Beyond the classical Stefan problem

Francesc Font Martinez

PhD thesis

Supervised by: Prof. Dr. Tim Myers

Submitted in full fulfillment of the requirements
for the degree of Doctor of Philosophy in Applied Mathematics
in the Facultat de Matemàtiques i Estadística
at the Universitat Politècnica de Catalunya

June 2014, Barcelona, Spain

Acknowledgments

First and foremost, I wish to thank my supervisor and friend Tim Myers. This thesis would not have been possible without his inspirational guidance, wisdom and expertise. I appreciate greatly all his time, ideas and funding invested into making my PhD experience fruitful and stimulating. Tim, you have always guided and provided me with excellent support throughout this long journey. I can honestly say that my time as your PhD student has been one of the most enjoyable periods of my life.

I also wish to express my gratitude to Sarah Mitchell. Her invaluable contributions and enthusiasm have enriched my research considerably. Her remarkable work ethos and dedication have had a profound effect on my research mentality. She was an excellent host during my PhD research stay in the University of Limerick and I benefited significantly from that experience. Thank you Sarah.

My thanks also go to Vinnie, who, in addition to being an excellent football mate and friend, has provided me with insightful comments which have helped in the writing of my thesis. I also thank Brian Wetton for our useful discussions during his stay in the CRM, and for his acceptance to be one of my external referees. Thank you guys.

Agraeixo de tot cor el suport i l'amor incondicional dels meus pares, la meva germana i la meva tieta. Ells han sigut des de sempre la meva columna vertebral i, sense cap dubte, mai no hauria arribat on sóc si no hagués estat per ells. També vull dedicar un record especial al meu avi que, tot i ja no ser entre nosaltres, sempre estava pendent de mi i dels meus progressos, i s'il·lusionava amb cada petit repte que anava aconseguint. Sempre el tindre present. També vull dedicar unes paraules especials a la Gloria que, a part dajudar-me en la

vessant artística de la tesi, ha esdevingut durant aquest últim any la meva font permanent de felicitat, calidesa i amor. Infinites gràcies a tots vosaltres.

També tinc paraules especials per (enumero per ordre alfabètic, perquè ningú se m'enfadi) en David, en Guillem, en Jordi, en Josep, en Marc, en Pau, en Roger i en Sergi, els meus eterns proveidors de somriures. Potser sense adonar-vos-en, però també heu format part de l'energia necessaria per dur a terme un projecte com aquest. Sou els millors.

M'agradaria també donar les gràcies als meus companys del CRM, l'Esther, l'Anita, el Dani, el Francesc i tota la tropa que han vingut després, pels bons moments i bon ambient viscuts al despatx. Ovbiously, a special shout out to Michelle for being the best possible PhD comrade and a good friend. També vull agrair-li a l'Albert el bon humor, les estones de fer petar la xerrada a la uni, els cafès i els dinars que hem fet. Moltes gràcies a tots.

Finalment, vull agrair al Centre de Recerca Matemàtica el finançament rebut per a la realització d'aquesta tesi doctoral. Dono les gràcies també a tots els membres de l'administració i la direcció del centre per tots aquests anys de bons moments i feina ben feta.

A tots vosaltres, gràcies de tot cor.

Outline

The main body of this thesis is based on the research papers published since I started my PhD in September 2010. The papers listed below, from 1 to 5, correspond to the chapters 2, 3, 4, 5, 6, respectively. Paper 6 is a review of this whole body of work, which will most likely be submitted to SIAM Review. Chapter 1 is an introduction to the topic. Chapter 7 contains the conclusions. Chapters 8 and 9 are the Appendix and Bibliography, respectively. The abstract and conclusions are written in both English and Catalan.

1. F. Font, T.G. Myers. *Spherically symmetric nanoparticle melting with a variable phase change temperature*, Journal of Nanoparticle Research, 15, 2086 (2013). *Impact factor: 2.175*, [29].

2. F. Font, T.G. Myers, S.L. Mitchell. *Mathematical model for nanoparticle melting with density change*, Microfluidics and Nanofluidics, DOI:10.1007/s10404-014-1423-x (May 2014). *Impact factor: 3.218*, [30].

3. F. Font, S.L. Mitchell, T.G. Myers. *One-dimensional solidification of supercooled melts*, International Journal of Heat and Mass Transfer, 62, 411-421 (2013). *Impact factor: 2.315*, [28].

4. T.G. Myers, S.L. Mitchell, F. Font. *Energy conservation in the one-phase supercooled Stefan problem*, International Communications in Heat and Mass Transfer, 39, 1522-1225 (2012). *Impact factor: 2.208*, [74].

5. T.G. Myers, F. Font. *On the one-phase reduction of the Stefan problem*, Submitted to International Communications in Heat and Mass Transfer (May 2014). *Impact factor:*

2.208, [75].

6. F. Font, T.G. Myers, S.L. Mitchell. *Beyond the classical Stefan problems*, To be submitted to SIAM Review (July 2014). *Impact factor: 8.414*.

Abstract

In this thesis we develop and analyse mathematical models describing phase change phenomena linked with novel technological applications. The models are based on modifications to standard phase change theory. The mathematical tools used to analyse such models include asymptotic analysis, similarity solutions, the Heat Balance Integral Method and standard numerical techniques such as finite differences.

In chapters 2 and 3 we study the melting of nanoparticles. The Gibbs-Thomson relation, accounting for melting point depression, is coupled to the heat equations for the solid and liquid and the associated Stefan condition. A perturbation approach, valid for large Stefan numbers, is used to reduce the governing system of partial differential equations to a less complex one involving two ordinary differential equations. Comparison between the reduced system and the numerical solution shows good agreement. Our results reproduce interesting behaviour observed experimentally such as the abrupt melting of nanoparticles. Standard analyses of the Stefan problem impose constant physical properties, such as density or specific heat. We formulate the Stefan problem to allow for variation at the phase change and show that this can lead to significantly different melting times when compared to the standard formulation.

In chapter 4 we study a mathematical model describing the solidification of supercooled liquids. For Stefan numbers, β, larger than unity the classical Neumann solution provides an analytical expression to describe the solidification. For $\beta \leq 1$, the Neumann solution is no longer valid. Instead, a linear relationship between the phase change temperature and the front velocity is often used. This allows solutions for all values of β. However, the

linear relation is only valid for small amounts of supercooling and is an approximation to a more complex, nonlinear relationship. We look for solutions using the nonlinear relation and demonstrate the inaccuracy of the linear relation for large supercooling. Further, we show how the classical Neumann solution significantly over-predicts the solidification rate for values of the Stefan number near unity.

The Stefan problem is often reduced to a 'one-phase' problem (where one of the phases is neglected) in order to simplify the analysis. When the phase change temperature is variable it has been claimed that the standard reduction loses energy. In chapters 5 and 6, we examine the one-phase reduction of the Stefan problem when the phase change temperature is time-dependent. In chapter 5 we derive a one-phase reduction of the supercooled Stefan problem, and test its performance against the solution of the two-phase model. Our model conserves energy and is based on consistent physical assumptions, unlike one-phase reductions from previous studies. In chapter 6 we study the problem from a general perspective, and identify the main erroneous assumptions of previous studies leading to one-phase reductions that do not conserve energy or, alternatively, are based on non-physical assumptions. We also provide a general one-phase model of the Stefan problem with a generic variable phase change temperature, valid for spherical, cylindrical and planar geometries.

Resum

En aquesta tesi construirem i analitzarem models matemàtics que descriuen processos de transició de fase vinculats a noves tecnologies. Els models es basen en modificacions de la teoria estàndard de canvis de fase. Les tècniques matemàtiques per resoldre els models es basen en l'anàlisi asimptòtic, solucions autosimilars, el mètode de la integral del balanç de la calor i mètodes numèrics estàndards com ara el mètode de les diferències finites.

En els capítols 2 i 3 estudiarem la transició solid-líquid d'una nanopartícula, acoblant la relació de Gibbs-Thomson, que descriu la depressió de la temperatura de fusió en una superfície corba, amb l'equació de la calor per la fase sòlida i líquida, i la condició de Stefan. Mitjançant el mètode de pertorbacions, per a valors grans del nombre de Stefan, el problema d'equacions en derivades parcials inicial és reduït a un sistema més senzill de dues equacions diferencials ordinàries. La solució del sistema reduït concorda perfectament amb la solució numèrica del sistema inicial d'equacions en derivades parcials. Els resultats confirmen la transició ultra ràpida de sòlid a líquid observada en experiments amb nanopartícules. Els anàlisis estàndards del problema de Stefan consideren propietats físiques com la densitat i el calor específic constants en la fase sòlida i líquida. En aquesta tesi, formularem el problema de Stefan relaxant la condició de densitat constant, el que portarà a diferències molt significatives en els temps totals de fusió al comparar-los amb els temps obtinguts mitjançant la formulació habitual del problema de Stefan.

En el capítol 4 estudiarem un model matemàtic que descriu la solidificació de líquids sota-refredats. Per nombres de Stefan, β, més grans que la unitat la solució clàssica de Neumann dona una expressió analítica que descriu el procés. Per valors $\beta \leq 1$, la solució de Neumann no es vàlida i, habitualment, per tal de trobar solucions en aquest règim, s'estableix una relació lineal entre la temperatura de canvi de fase i la velocitat del front de solidificació. Aquesta relació lineal però, és una aproximació per sota-refredaments moderats d'una relació no lineal més complexa. En aquest capítol, buscarem solucions del problema incorporant la relació no lineal al model, i demostrarem la poca precisió a l'utilitzar l'aproximació lineal. A més a més, veurem com la solució de Neumann sobre estima de manera significativa la velocitat del procés per valors propers a la unitat.

Habitualment, el problema de Stefan, que te en compte les fases solida i líquida de la transició, és simplificat a un problema d'una fase (on una de les fases és omesa) per tal de reduir la dificultat de l'anàlisi. En casos on la temperatura de transició de fase és variable s'ha manifestat que la simplificació d'una fase no conserva l'energia. En els capítols 5 i 6, examinarem les diferents reduccions d'una fase del problema de Stefan en el cas on la temperatura de transició depèn del temps. En el capítol 5 derivarem el problema de Stefan d'una fase associat a la solidificació de líquids sota-refredats, i compararem la solució del sistema resultant amb la solució del problema de Stefan estàndard de dues fases. A diferència dels models d'una fase descrits en estudis previs, el nostre model reduït conserva l'energia i està basat en suposicions físiques consistents. En el capítol 6 estudiarem el problema des d'una perspectiva més general i identificarem les suposicions errònies d'estudis previs que porten a la no conservació de l'energia o que, alternativament, estan basades en suposicions físiques poc consistents. A més a més, derivarem un model d'una fase amb temperatura de canvi de fase variable, vàlid per geometries esfèriques, cilíndriques i planes.

Contents

List of Figures

List of Tables

Chapter 1

Introduction

The phenomena of melting and solidification occurs in a multitude of natural and industrial situations, from the melting of the polar ice caps or the solidification of lava from a volcano to the manufacture of ice cream or the production of steel. For a material to undergo a solid-liquid phase change, thermal energy has to be delivered to the solid to break the bonds that maintain its molecules or atoms in an organized lattice structure. For the opposite process, energy must be taken from the liquid phase to slow down the motion of its molecules and organize them back into a stable lattice structure. The mathematical formulation describing this intuitively simple physical process is known as the Stefan problem, named after the Slovene physicist Josef Stefan.

Scientific discoveries are being made every day that are changing the world we live in. New observations and experiments lead to established scientific theories being revisited, updated and possibly started from scratch. Following the philosophy of the pioneers of the Stefan problem this thesis provides a mathematical description and analysis of new observed physical phenomena, introducing appropriate modifications to classical phase change theory. The mathematical models discussed in this thesis are linked with industrial processes on materials manufacturing and the working mechanisms of new technological applications. In particular, we develop mathematical models describing the melting process of nanoparticles and the solidification of supercooled liquids. In addition, more fundamental questions, for

example concerning the energy conservation of such systems, arose during the development of the models and led to a revision of the standard formulation of Stefan problems.

Note, this thesis is built from five published papers, each of which contain an introduction and literature survey. Consequently in this chapter we will not go into great detail on the literature, all the relevant sources will be cited in the introduction section of each chapter.

In chapters 2 and 3 we present mathematical models describing the melting process of nanoparticles. In these models the characteristic melting point depression of nanoparticles is described by the Gibbs-Thomson relation. In chapter 2 we present a generalized version of the Gibbs-Thomson relation that shows good agreement with experimental data down to a few nanometers. Then, the relation is coupled with the heat equations for the solid and liquid phase, and the Stefan condition. The standard perturbation method for large Stefan number is utilized to reduce the system to a pair of easily solvable ordinary differential equations (ODE). We highlight the strong effect of the melting point depression when compared to the equivalent classical Stefan problem solution. The solutions found show interesting features observed experimentally, such as the ultra-fast melting velocity as the radius of the nanoparticle tends to zero. In chapter 3 the model studied in chapter 2 is extended, allowing for the densities of the solid and liquid phases to take different values. This seemingly inoffensive assumption leads to a remarkably different model formulation; requiring an advection term in the heat equation for the liquid, an extra cubic term for the velocity in the Stefan condition and a second moving boundary tracking the expansion of the liquid phase. The solution methodology is analogous to that in chapter 2. The introduction of the density jump between phases has a profound effect on the solution, showing more than a 50% difference in the melting times with the equivalent model assuming equal densities.

In chapter 4 we study the solidification process of a supercooled liquid. Again the phase change temperature is variable but now it is related to the reduced mobility of the supercooled liquid molecules. The interface temperature, which is lower than the ideal freezing point, depends nonlinearly on the velocity of the solidification front. Previous studies have focused on the standard problem with a constant phase change temperature or on the case of very small supercooling, where the relation between the velocity of the solidification front and the

phase change temperature is approximately linear. We analyse the problem in three possible scenarios; with the full nonlinear relation, the linearized approximation and the standard case, with constant interface temperature. Asymptotic solutions for small and large times are provided and compared with numerical and approximate solutions by the Heat Balance Integral Method. The introduction of the characteristic nonlinear behaviour of the phase change temperature shows the unsuitability of the classical Neumann solution to describe the solidification of supercooled melts.

In general, finding a solution to the Stefan problem requires solving heat equations for the solid and liquid phases subject to a condition in the solid-liquid interface describing the evolution of the phase change front. Sometimes, it is convenient to reduce the problem by assuming the solid or the liquid to be at the phase change temperature and only solve the heat equation for the remaining phase. This simplified model is commonly referred to as the one-phase Stefan problem. In chapters 2, 3 and 4 we propose models where the phase change temperature varies, meaning that a truly one-phase problem will never exist (since the melting or freezing temperature is a function of time). Hence, the one-phase reduction based on assuming one of the phases at the constant phase change temperature does not hold. This leads us to look for consistent ways to formulate the one-phase Stefan problem for cases where the phase change temperature is variable. In chapter 5 we specifically deal with the derivation of an accurate one-phase reduction of the Stefan problem for the solidification of supercooled melts. Previous formulations of the one-phase reduction have appeared not to conserve energy or relied on non-physical assumptions. In chapter 5, we derive an energy conserving formulation for the one-phase supercooled Stefan problem. Numerical solutions for the proposed one-phase model are tested against solutions for the full two-phase problem. The results show excellent agreement and improve considerably on the accuracy of previous one-phase formulations.

The study of the one-phase reduction of the Stefan problem with linear supercooling carried out in chapter 5 opens the door to tackle the problem from a more general point of view. With the advent of new technologies, phase change processes where solid-liquid interface temperature differ from the bulk phase change temperature are becoming more

frequent. This serves as the motivation for chapter 6 where the derivation of the one-phase reduction of the Stefan problem is examined in detail via energy arguments. A general one-phase model of the Stefan problem with a generic variable phase change temperature, valid for spherical, cylindrical and planar geometries, is provided. Finally, the model is solved numerically for the case where the phase change temperature depends on the inverse of the melting front (which is related to the melting process of nanoparticles studied in chapters 2 and 3). As in chapter 5 the results are compared to the two-phase model and show excellent accuracy.

In the following section of this introduction we briefly describe the historical roots of the Stefan problem. In the second section we introduce the formulation of the problem and summarize some of the standard analytical techniques used to tackle Stefan problems. Then, we present the extensions that have to be introduced to the standard problem to account for the variable phase change temperature of nanoparticles and supercooled liquids, and the appropriate way to formulate the one-phase Stefan problem for such situations.

1.1 Historical roots of the Stefan problem

The Stefan problem, named after the Slovene physicist Jožef Stefan (1835-1893), is a particular kind of moving boundary value problem that originally aimed to describe the solid-liquid phase change process [53, 94, 107, 117]. Stefan problems, are characterized by having a boundary of the domain which is moving and, therefore, its position is unknown "a priori". The position of the moving boundary is a function of time (and sometimes space) and must be determined as part of the solution. The differential equations in a Stefan problem are generally, but not restricted to, of parabolic type. The most common example of a Stefan problem is that describing the ice-water phase transition. This requires solving heat equations for the ice and water phases, while the position of the front separating the two states, the moving boundary, is determined from an energy balance, referred to as the Stefan condition.

Stefan carried out extensive analytical and experimental work on physical situations involving a moving boundary: solid-liquid phase change [102, 104, 105, 107], chemical reac-

tions [101] and liquid-vapor phase change [100, 103, 106]. Indeed, his most popular and cited work in the field is [107] (a reprinted version of [102] for the journal *Annalen der Physics und Chemie*) where he studied ice formation in the polar Arctic seas. His model described the seawater initially at the freezing temperature and the air in contact with the water to be at a constant temperature below the freezing point, thus, triggering ice formation at the air-water interface [115]. The resulting growing ice layer was found to be proportional to the square root of time. However, Stefan's major contribution to science was the experimental finding that states the thermal energy radiated by an object is proportional to the fourth power of its temperature, the law of Stefan-Boltzmann. The second name is due to the Austrian physicist Ludwig Boltzmann (1844-1906), Stefan's pupil, who derived the relationship from first principles. Above all, Stefan was a brilliant experimentalist who is also known for being the first to accurately measure the thermal conductivity of gases [17].

Although Stefan carried out wide ranging research concerning phase change, from experimental to theoretical work, and the Stefan problem was named after him, he was not the first to formalize and solve the problem. In the 18^{th} century, the Scottish medical doctor Joseph Black (1728-1799) introduced for the first time the concept of latent heat, a key ingredient to understanding the physical mechanism of phase change. Later on, Jean Baptiste Joseph Fourier (1768-1830), a French mathematician and physicist, provided the necessary physics and mathematics to the theory of heat conduction. In the 19^{th} century, the physicist Gabriel Lamé (1795-1850) and the mechanical engineer Emile Clapeyron (1799-1864) were the first to mathematically couple the concept of latent heat with the heat conduction equation, whilst extending Fourier's work on the estimate of the time elapsed since the Earth began to solidify from its initial molten state [53, 94]. They initially assumed the Earth to be in a liquid phase at the melting temperature (a one-phase problem). Due to an abrupt temperature drop at the surface the freezing process was initiated. They found the solid crust to grow proportional to the square root of time (just as Stefan later found in his work [102, 107]). Unlike Stefan, Lamé and Clapeyron did not determine the value of the constant of proportionality. In a series of lectures in the early 1860s, Franz Ernst Neumann (1798-1895), a German physicist and mathematician, solved in detail a problem similar to the one

of Lamé and Clapeyron [53], with the initial temperature above the melting point [17, 94] (so dealing with a two-phase problem). However, his work was not published until 1901 by Heinrich Weber in [117]. Today, the solution to the classical Stefan problem receives the name of Neumann solution in honor of the German scientist.

The motivation of the Stefan problem was the need to mathematically formulate and describe observed natural physical phenomena, such as the melting, solidification or evaporation of a substance. Nowadays, it is well known that Stefan problems arise in numerous industrial and technological applications, such as the manufacture of steel, ablation of heat shields, contact melting in thermal storage systems, ice accretion on aircraft, evaporation of water, and a long etcetera [3, 16, 27, 40, 43, 108]. The fact that the Stefan problem has been studied and applied in a wide variety of situations is evident by simply looking at the review on the subject from 1988 [108], where around 2500 references were given. Over 20 years later, the number of references has exponentially increased. A quick search in Google Scholar gives around 422K references in the period 1999-2014. Hence, it is clearly impossible to establish here a complete list of references of papers on the subject. However, there are some reference books on Stefan problems and its applications that have been particularly important for the elaboration of this thesis that the interested reader may wish to consult [3, 16, 19, 38, 40].

1.2 Formulation and standard mathematical techniques

The Stefan problem is a mathematical model describing the process of a material undergoing a phase change. The mathematical formulation of the problem involves heat equations for the solid and liquid phases and a condition at the solid-liquid interface, the Stefan condition, that describes the position of the phase change front. At the moving phase change boundary, $x = s(t)$, the temperature is fixed at the constant bulk phase change temperature, T_m^*. The most basic form of Stefan problem arises when considering the melting of a semi-infinite, one-dimensional slab occupying $x \geq 0$, where the phase change is driven by a heat source at the boundary $x = 0$. A configuration of the model is shown in figure 1.1.

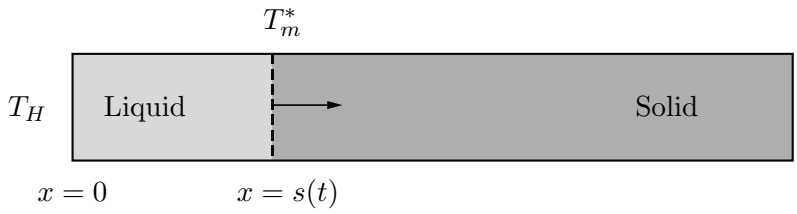

Figure 1.1: Semi-infinite slab melting from $x = 0$ due to the high temperature T_H. Dashed line depicts the liquid-solid interface, $s(t)$, and the arrow the direction of motion of the phase change front.

The governing equations of the model are

$$c_l \rho_l \frac{\partial T}{\partial t} = k_l \frac{\partial^2 T}{\partial x^2} \qquad \text{on} \qquad 0 < x < s(t) \ , \tag{1.1}$$

$$c_s \rho_s \frac{\partial \theta}{\partial t} = k_s \frac{\partial^2 \theta}{\partial x^2} \qquad \text{on} \qquad s(t) < x < \infty \ , \tag{1.2}$$

where T represents the temperature in the liquid, θ the temperature in the solid, $s = s(t)$ the position of the moving boundary, k the thermal conductivity, ρ the density, c the specific heat and subscripts s and l indicate solid and liquid, respectively. The position of the moving front $s(t)$ is determined by the Stefan condition

$$\rho_l L_m \frac{ds}{dt} = k_s \frac{\partial \theta}{\partial x} - k_l \frac{\partial T}{\partial x} \qquad \text{on} \qquad x = s(t) \ , \tag{1.3}$$

where L_m is the latent heat. At the interface $x = s(t)$ we have $T(s,t) = \theta(s(t),t) = T_m^*$ and, defining the heat source driving the melting as a constant temperature $T_H > T_m^*$, at $x = 0$ we have $T(0,t) = T_H$. Obviously, at $t = 0$ the liquid phase does not exist, so $s(0) = 0$. From a formal point of view we still need to define a boundary and an initial condition for θ but for the following argument this is unnecessary.

A very common simplification of the Stefan problem consists of assuming one of the phases to be initially at the phase change temperature [40]. This removes one of the two heat equations and provides a simpler form of the Stefan condition by eliminating one of the temperature gradients. In this way, one of the two phases is effectively omitted and the resulting system is referred to as the one-phase Stefan problem. For instance, by assuming

the solid region initially at the melting temperature in the system (1.1)-(1.3) the problem reduces to

$$c_l\rho_l \frac{\partial T}{\partial t} = k_l \frac{\partial^2 T}{\partial x^2} \quad \text{on} \quad 0 < x < s(t) \ , \tag{1.4}$$

$$T(0,t) = T_H \ , \tag{1.5}$$

$$T(s,t) = T_m^* \ , \tag{1.6}$$

$$\rho_l L_m \frac{ds}{dt} = -k_l \frac{\partial T}{\partial x} \quad \text{on} \quad x = s(t). \tag{1.7}$$

Only one practically useful exact solution exists for problems of the form (1.4)-(1.7), which is expressed in terms of the error function [38, 40, 53, 107]. Several analytical, approximate and numerical methods have been employed in the past to analyse Stefan problems when no analytical solution exists [3, 10, 40, 43, 55, 64, 66, 113]. In this thesis we mainly focus on analytical and approximate techniques. Numerical solutions are generally provided to verify approximate solutions. Now, we provide a quick overview of some standard mathematical techniques for Stefan problems that will be used later in this thesis.

1.2.1 Similarity variables

The order of a partial differential equation can often be reduced by rewriting the equation in terms of a similarity variable, grouping in the new variable two or several former independent variables, and thus reducing the order of the equation. For instance, if we have a partial differential equation whose independent variables are x and t we may look for a similarity variable of the form $\xi = c\, t^{\nu} x^{\gamma}$ [16, 40]. Assuming the nondimensional version of (1.4)–(1.7)

$$\frac{\partial T}{\partial t} = \frac{\partial^2 T}{\partial x^2} \quad \text{on} \quad 0 < x < s(t) \ , \tag{1.8}$$

$$T(0,t) = 1 \ , \tag{1.9}$$

$$T(s,t) = 0 \ , \tag{1.10}$$

$$\beta \frac{ds}{dt} = -\frac{\partial T}{\partial x} \quad \text{on} \quad x = s(t) \ , \tag{1.11}$$

where $\beta = L/c(T_H - T_m^*)$ is the Stefan number, and applying the similarity transformation $\xi = x/\sqrt{t}$ to (1.8), the PDE is reduced to

$$F_{\xi\xi} = -\frac{\xi}{2} F_\xi \ , \tag{1.12}$$

where $F(\xi) = T(x,t)$. This has the general solution

$$F(\xi) = C_1 + C_2 \operatorname{erf}\left(\frac{\xi}{2}\right). \tag{1.13}$$

This may be solved in terms of the error function. Imposing the boundary conditions and rewritting in terms of the original variables, the solution to the problem (1.8)–(1.11) is

$$T(x,t) = 1 - \frac{\operatorname{erf}\left(\frac{x}{2\sqrt{t}}\right)}{\operatorname{erf}(\lambda)} \ , \qquad s(t) = 2\lambda\sqrt{t} \ , \tag{1.14}$$

where the constant λ is the solution of

$$\beta\sqrt{\pi}\lambda e^{\lambda^2} \operatorname{erf}(\lambda) = 1. \tag{1.15}$$

Expressions (1.14)-(1.15) receive the name of Neumann solution.

Although similarity transformations can only provide exact solutions to a very small number of Stefan problems, they represent the basis for analytical progress to other formulations when combined with other techniques such as perturbation methods, as in chapter 4.

1.2.2 Boundary–fixing transformations

Another useful tool to simplify problems like (1.4)–(1.7) is the boundary–fixing transformation [16, 41, 40]. This is of particular interest when looking for numerical solutions, where working with a moving boundary is always troublesome. For example, the boundary immobilising coordinate $\eta = x/s(t)$ applied to (1.4)–(1.7) yields

$$\frac{\partial F^2}{\partial \eta^2} = s^2 \frac{\partial F}{\partial t} - \eta s \frac{ds}{dt} \frac{\partial F}{\partial \eta} \ , \tag{1.16}$$

and boundary conditions

$$F(0,t) = 1 \ , \qquad F(1,t) = 0 \ , \qquad \beta s \frac{ds}{dt} = -\frac{\partial F}{\partial \eta}\bigg|_{\eta=1} \ , \tag{1.17}$$

where $F(\eta, t) = T(x, t)$. This fixes the problem of a moving domain, since the original domain $x \in [0, s(t)]$ is now mapped on to $\eta \in [0, 1]$. However, with the standard Stefan problem we find $s \sim \sqrt{t}$ and so $s_t \sim 1/\sqrt{t}$ (which appears in (1.16)) is singular at $t = 0$. This difficulty may be removed by working in terms of $z = s^2$, so

$$\frac{\partial F^2}{\partial \eta^2} = z\frac{\partial F}{\partial t} - \frac{\eta}{2}\frac{dz}{dt}\frac{\partial F}{\partial \eta} \ , \qquad \frac{\beta}{2}\frac{dz}{dt} = -\frac{\partial F}{\partial \eta}\bigg|_{\eta=1} \ . \tag{1.18}$$

In this form the equations are amenable to standard finite difference techniques.

The variable $\eta = x/s(t)$ transforms the domain $[0, s(t)]$ into $[0, 1]$. However, the one-phase reduction of the Stefan problem can be such that the heat equation lies in the region $s(t) < x < \infty$ instead of $0 < x < s(t)$. If this is the case, then the boundary fixing variable that we use is $\eta = x - s(t)$, which transforms the domain from $[s(t), \infty]$ into $[0, \infty]$. In the case of solving the two-phase problem we could use both transformations, one for each phase, i.e., $\eta_1 = x/s(t)$ and $\eta_2 = x - s(t)$. Indeed, other transformations arise depending on the nature of each problem, as in chapters 2 and 3 where the geometry of the domain is spherical.

1.2.3 Perturbation method

The aim of this method is to find an approximate solution to a problem, which cannot be solved analytically, by means of a power series solution in terms of a small parameter [42]. For instance, we will now describe what is known as the large Stefan number expansion, see [40]. Consider the problem (1.8)–(1.11). For large values of β we can define the small parameter $\epsilon = 1/\beta \ll 1$ and the Stefan condition may be written as

$$\frac{ds}{dt} = -\epsilon \, \frac{\partial T}{\partial x}\bigg|_{x=s} . \tag{1.19}$$

From (1.19) we see that at leading order $s_t = 0$ and, after applying the initial condition, $s = 0$, meaning that the front is approximately stationary. This indicates that a large Stefan number corresponds to slow melting (as can be seen from $\beta \propto 1/(T_H - T_m^*)$, so large β implies small heating). In order for the front to move (at leading order) we need to rescale time $t = \tau/\epsilon$. This leads to

$$\epsilon \frac{\partial T}{\partial \tau} = \frac{\partial^2 T}{\partial x^2} \ , \qquad \frac{ds}{d\tau} = - \left. \frac{\partial T}{\partial x} \right|_{x=s} . \tag{1.20}$$

Hence, we try the expansion

$$T = T_0 + \epsilon T_1 + \epsilon^2 T_2 + \dots \ , \tag{1.21}$$

and find

$$\mathcal{O}(\epsilon^0): \qquad 0 = \frac{\partial^2 T_0}{\partial x^2} \qquad \rightarrow \qquad T_0 = 1 - \frac{x}{s} \tag{1.22}$$

$$\mathcal{O}(\epsilon^1): \qquad \frac{\partial T_0}{\partial \tau} = \frac{\partial^2 T_1}{\partial x^2} \qquad \rightarrow \qquad T_1 = \frac{s_\tau}{6} \left(\frac{x^3}{s^2} - x \right) \tag{1.23}$$

$$\mathcal{O}(\epsilon^2): \qquad \frac{\partial T_1}{\partial \tau} = \frac{\partial^2 T_2}{\partial x^2} \qquad \dots \tag{1.24}$$

If we substitute these solutions into the Stefan condition we find

$$\frac{ds}{d\tau} = - \left(-\frac{1}{s} + \epsilon \frac{1}{3} \frac{ds}{d\tau} \right) \ , \tag{1.25}$$

which gives

$$s = \sqrt{\frac{6\tau}{3+\epsilon}} = \sqrt{2\tau} \left(1 - \frac{\epsilon}{6} + \dots \right) . \tag{1.26}$$

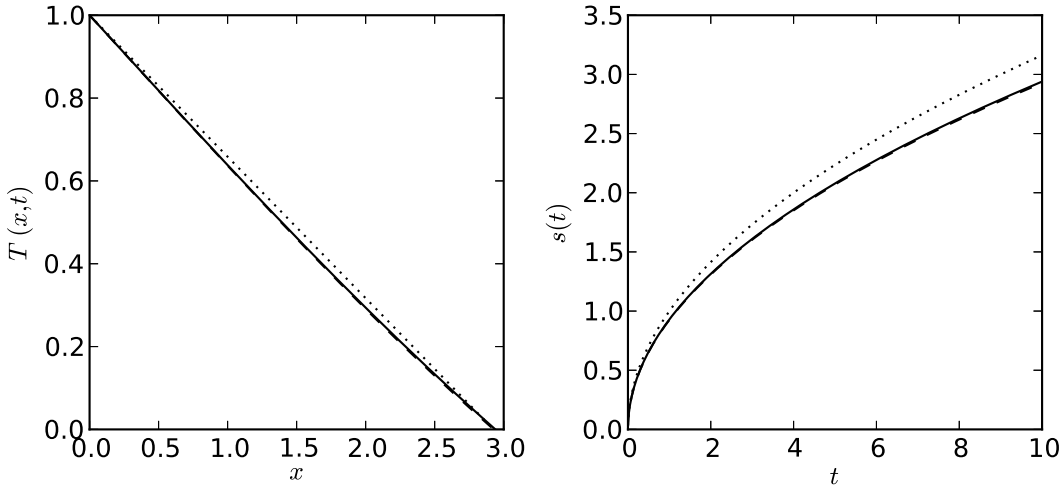

Figure 1.2: Exact (solid), leading order perturbation (dotted) and first order perturbation (dashed) solution for the one-phase Stefan problem (1.8)-(1.11) for $\beta = 2$. Left: temperature of the liquid at $t = 10$. Right: evolution of the melting front.

In figure 1.2 we compare the exact solution, the leading order perturbation solution and the perturbation solution to $\mathcal{O}(\epsilon)$. We observe that the correction introduced by the $\mathcal{O}(\epsilon)$ term from (1.23) has a strong effect, and even for the relatively large value of the small parameter used, $\epsilon = 0.5$, the solution converges very quickly to the exact solution.

We note that after the $\mathcal{O}(\epsilon)$ solution, equation (1.23), we cannot take the perturbation solution further. We stopped the series in T_2 since it depends on $\frac{\partial T_1}{\partial \tau}$ and so involves a term $s_{\tau\tau}$. Since we only have a single initial condition we cannot deal with this extra term that makes the Stefan condition second order in time. We may overcome this problem by defining the boundary–fixing transformation $\eta = x/s$ and a new time variable $\tau(t) = s(t)$, so that $T(x,t) = F(\eta,\tau)$ [40]. Then the problem (1.8)–(1.11) becomes

$$F_{\eta\eta} = \tau\tau_t\left(\tau F_\tau - \eta F_\eta\right), \qquad \beta\tau\tau_t = -F_\eta|_{\eta=1}, \qquad F(0,\tau) = 1, \qquad F(1,\tau) = 0\ , \tag{1.27}$$

and for a large Stefan number we have

$$\tau\tau_t = -\epsilon F_\eta|_{\eta=1}\,. \tag{1.28}$$

Since (1.27a) contains $\tau\tau_t$ we substitute (1.28) into it and perform the following expansion

$$F(\eta,\tau) = F_0 + \epsilon F_1 + \epsilon^2 F_2 + \dots \ , \tag{1.29}$$

to give

$$\mathcal{O}(\epsilon^0): \qquad 0 = \frac{\partial^2 F_0}{\partial \eta^2} \qquad \rightarrow \qquad F_0 = 1-\eta \tag{1.30}$$

$$\mathcal{O}(\epsilon^1): \qquad -C(\tau)\left(\tau F_{0\tau} - \eta F_{0\eta}\right) = \frac{\partial^2 F_1}{\partial \eta^2} \qquad \rightarrow \qquad F_1 = \frac{C(\tau)}{6}\left(1-\eta^2\right)\eta \tag{1.31}$$

$$\mathcal{O}(\epsilon^2): \qquad -C(\tau)\left(\tau F_{1\tau} - \eta F_{1\eta}\right) = \frac{\partial^2 F_2}{\partial \eta^2} \qquad \rightarrow \qquad \dots \ , \tag{1.32}$$

where $C(\tau) = F_\eta|_{\eta=1}$. An important point is that we could take this expansion as far as we like as there is no issue with derivatives of τ, and the only reason to stop is that the algebra becomes tedious. Once, we have enough terms in the expansion we replace F in the Stefan condition and solve the equation for τ.

1.2.4 The Heat Balance Integral Method

The heat balance integral method (HBIM) introduced by Goodman [32] is a well-known approximate method for solving Stefan problems [3, 10, 64, 73, 71]. The basic idea behind the method is to approximate the temperature profile, usually with a polynomial, over some distance $\delta(t)$ known as the heat penetration depth. This is a fictitious measure of the point where the thermal boundary layer ends. The heat equation is then integrated to determine a ordinary differential equation for $\delta(t)$. The solution of this equation, coupled with the Stefan condition then determines the temperature and position $s(t)$. In chapter 4 we apply the HBIM to a one-phase Stefan problem related to the solidification of a supercooled melt. We will now use this physical situation to illustrate the HBIM.

Consider the solidification of a supercooled liquid which initially occupies the semi-infinite space $[0,\infty]$ and starts to solidify from the edge $x = 0$. The nondimensional version of the

one-phase Stefan problem describing this situation may be written as

$$\frac{\partial T}{\partial t} = \frac{\partial^2 T}{\partial x^2} \qquad \text{on} \qquad s < x < \infty \ , \tag{1.33}$$

$$T(s,t) = 0, \qquad T(\infty,t) = -1, \qquad T(x,0) = -1 \ , \tag{1.34}$$

where T represents the temperature of the supercooled liquid, the temperature $T = 0$ represents the freezing temperature and $T = -1$ is the far field and initial temperature of the liquid. The Stefan and the initial condition at the solidification front $s(t)$ are

$$\beta \frac{ds}{dt} = - \left. \frac{\partial T}{\partial x} \right|_{x=s}, \qquad s(0) = 0 \ . \tag{1.35}$$

The system (1.33)-(1.35) can be solved analytically by means, for instance, of similarity variables and has the exact solution

$$T = -1 + \frac{\operatorname{erfc}\left(x/2\sqrt{t}\right)}{\operatorname{erfc}(\lambda)}, \qquad s = 2\lambda\sqrt{t} \ , \tag{1.36}$$

where the value of λ is obtained by solving the transcendental equation

$$\beta\sqrt{\pi}\lambda \operatorname{erfc}(\lambda) e^{\lambda^2} = 1 \ . \tag{1.37}$$

The solution (1.36)-(1.37) represents the particular form of the classical Neumann solution for the one-phase supercooled Stefan problem (1.33)-(1.35).

The first step when using the HBIM consists in defining the heat penetration depth $\delta(t)$, the point after which we consider the temperature gradient to be negligible. In our model, $x = \delta(t)$ represents the point where the temperature of the liquid is sufficiently close to the far field temperature $T = -1$. Note, this means we work over the domain $[s(t), \delta(t)]$. The second step consists in assuming a temperature profile describing the thermal response of the material. This involves typically polynomials, although logarithmic, exponential and error functions have been also utilized in the literature [15, 65, 69]. The profile will include a number of parameters that will be chosen to match the boundary conditions. For the

current problem, we propose

$$T(x,t) = a_1 + a_2\left(\frac{\delta - x}{\delta - s}\right) + a_3\left(\frac{\delta - x}{\delta - s}\right)^n . \tag{1.38}$$

The final step, is the integration of the heat equation over the spatial variable x to produce the heat balance integral.

In summary, using the HBIM, the problem (1.33)–(1.34) translates into

$$\int_s^\delta \frac{\partial T}{\partial t}\, dx = \int_{s(t)}^\delta \frac{\partial^2 T}{\partial x^2}\, dx \qquad \text{on} \qquad s < x < \delta \ , \tag{1.39}$$

$$T(s,t) = 0, \qquad T(\delta,t) = -1, \qquad T_x(\delta,t) = 0 \ . \tag{1.40}$$

It is straightforward to see that the parameters a_1, a_2 and a_3 from the assumed profile (1.38) are readily found from the boundary conditions (1.40). Hence, the temperature profile becomes

$$T(x,t) = -1 + \left(\frac{\delta - x}{\delta - s}\right)^n . \tag{1.41}$$

Equation (1.39) may be rearranged by means of the Leibniz integral rule to give

$$\frac{\mathrm{d}}{\mathrm{d}t}\int_s^\delta T\,\mathrm{d}x - T\big|_{x=\delta}\delta_t + T\big|_{x=s}s_t = T_x\big|_{x=\delta} - T_x\big|_{x=s} \ . \tag{1.42}$$

Then, assuming the polynomial to be quadratic, $n = 2$, and replacing (1.41) into (8.6) and (1.35) results in two ordinary differential equations

$$\frac{d\delta}{dt} = (3\beta - 2)\frac{ds}{dt}, \qquad \delta(0) = 0 \ , \tag{1.43}$$

$$\frac{ds}{dt} = \frac{2}{\beta(\delta - s)}, \qquad s(0) = 0 \ , \tag{1.44}$$

with solutions

$$\delta = (3\beta - 2)s, \qquad s = \sqrt{\frac{4t}{2\beta(\beta - 1)}} \ . \tag{1.45}$$

Substituting the expressions (1.45) in (1.41) the temperature profile is completely determined.

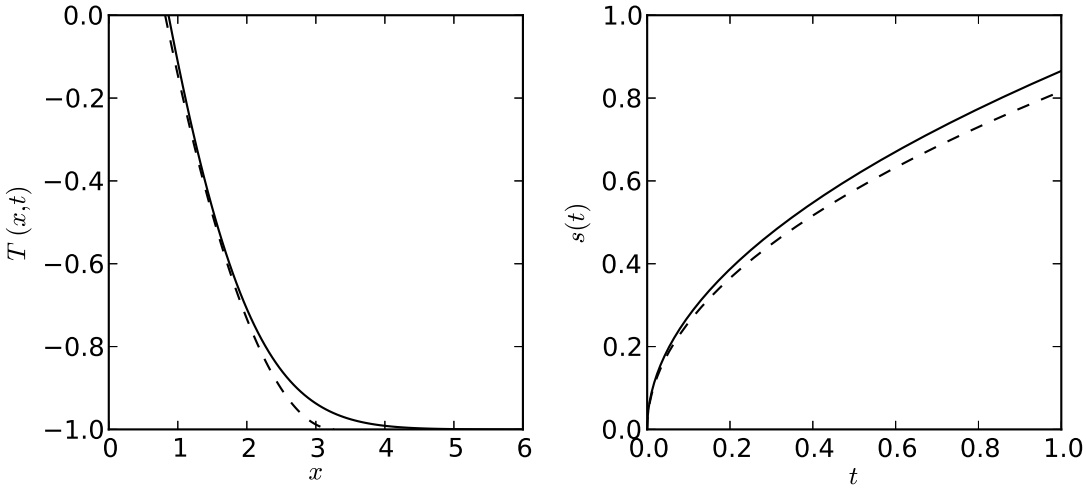

Figure 1.3: Exact (solid) and HBIM (dashed) solution for the one-phase supercooled Stefan problem for $\beta = 2$. Left: temperature of the liquid at $t = 1$. Right: time evolution of the solidification front.

The main advantage of the HBIM is that it reduces a difficult problem such as (1.33)–(1.35) into a pair of easily solvable ODEs. In this case it may not seem of great use, since an exact solution exists, but for more complex problems such as the ones developed in this thesis, the HBIM is sometimes of incalculable help. In figure 1.3 we compare the exact solution (1.36) and the HBIM solution with $n = 2$. It is clear that even for $n = 2$, the simplest realistic choice, the HBIM captures satisfactorily the behaviour of the exact solution. However, we note that even though Goodman's original choice was $n = 2$ the method may be improved by assuming n as an unknown in the problem and determining it as part of the solution. One option, known as the Optimal HBIM [70, 71], consists in choosing an exponent n that minimizes the least squares error

$$E_n = \int_s^\delta f(x,t)^2 dx \qquad \text{where} \qquad f(x,t) = \frac{\partial T}{\partial t} - \frac{\partial^2 T}{\partial x^2}. \tag{1.46}$$

This method significantly improves the accuracy of the HBIM and provides an error measure that does not require knowledge of an exact or numerical solution. For certain problems, for example when the boundary conditions are time–dependent, n may vary with time. Sometimes, to keep the method simple n is then given its initial value since this is where the

largest value of E_n usually occurs. Other extensions of the HBIM based on determining n as part of the solution exist. This is the case of the Refined Integral Method (RIM) [64, 91], that integrates the heat equation twice to obtain an extra equation for n, or the Combined Integral Method [65, 73], a combination of the Optimal HBIM and the RIM.

1.3 Extensions to the standard problem

To understand phase change in a more general situation several modifications must be introduced in the formulation of the standard Stefan problem, for example to include phenomena such as the melting point depression of nanoparticles, the velocity dependent freezing temperature in supercooled liquids or the expansion upon melting of the liquid phase of a material. Such modifications require us to review the derivation of the governing equations of the Stefan problem, so, we briefly describe how to derive the heat equation from the energy conservation equation and the Stefan condition from an energy balance at the solid-liquid interface. This will provide general mathematical expressions that will be easily adapted for modeling each physical problem dealt with within this thesis.

Bird, Stewart and Lightfoot [7] write down an energy balance, stating that the gain of energy per unit volume equals the energy input by convection and conduction and the work done by gravity, pressure and viscous forces. Assuming the effects of gravity, viscous dissipation and pressure are negligible an appropriately simplified version of their energy conservation equation is

$$\frac{\partial}{\partial t}\left[\rho\left(I+\frac{v^2}{2}\right)\right] = -\nabla\cdot\left[\rho\mathbf{v}\left(I+\frac{v^2}{2}\right)+\mathbf{q}\right] \ , \tag{1.47}$$

where ρ is the density, I the internal energy per unit mass, $\mathbf{v}$ the velocity, $v=|\mathbf{v}|$, and the conductive heat flux $\mathbf{q}=-k\nabla T$. The quadratic term in the velocity is the kinetic energy component. The internal energy is defined by

$$I = c_l(T-T_m^*)+L_m \qquad \text{in the liquid} \ , \tag{1.48}$$

$$I = c_s(\theta-T_m^*) \qquad \text{in the solid} \ , \tag{1.49}$$

where T represents the temperature in the liquid and θ that in the solid. Again neglecting the work done by gravity, pressure and viscosity conservation of mechanical energy for a flowing liquid is

$$\frac{\partial}{\partial t}\left(\frac{1}{2}\rho_l v^2\right) = -\nabla \cdot \left(\frac{1}{2}\rho_l v^2 \mathbf{v}\right) \ . \tag{1.50}$$

Noting that

$$\nabla \cdot (\rho I \mathbf{v}) = \mathbf{v} \cdot \nabla(\rho I) + \rho I \nabla \cdot \mathbf{v} = \mathbf{v} \cdot \nabla(\rho I) \ , \tag{1.51}$$

for an incompressible fluid, then equations (1.47) and (1.50) may be combined to give

$$\frac{\partial}{\partial t}\left[\rho I\right] = -\nabla \cdot \left[\rho \mathbf{v} I + \mathbf{q}\right] = -\mathbf{v} \cdot \nabla(\rho I) - \nabla \cdot \mathbf{q} \ . \tag{1.52}$$

All versions of the heat equation analysed in the thesis can be deduced from expression (1.52). For example, in the one-dimensional case, $\nabla = \partial/\partial x$, substituting (1.48)-(1.49) in (1.52) and assuming that none of the phases is moving, $\mathbf{v} = 0$, yields (1.1)-(1.2), the most basic form of the heat equation for the Stefan problem.

By means of (1.47) we have specified energy conservation in the solid and liquid phases. The study of the energy conservation across the solid-liquid interface will lead to the Stefan condition. To examine the energy conservation at the phase change boundary, $s(t)$, requires the Rankine-Hugoniot condition

$$\frac{\partial f}{\partial t} + \nabla \cdot \mathbf{g} = 0 \quad \Rightarrow \quad [f]_-^+ \, s_t = [\mathbf{g} \cdot \mathbf{n}]_-^+ \ , \tag{1.53}$$

where $\mathbf{n}$ is the unit normal and f, $\mathbf{g}$ are functions evaluated on either side of $s(t)$ [3] (for a derivation of (1.53) in the one-dimensional case, see Appendix). Applying (1.53) to the energy balance (1.47) in the one-dimensional case, where

$$f = \rho\left(I + \frac{v^2}{2}\right) \ , \qquad \mathbf{g} \cdot \mathbf{n} = \rho v \left(I + \frac{v^2}{2}\right) + q \ , \tag{1.54}$$

and $q = -k_s\,\partial\theta/\partial x$ or $q = -k_l\,\partial T/\partial x$ (for solid and liquid, respectively), and assuming that the solid is stationary, gives the Stefan condition

$$\left\{\rho_l\left[\left(c_l(T(s,t)-T_m^*)+L_m+\frac{v^2}{2}\right)\right]-\rho_s c_s(\theta(s,t)-T_m^*)\right\}s_t = \rho_l v\left[c_l(T(s,t)-T_m^*)+L_m+\frac{v^2}{2}\right] - k_l\left.\frac{\partial T}{\partial x}\right|_{x=s(t)} + k_s\left.\frac{\partial\theta}{\partial x}\right|_{x=s(t)}. \tag{1.55}$$

Equivalent to (1.52) for the heat equations, equation (1.55) serves as starting point to obtain all the Stefan conditions used throughout the thesis. For example, if the liquid does not move ($v = 0$) and the temperature at $s(t)$ is the bulk phase change temperature, $T(s,t) = \theta(s,t) = T_m^*$, then the standard form of the Stefan condition, (1.3), is retrieved.

In the following sections we will use (1.52) and (1.55) to obtain heat equations and Stefan conditions that will be used later in subsequent chapters. In section 1.3.1 we introduce the specific form of the Stefan condition for cases where the interface temperature differs from the standard phase change temperature. Then, we specify the particular expressions describing the interface temperature for the phase change processes of nanoparticles and supercooled melts. In section 1.3.2 we present the changes in the governing equations and boundary conditions induced by considering a density jump between the solid and liquid phases. Finally, in section 1.3.3 we discuss the effect of a variable phase change temperature when reducing the two-phase Stefan problem to a one-phase problem. In addition, we show how to derive an accurate one-phase model based on consistent physical assumptions.

1.3.1 Variable phase change temperature

There are many practical situations where the phase change temperature cannot be considered constant, e.g. when the phase change occurs in the presence of a curved interface or in supercooled conditions [3, 4, 19, 38]. In both cases the interface temperature is a function of time. With the standard Stefan problem, $T(s(t),t) = \theta(s(t),t) = T_m^*$, where T_m^* is the bulk phase change temperature. With a time-dependent phase change temperature this condition

is replaced by

$$T(s(t),t) = \theta(s(t),t) = T_I(t) \ , \tag{1.56}$$

where the form of $T_I(t)$ will depend on the physical problem. Substituting (1.56) in (1.55), assuming the liquid is stationary and phases with the same density, the Stefan condition becomes

$$\rho_l \left[L_m - (c_l - c_s)(T_m^* - T_I)\right] s_t = k_s \frac{\partial \theta}{\partial x} - k_l \frac{\partial T}{\partial x} \qquad \text{on} \qquad x = s(t). \tag{1.57}$$

The difference between (1.57) and the standard Stefan condition (1.3) is the term $(c_l - c_s)(T_m^* - T_I)$. Inspection of (1.57) reveals that, if $T_I = T_m^*$ the standard form is retrieved. One way to reduce (1.57) to its standard form, but keeping (1.56) in the model, is by assuming the specific heat for the liquid and solid phase are equal, i.e. $c_l = c_s$. However, as shown in chapter 2, in the context of nanoparticle melting, this assumption leads to inaccurate results.

In the two subsequent sections, we introduce the concept of a nanoparticle and provide motivation for the study of its phase change process. We present the Gibbs-Thomson equation, the mathematical expression for T_I describing the melting point depression of nanoparticles. Then, we discuss supercooled liquids and the interest in their solidification process. Further, we provide a nonlinear expression for T_I modeling the dynamics of the molecules at the solid-liquid interface.

Nanoparticles

According to the International Union for Pure and Applied Chemistry, a nanoparticle is a particle of any shape with dimensions in the range 10^{-9}-10^{-7}m [110]. Nanoparticles have fascinated the scientific community since the second half of the last century, due to their remarkable physical properties, which are not obseerved at the bulk scale [35, 36, 87]. Despite the reduced size of nanoparticles, continuum theory describing phase change processes is considered to be valid for particles with radii larger than 2 nm [36]. Kofman *et al* [48] state that at scales smaller than 5 nm the melting process is discontinuous and dominated by fluctuations. Kuo *et al* [50] observed structural changes and a quasi-molten state in their

study of nanoparticle melting between 2-5 nm.

From a practical point of view, nanoparticles are very interesting because they are currently being used for new and revolutionary technological applications such as phase change memories [22, 99], phase change materials [46], nanofluids [116] and in biological applications such as drug carriers [6, 31, 57, 88] or thermal agents for hyperthemia treatments of tumours [44]. Some of the aforementioned applications work directly in the phase change regime or occur at very high temperatures, indicating the importance of understanding the thermal response and likely phase change behaviour of nanoparticles.

An interesting property directly affecting the melting process of nanoparticles is the melting point depression or Gibbs-Thomson effect [3, 8, 18, 98], which is a well-known physical phenomena that occurs on surfaces with a high curvature. A nanoparticle can be imagined as a cluster of atoms. The surface atoms are more weakly bound to the cluster than the bulk atoms and melting proceeds by exciting the surface atoms and separating them from the bulk. For a sufficiently large cluster the energy required is relatively constant since each surface atom is affected by the same quantity of bulk atoms. However, as the cluster decreases in size the surface atoms are surrounded by an inferior number of bulk atoms and, so feel less attraction to the bulk. Consequently, less energy is required for separation. This translates into a decrease of the melting temperature at the surface of nanoparticles. The most general form of the Gibbs-Thomson equation is given by

$$\left(\frac{1}{\rho_l}-\frac{1}{\rho_s}\right)(p_l-p_a)=L_m\left(\frac{T_I}{T_m^*}-1\right)+(c_l-c_s)\left[T_I\ln\left(\frac{T_I}{T_m^*}\right)+T_m^*-T_I\right]+\frac{2\sigma_{sl}\kappa}{\rho_s}\ , \quad (1.58)$$

where ρ is the density, L_m the latent heat, c the specific heat, p the pressure and σ the surface tension [3]. The subscripts s and l indicate solid and liquid, respectively. The mean curvature κ is given by

$$\kappa=\frac{1}{2}\left(\frac{1}{R_1}+\frac{1}{R_2}\right)\ , \quad (1.59)$$

where R_1 and R_2 are the two principal radii of curvature. If R is the radius of a sphere or cylinder, then $\kappa = 1/R$ or $\kappa = 1/2R$, respectively.

In chapter 2 the spherical Stefan problem with a variable phase change temperature,

described by (1.58), is analysed. Pressure differences are not considered and thus the left hand side of (1.58) is set to zero. In the presence of a high curvature, as on the nanoparticle surface, even if the pressure variation is relatively high, the term is small compared to the rest, as will be discussed in chapter 2. Under the assumption that the specific heat remains constant throughout the liquid and solid phase ($c_l = c_s$), expression (1.58) yields the classical form of the Gibbs-Thomson relation

$$T_I = T_m^* \left(1 - \frac{2\sigma_{sl}\kappa}{\rho_s L_m}\right). \tag{1.60}$$

In chapter 3 we study the effect of a density change between the solid and liquid phase in the nanoparticle melting process. In this case, to obtain a more tractable mathematical model we consider $c_l = c_s$ and use (1.60) instead of (1.58).

In chapters 2 and 3 we consider models with a spherical geometry. In these models, melting begins due to a high temperature at the surface of the nanoparticle. As the liquid phase grows at the nanoparticle surface, the solid phase is reduced in turn. The solid-liquid interface, which also defines the radius of the solid portion, is denoted by $R = R(t)$. As melting proceeds the curvature of the interface $R(t)$ increases rapidly. Therefore, the melting point depression due to the Gibbs-Thomson effect at $R(t)$ is larger as the process continues leading to a remarkable increase in the velocity of the nanoparticle melting process.

High curvature induces a variable phase change temperature on the surface. In supercooling conditions the molecular attaching mode at the solid-liquid interface plays a role and leads to a decrease of the phase change temperature, which we now introduce.

Supercooled melts

Supercooling is the action of cooling down a liquid below its standard freezing point. These liquids are trapped in a metastable state and are ready to solidify as soon as the opportunity arises. The supercooled state of a liquid can be achieved, for instance, by applying very high cooling rates, cooling down a liquid adjacent to a material surface with a particular molecular arrangement or cooling the liquid down while it is being levitated [34, 56, 96, 121]. Clouds

at high altitude are a good example of this as they contain tiny droplets of water that in the absence of seed crystals do not form ice despite the low temperatures. Freezing rain is caused by the precipitation of these drops that, upon impact with any surface, instantly freeze, and sometimes accumulate to a thickness of several centimeters. In fact, when an aircraft flies through a cloud of supercooled droplets it provides a large nucleation site. As a consequence there can be significant ice accretion, which can have a detrimental effect on the plane's performance [72]. However, materials formed from supercooled melts have desirable properties for many technological applications, such as metallic glass [109]. The interest in these kind of materials lies in the fact that they lack a crystalline structure, which provides them with increased strength, durability and elasticity [109]. Furthermore, phase change techniques in supercooled conditions are also being examined for the cryopreservation of human ovarian cortex tissues and food storage [54, 68].

As a liquid is cooled down below its freezing point, the energy of the molecules and hence their motion is decreased. As the solidification of a supercooled liquid begins the reduced molecular motion in the liquid phase affects the ability of the molecules to move onto the solid interface [4, 19]. In this situation the temperature at which the liquid solidifies is not constant and depends on the velocity of the solidification front, s_t. The relationship between the velocity and the temperature at the solid-liquid interface, T_I, is given by

$$s_t = \frac{d\Delta h}{6hT_m^*} e^{-\frac{q}{kT_I}} (T_m^* - T_I) \ , \tag{1.61}$$

where d is the molecular diameter, h Planck's constant, q the activation energy and k the Boltzmann constant [4]. The parameter Δh is the product of the latent heat and the molecular weight divided by Avogadro's number. If the degree of supercooling, $(T_m^* - T_I)$, is small (1.61) can be approximated in the linear form

$$T_I(t) = T_m^* - \phi s_t \ , \tag{1.62}$$

where $\phi = 6hT_m e^{\frac{q}{kT_m}}/(d\Delta h)$. We note that (1.61), as with the generalized Gibbs-Thomson equation (1.58), represents an extra equation in the Stefan problem that has to be solved

in combination with the heat equations and the Stefan condition. The role of the linear approximation (1.62) in the Stefan problem is the same as that of the classical Gibbs-Thomson relation (1.60); they can be directly incorporated as time-dependent boundary conditions in the model.

In chapter 4 we study the solidification of supercooled melts by introducing (1.61) into the one-phase Stefan problem. In previous studies of the supercooled Stefan problem the linear approximation (1.62) has been used extensively, regardless of the degree of supercooling. Hence, we analyse the problem with the linear approximation and we test its performance against the solution using the nonlinear form (1.61). In addition, we show how the Neumann solution (1.36) remarkably overestimates the velocity of propagation of the freezing front in contrast with the solutions obtained using (1.61) and (1.62).

1.3.2 The effect of density change

One of the basic assumptions in standard analyses of Stefan problems is that of constant density, $\rho_l = \rho_s$. However, in reality, melting and solidification processes are always affected by changes in the density, which translate physically to the shrinkage or expansion of one of the phases. For instance, in countries with cold climates, pipe bursting is a recurrent problem. As water freezes, the molecules crystallize into a hexagonal form, which takes up more space than molecules in the liquid form, thus, causing the pipe to burst.

The changes in the mathematical model when the density jump between phases is introduced are significant. To demonstrate this we will now focus on the case where the liquid phase moves due to expansion upon melting. Then, expression (1.52) combined with (1.48) and the heat flux $\mathbf{q} = -k_l \nabla T$, yields the heat equation

$$\rho_l c_l \left(\frac{\partial T}{\partial t} + \nabla T \cdot \mathbf{v} \right) = k_l \nabla^2 T \ , \tag{1.63}$$

where $\mathbf{v}$ is the velocity of the fluid [3, 7]. The solid does not move and the standard heat equation (1.2) holds. For one-dimensional Cartesian problems the velocity due to expansion

of the fluid takes the form

$$v = \left(1 - \frac{\rho_s}{\rho_l}\right) s_t \ . \tag{1.64}$$

Expression (1.64) can be easily derived from mass conservation arguments [3]. In chapter 3 we derive an analogous form of (1.64) for a one-dimensional spherically symmetric problem.

In addition to the heat equation, the kinetic energy due to the moving fluid also affects the energy balance at the solid-liquid interface. Equation (1.55) in combination with (1.64), for the general case $T(s,t) = \theta(s,t) = T_I(t) \neq T_m^*$, leads to the Stefan condition

$$\begin{aligned} \rho_s \left[L_f + (c_l - c_s)\left(T_I - T_m^*\right)\right] s_t + \\ \frac{\rho_s}{2}\left(1 - \frac{\rho_s}{\rho_l}\right)^2 s_t^3 = k_s \left.\frac{\partial \theta}{\partial x}\right|_{x=s} - k_l \left.\frac{\partial T}{\partial x}\right|_{x=s} . \end{aligned} \tag{1.65}$$

A complete derivation of (1.65) for the case $c_l = c_s$ can be found in [3]. The expression (1.65) contains a new term proportional to the third power of the front velocity s_t. The cubic term in (1.65) impedes one from finding an exact solution to the problem, and this is one reason why the assumption $\rho_s = \rho_l$ is used so extensively in the literature. However, as will be shown in chapter 3 this reduction leads to significant inaccuracies. Obviously, if we set $\rho_l = \rho_s$ in (1.65) we retrieve the Stefan condition (1.57). If we also set $T_I = T_m^*$, we obtain the standard Stefan condition (1.3).

In chapter 3 we study the influence of a density change between phases in the melting process of nanoparticles. In this case, the Stefan problem consists of the heat equation (1.65) for the liquid and the standard heat equation (1.2) for the solid phase. Given that we focus on the effect of $\rho_l \neq \rho_s$, we assume the specific heats between phases to be equal, $c_l = c_s$, to reduce the complexity of the model. This enables us to neglect the term $(c_l - c_s)(T_I - T_m^*)$ in (1.65) and use the classical Gibbs-Thomson relation (1.60) instead of the generalized version (1.58). The effect of density change combined with melting point depression leads, in some cases, to an increase in the melting times of more than 50% when compared to the solution assuming $\rho_s = \rho_l$.

In the next section we briefly introduce the problems induced by having a variable phase change temperature when reducing the two–phase Stefan problem to a one–phase problem.

1.3.3 One–phase reductions and energy conservation

The two–phase Stefan problem is typically difficult to solve, given that it involves solving two partial differential equations on an a priori unknown, moving domain. The associated one–phase problem is a significantly less challenging prospect. The key to obtaining the one–phase reduction of the standard two–phase Stefan problem is by assuming that the phase change temperature is constant. For example, in section 1.2 we transformed the two–phase problem describing the melting of a semi–infinite slab (1.1)-(1.3) into the associated one–phase problem (1.4)-(1.7) by assuming the temperature of the solid phase to be at the phase change temperature, $\theta(x,t) = T_m^*$. This was sufficient to avoid the heat equation for the solid and remove a temperature gradient term in the Stefan condition.

In this thesis we deal with Stefan problems where, for physical reasons, the phase change temperature is time-dependent. With a phase change temperature that depends on time, assuming the solid at $\theta(x,s) = T_m^*$ is not consistent with the boundary condition at the phase change boundary where $\theta(s,t) = T(s,t) = T_I(t)$. An a priori sensible assumption is to consider $\theta(x,t) = T_I(t)$, which allows one to neglect the solid temperature gradient from the Stefan condition. However, the heat equation for the solid then reduces to $\theta_t = 0$, which is inconsistent with the temperature in the solid being a function of time. The question is how can we obtain a one-phase reduction in such a situation? The key to answering this question lies in the energy conservation principle and this will be dealt with in chapters 5 and 6.

In chapter 5 we formulate a one-phase reduction of the two-phase Stefan problem with supercooling based on energy conservation arguments. In chapter 6 we discuss the problem from a more general perspective, identifying the main erroneous assumptions of previous studies leading to one-phase reductions that do not conserve energy or, alternatively, are based in non-physical assumptions. Finally, we provide a general one–phase formulation of the Stefan problem with a generic variable phase change temperature, valid for spherical, cylindrical and planar geometries.

Chapter 2

The melting of spherical nanoparticles

F. Font, T.G. Myers. *Spherically symmetric nanoparticle melting with a variable phase change temperature*
Journal of Nanoparticle Research, 15, 2086 (2013)
Impact factor: 2.175

Abstract

In this chapter we analyse the melting of a spherically symmetric nanoparticle, using a continuum model which is valid down to a few nanometres. Melting point depression is accounted for by a generalised Gibbs-Thomson relation. The system of governing equations involves heat equations in the liquid and solid, a Stefan condition to determine the position of the melt boundary and the Gibbs-Thomson equation. This system is simplified systematically to a pair of first-order ordinary differential equations. Comparison with the solution of the full system shows excellent agreement. The reduced system highlights the effects that dominate the melting process and specifically that rapid melting is expected in the final stages, as the radius tends to zero. The results agree qualitatively with limited available experimental data.

2.1 Introduction

Nanomaterials are currently the subject of intense investigation due to their unique properties and a wide range of novel applications such as in optical, electronic, catalytic and biomedical applications, single electron tunneling devices, nanolithography etc. [2, 45, 92, 98]. One reason for their interesting behaviour is that they have a very large ratio of surface to volume atoms which can have a significant effect on the material properties [36]. A particular example of this is the well-documented decrease in phase change temperature as the material dimensions decrease [98]. The experiments of Buffat and Borel [8] show a decrease of around 500 K for gold particles with radius slightly greater than 1 nm. The molecular dynamics simulations of Shim *et al* [98] show a 60% decrease (more than 800 K) below the bulk melt temperature for gold nanoparticles with a radius around 0.8 nm. Experiments on tin and lead have shown decreases of the order 70 K and 200 K respectively [18]. Drugs with poor water solubility may be administered as nanoparticles to improve their uptake. Bergese *et al* [6] and Liu *et al* [57] study antibiotic and antianginal drugs, which exhibit a melting point depression of around 30 K (a 10% decrease from the bulk value). Since gold has low toxicity, gold nanoparticles also make good carriers for drug and gene delivery [31, 88].

Given the diversity of applications of nanoparticles and that many occur at high temperatures it is important to understand their thermal response and likely phase change behaviour [98]. The present study is undertaken with this purpose in mind. In the following we will analyse the melting of a nanoparticle using continuum theory. The analysis will be based on standard phase change theory, with appropriate modification to account for the variation in the phase change temperature. We will present results primarily for the melting of gold, since much data is available for this material, however the theory is general and may be applied to other materials by using the appropriate parameter values.

Continuum theory may be applied when there is a sufficiently large sample size to ensure that statistical variation of material quantities, such as density, is small. For fluids the variation is often quoted as 1% [1]. Assuming a spherical sample Nguyen and Werely [81] suggest this level of variation requires a minimum of 10^4 atoms and so deduce a critical dimension of

the order 10 and 90 nm for liquids and gases respectively. By comparing molecular dynamics simulations to computations based on the Navier-Stokes equations Travis *et al* [112] show that continuum theory may be applied to water flow down to around 3 nm. In the field of heat transfer and phase change it has been suggested that continuum theory requires particle radii greater than 2 nm [36] (this is based on assuming a relative temperature variation of 3%). Kofman *et al* [48] state that at scales smaller than 5 nm the melting process is discontinuous and dominated by fluctuations, Kuo *et al* [50] observed structural changes and a 'quasi-molten' state in their study of nanoparticle melting between 2-5 nm. Indeed for very small particles it may be necessary to modify the model for heat flow, one method is to augment the heat equation with an inertia term, see [114] for example. At the end of §2.3 we discuss the effect of this extra term on the solutions for various particle sizes. We conclude that care should be taken when modelling the phase change of very small particles and also that the continuum limit will vary depending on the material.

The standard continuum model for phase change is known as the Stefan problem. The simplest example involves solving a one-dimensional heat equation in Cartesian co-ordinates subject to constant temperature boundary conditions over a time-dependent domain whose extent is unknown '*a priori*'. At the phase change boundary, $r = R(t)$, the temperature is fixed at the constant bulk phase change temperature $T(R(t), t) = T_m^*$. The material properties remain constant throughout the process. This problem has a well-known exact solution, for more details see [3, 19, 40]. However, in reality material properties vary and there is often a jump in property values when the phase change occurs. With high curvature (such as occurs in the nano context) the phase change temperature may vary significantly: this leads to a coupling between the phase change temperature and the standard governing equations for the Stefan problem and prevents an analytical solution.

In this chapter we will begin by discussing the generalised Gibbs-Thomson equation which describes the melt temperature variation. We will then describe the mathematical model appropriate for the melting of a nanosphere, subject to a fixed boundary temperature (greater than the phase change temperature). Noting that the Stefan number, the ratio of latent heat to sensible heat, is generally large for practical situations in §2.4 we seek

approximate solutions which exploit this feature. This is first carried out for a simple one-phase reduction, where the temperature of the solid is neglected, and then for the two-phase model where both solid and liquid regions are analysed. Results are presented in §2.5 comparing the numerical and approximate solutions. The relation between the results and limited experimental observations is also discussed.

2.2 Generalised Gibbs-Thomson relation

The vast majority of analyses on phase change assume that the melt temperature remains constant throughout the process. In situations where the melt temperature is variable and the density and specific heat remain approximately constant in each phase the melt temperature may be estimated from the following generalised Gibbs-Thomson relation

$$\left(\frac{1}{\rho_l}-\frac{1}{\rho_s}\right)(p_l-p_a)=L_m\left(\frac{T_m}{T_m^*}-1\right)+\Delta c\left[T_m\ln\left(\frac{T_m}{T_m^*}\right)+T_m^*-T_m\right]+\frac{2\sigma_{sl}\kappa}{\rho_s}\,, \qquad (2.1)$$

where T_m is the temperature at which the phase change occurs, T_m^* the bulk phase change temperature, c is the specific heat, $\Delta c = c_l - c_s$, p the pressure (and p_a the ambient pressure), σ the surface tension and κ the mean curvature, subscripts s, l indicate solid and liquid. A complete derivation of this equation from thermodynamical principles can be found in [3]. Various limits of equation (2.1) produce familiar relations. For example, with constant parameter values $\Delta\rho = \Delta c = 0$ the standard Gibbs-Thomson equation is retrieved

$$T_m = T_m^*\left(1-\frac{2\sigma_{sl}\kappa}{\rho_s L_m}\right). \qquad (2.2)$$

This demonstrates how the melt temperature decreases as the curvature at the interface increases. If $\sigma_{sl}\kappa \ll \rho_s L_m$ then $T_m \approx T_m^*$ is the standard constant melt temperature boundary condition.

The use of equation (2.2) rather than $T_m = T_m^*$ may appear to be a rather simple modification, however it significantly complicates the system. If we consider the problem of melting a spherical particle the mean curvature will be related to the position of the

phase change front $\kappa = 1/R(t)$ and so the boundary condition $T(R(t), t) = T_m(t)$ is time-dependent where $T_m(t)$ must be calculated as part of the solution process. Further, the standard reduction of the two-phase to a one-phase problem ceases to make physical sense. If $T_m = T_m^*$ is constant we may define a one-phase problem by setting the solid temperature to T_m^* for all time. If T_m is a function of time then the one-phase problem requires the solid temperature to equilibrate instantaneously to the boundary temperature. Evans and King [25] show that the standard one-phase reduction loses energy. Myers *et al* [74] present a one-phase reduction that conserves energy and matches closely to numerical solutions of the two-phase formulation.

The relative size of the terms in (2.1) indicate their importance in the melting process. If the melting temperature deviates significantly from the bulk value due to curvature effects then the first term on the right hand side must have a similar magnitude to the final term. For a gold nanoparticle with radius 6 nm we find using expression (2.1) that $T_m \approx T_m^* - 100\,\mathrm{K}$. Taking $p_l - p_a = 10^5\,\mathrm{Pa}$ and using the parameter values from Table 2.1 gives

$$\begin{aligned} L_m\left(\frac{T_m}{T_m^*} - 1\right) \sim \frac{2\sigma_{sl}\kappa}{\rho_s} = \mathcal{O}(4700) \gg \\ \Delta c\left[T_m \ln\left(\frac{T_m}{T_m^*}\right) + T_m^* - T_m\right] = \mathcal{O}(130) \gg \\ \left(\frac{1}{\rho_l} - \frac{1}{\rho_s}\right)(p_l - p_a) = \mathcal{O}(0.6)\ , \end{aligned} \tag{2.3}$$

Obviously in such a situation it is the pressure term that should be neglected first (this is achieved by setting $\rho_l = \rho_s$ in equation (2.1)). Of course there are physical situations where the pressure variation is much higher and so may be the driving mechanism for the melt temperature variation, see [21], however this will not be the focus in the following work. Therefore, the version of the Gibbs-Thomson equation that will be used here is

$$0 = L_m\left(\frac{T_m}{T_m^*} - 1\right) + \Delta c\left[T_m \ln\left(\frac{T_m}{T_m^*}\right) + T_m^* - T_m\right] + \frac{2\sigma_{sl}\kappa}{\rho_s}. \tag{2.4}$$

In Figure 2.1 we show a comparison of the experimentally measured melt temperature against particle radius for gold and the prediction of (2.4). The parameter values used in the figures

are given in Table 2.1. The diamonds represent the experimental points, solid lines come from (2.4) (i.e. with $\Delta c \neq 0$) and dashed lines from (2.2) (i.e. $\Delta c = 0$). The agreement between equation (2.4) and experiment is excellent. The curves for $\Delta c \neq 0$ and $\Delta c = 0$ may appear close, but there is a significant difference in the prediction of melt temperatures. At 2 nm the two models differ by approximately 35K. In the results section we will see that this can have a large effect on the melt rate. For radii below approximately 1 nm, where $T_m \approx 329$K, equation (2.4) becomes multi-valued, this is shown in the inset. So we may assume that the generalised Gibbs-Thomson relation should not be applied below this value. Of course, since continuum theory is invalid for such small particles this does not place any extra restrictions on the mathematical model. In §2.5 we will cut-off solutions at $R = 1$ nm. In fact there are a number of different expressions for the melting point depression derived from distinct hypotheses, all of them agreeing in $T_m - T_m^* \propto \kappa$ when the parameter values are constant [8, 48, 52, 78]. The main difference between them lies in the dependence on the interfacial energy between phases σ_{sl} [26, 78]. We show one example, the dash-dot curve which represents Pawlow's formula[37, eq. 1], [118] (Pawlow's formula is a form of Gibbs-Thomson relation, equation (2.2) where the solid-liquid surface tension σ_{sl} is replaced by $\sigma_{sv} - \sigma_{lv}(\rho_s/\rho_l)^{2/3}$ and the subscript v denotes vapour). Obviously this does not accurately capture the current data set.

Nanda [78] points out that different research groups have found different dependences of T_m on the system parameters, even when examining the same material. This is attributed to different types of melting, such as liquid skin melting or homogeneous melting. Another cause for deviation at very small radius may be explained by considering the particle as a cluster of atoms. The particle is made up of bulk and surface atoms: the surface atoms are more weakly bound to the cluster than the bulk atoms and melting proceeds by the surface atoms separating from the bulk. Obviously this separation is paid for with energy (the latent heat). With a sufficiently large cluster the energy required is relatively constant since each surface molecule is affected by the same quantity of bulk molecules. However, as the cluster decreases in size the surface molecules feel less attraction to the bulk, consequently less energy is required for separation. The change in the ratio of surface to bulk energy

may also lead to a structural transition and a reduction in surface tension. Kofman et al [48] suggest that around 5 nm there is a surface induced transition in the melting process. The molecular dynamic simulations of Koga et al [49] indicate that for gold nanoparticles a structural transition occurs between 3 and 14 nm. The new particle configuration will then have a different value for the interfacial free energy. Samsonov *et al* [93] state that for metal melt nanodroplets when $R < 4\,\text{nm}$ the surface tension takes the form $\sigma_{sl} \propto R$ and their MD simulations also indicate a structural transition around this value. Sheng et al [97] specify a decrease in latent heat proportional to $1/R$. This leads us to the simple conclusion that the present mathematical model should not be applied down to $R = 0$ and as already mentioned we cannot apply Gibbs-Thomson below 1 nm for gold.

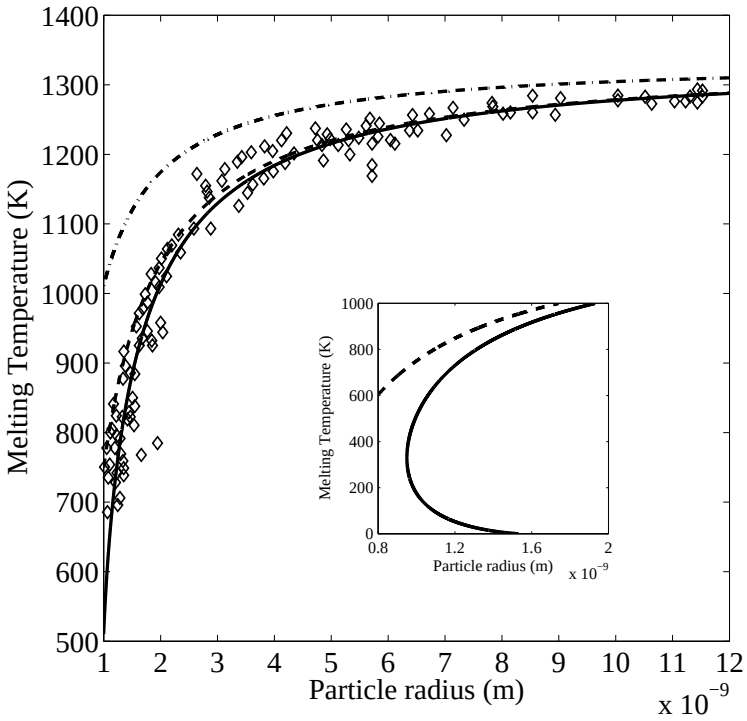

Figure 2.1: Size dependence of the melting temperature of gold nanoparticles. Solid line represents T_m from (2.4), dashed line corresponds to (2.2) and dash-dotted line to Pawlow model. Diamonds are experimental data from [8]. The subplot shows T_m from (2.2) and (2.4) for radius below 2 nm.

Table 2.1: Approximate thermodynamical parameter values for water, gold, and lead. The values for σ_{sl} are taken from [8, 48, 83].

Substance	T_m^* (K)	L_m (J/Kg)	c_l, c_s (J/Kg·K)	ρ_l, ρ_s (kg/m^3)	k_l, k_s (W/m·K)	σ_{sl} (N/m)
Water	273	3.34×10^5	4181/2050	$1.00\times10^3/0.92\times10^3$	0.55/2.20	0.03
Gold	1337	6.37×10^4	163/129	$1.73\times10^4/1.93\times10^4$	106/317	0.27
Lead	600	2.30×10^4	148/128	$1.07\times10^4/1.13\times10^4$	16/35	0.05

2.3 Mathematical model

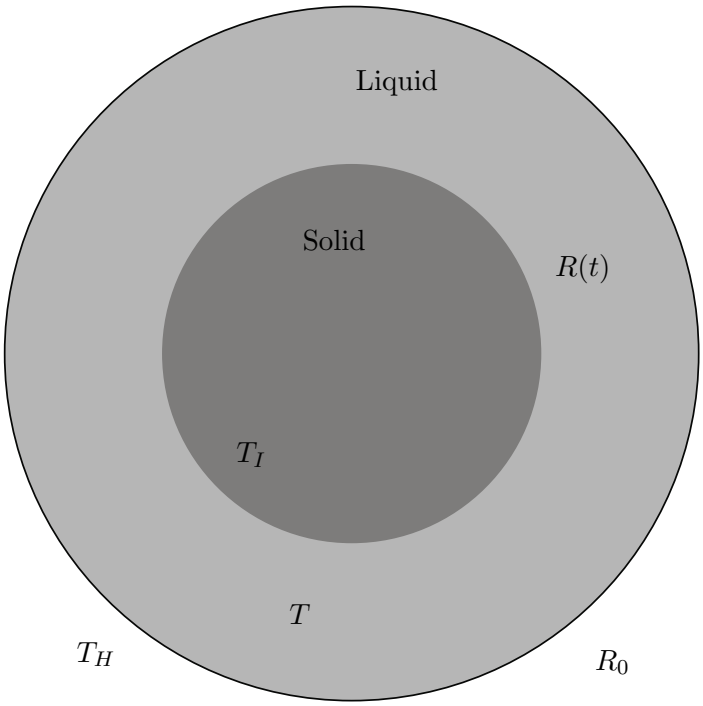

Figure 2.2: Sketch of the problem configuration.

The practical situation motivating the present study is the melting of nanoparticles, consequently the mathematical model is formulated as spherically symmetric. A typical configuration of the problem is illustrated in Figure 2.2. This depicts an initially solid, spherical nanoparticle which is heated at the surface to a temperature $T_H > T_m^*$. The outer region of the particle starts to melt, and the new liquid phase grows inwards until the whole

solid is melted. The location of the solid–liquid interface is represented by $R = R(t)$. The governing equations for the two-phase problem may be written as

$$c_l\rho_l\frac{\partial T}{\partial t} = k_l\,\frac{1}{r^2}\frac{\partial}{\partial r}\left(r^2\frac{\partial T}{\partial r}\right), \qquad R < r < R_0\ , \tag{2.5}$$

$$c_s\rho_s\,\frac{\partial \theta}{\partial t} = k_s\,\frac{1}{r^2}\frac{\partial}{\partial r}\left(r^2\frac{\partial \theta}{\partial r}\right), \qquad 0 < r < R\ , \tag{2.6}$$

where T represents the temperature in the liquid, θ the temperature in the solid, R_0 the initial radius of the particle and k the thermal conductivity. These equations are subject to the following boundary conditions

$$T(R_0,t) = T_H \qquad T(R,t) = \theta(R,t) = T_m \qquad \theta_r(0,t) = 0\ , \tag{2.7}$$

and the Stefan condition

$$\rho_l\left[L_m + \Delta c(T_m - T_m^*)\right]\frac{dR}{dt} = k_s\frac{\partial\theta}{\partial r}\bigg|_{r=R} - k_l\frac{\partial T}{\partial r}\bigg|_{r=R}\ , \tag{2.8}$$

where $R(0) = R_0$ and T_m is specified by (2.4). No initial condition is imposed on the temperature in the liquid, since it does not exist at $t = 0$. In the solid we set $\theta(r,0) = T_m(0)$, which allows us to compare the one and two phase solutions analysed in the following sections. Mathematical analyses typically invoke numerous simplifications, such as applying a single value for the thermal properties irrespective of phase or a constant phase change temperature. In the following we will only impose constant density (in line with neglecting pressure variation in the Gibbs-Thomson relation). This significantly simplifies the analysis and it is the material property which has the least variation (from Table 2.1 we see that ρ increases by approximately 10% when ice melts whilst c doubles and k decreases by a factor 4).

Introducing the dimensionless variables

$$\hat{T} = \frac{T - T_m^*}{T_H - T_m^*}\ , \qquad \hat{\theta} = \frac{\theta - T_m^*}{T_H - T_m^*}\ , \qquad \hat{r} = \frac{r}{R_0}\ , \qquad \hat{R} = \frac{R}{R_0}\ , \qquad \hat{t} = \frac{k_l}{\rho_l c_l R_0^2}t\ , \tag{2.9}$$

in (2.5)–(2.8) and dropping the hats the following nondimensional formulation is obtained

$$\frac{\partial T}{\partial t} = \frac{1}{r^2}\frac{\partial}{\partial r}\left(r^2\frac{\partial T}{\partial r}\right), \quad R < r < 1 , \tag{2.10}$$

$$\frac{\partial \theta}{\partial t} = \frac{k}{c}\frac{1}{r^2}\frac{\partial}{\partial r}\left(r^2\frac{\partial \theta}{\partial r}\right), \quad 0 < r < R , \tag{2.11}$$

with boundary conditions $T(1,t) = 1$, $T(R,t) = \theta(R,t) = T_m(t)$, $\theta_r(0,t) = 0$ and the Stefan condition

$$[\beta + (1-c)T_m]\frac{dR}{dt} = k\frac{\partial \theta}{\partial r} - \left.\frac{\partial T}{\partial r}\right|_{r=R} . \tag{2.12}$$

The nondimensional melting temperature T_m is scaling in the same manner as T and determined from

$$0 = \beta\left(T_m + \frac{\Gamma}{R}\right) + \frac{(1-c)}{\delta T}\left[\left(T_m + \frac{1}{\delta T}\right)\ln\left(T_m\,\delta T + 1\right) - T_m\right] . \tag{2.13}$$

The dimensionless parameters are defined by

$$c = c_s/c_l , \qquad k = k_s/k_l , \qquad \beta = L_m/c_l\Delta T ,$$

$$\delta T = \Delta T/T_m^* , \qquad \Gamma = 2\sigma_{sl}T_m^*/R_0\rho_l L_m\Delta T$$

where $\Delta T = T_H - T_m^*$.

McCue et al [60] carry out a mathematical analysis of a similar system using the standard Gibbs-Thomson relation, equation (2.2). Their expression for interfacial energy makes this equivalent to Pawlow's formula. This choice corresponds to setting $c = 1$ in equation (2.13) and changing the value of Γ. In the Stefan condition they apply $c \neq 1$. They go on to analyse small time and large Stefan number solutions and discuss the system behaviour as $R \to 0$. In the following we will focus more on the physical problem, which requires large Stefan number. Accepting that continuum theory does not hold as $R \to 0$ we do not analyse that limit. We retain all terms in equation (2.13) and show that setting $c = 1$ is only valid for large particles. In [120] the one-phase limit with $c = 1$ is analysed for inward solidification, so the phase change temperature increases as the solidification front moves inwards.

Note, as the particle size decreases the heat equations may require some adjustment. One such method is to include an additional inertia term $\tau_v/\tau\, T_{tt}$, see [114] for example, where τ_v is a relaxation time (of the order 1ps) and $\tau = \rho_l c_l L^2/k_l$ is the diffusive time-scale. For a 100 nm gold nanoparticle, neglecting this term will lead to errors of the order 0.3% however, due to the L^2 term, with a 10 nm particle the error may be as much as 30%. Consequently, as pointed out in the introduction the present theory will lose accuracy as the particle size decreases.

2.4 Solution method

To clarify the analytical methods used in the following section, we will begin by analysing the one-phase problem. There is a long history of studies of one-phase solidification typically neglecting melting point depression, see [59, 89] for example. This approximation involves setting the solid to the melt temperature $\theta = T_m(t)$. It may also be viewed as a large k/c approximation (for gold $k/c \approx 3.8$). Evans and King [25] point out that in this limit a thermal boundary layer will exist and the one-phase formulation loses energy. However, their proposed solution to the problem is not valid for physically realistic systems and, whilst conserving energy, is less accurate than the standard reduction. An accurate one-phase formulation which conserves energy is derived in [74], this adds an acceleration term R_{tt} to the Stefan condition. However, in §2.4.1 we will use the standard reduction since it is simple to formulate and leads to relatively small errors (when compared to those introduced by using continuum theory on very small particles). In §2.4.2 we extend the one-phase solution to the more physically realistic two-phase case and in §2.5 we show that the one-phase approximation of §2.4.1 is accurate for large particles.

2.4.1 One-phase reduction

Assuming $k/c \gg 1$ in (2.11) at leading order we may neglect the θ_t term and find $\theta = T_m(t)$ is the solution satisfying the reduced equation and boundary conditions. This permits us to

eliminate the term $k\theta_r$ from (2.12) and the problem reduces to

$$\frac{\partial T}{\partial t} = \frac{1}{r^2}\frac{\partial}{\partial r}\left(r^2\frac{\partial T}{\partial r}\right), \quad T(1,t) = 1, \quad T(R,t) = T_m \ , \tag{2.14}$$

where T is the temperature of the liquid phase, T_H is the temperature at the surface of the particle and T_m is the melting temperature specified by (2.13), with the Stefan condition

$$[\beta + (1-c)T_m]\,\frac{dR}{dt} = -\left.\frac{\partial T}{\partial r}\right|_{r=R}. \tag{2.15}$$

The system requires no initial condition on the temperature, since at $t = 0$ there is no liquid, however we must then apply a condition on the domain, $R(0) = 1$. The Stefan number, $\beta = L_m/c_l\Delta T$, is a characteristic nondimensional parameter of our system that provides a measure of the importance of the latent heat released in the phase change, L_m, relative to the heat required to increase the temperature of the material by ΔT (that is $c_l\Delta T$). For example, for a temperature increase of $\Delta T = 10\,\mathrm{K}$ we have $\beta \approx 8$, 40, 12 for water, gold and lead, respectively. Obviously, the smaller the increase ΔT the larger the value of β. Due to the small volume of the nanoparticles the energy required to melt them is also small: any increase above the melting temperature, ΔT, on the nanoparticle surface is enough to almost instantaneously melt it. Hence, working in a large Stefan number regime, where $\beta \gg 1$, is a sensible assumption.

The standard large β reduction of the Stefan problem involves re-scaling time, $t = \beta\tau$, so that equations (2.14)–(2.15) become

$$\frac{1}{\beta}\frac{\partial T}{\partial \tau} = \frac{1}{r^2}\frac{\partial}{\partial r}\left(r^2\frac{\partial T}{\partial r}\right), \qquad T(1,\tau) = 1, \qquad T(R,\tau) = T_m, \tag{2.16}$$

$$\left[1 + \frac{(1-c)}{\beta}T_m\right]\frac{dR}{d\tau} = -\left.\frac{\partial T}{\partial r}\right|_{r=R}. \tag{2.17}$$

Assuming $1/\beta \ll 1$, it may be used as the small parameter for a perturbation solution of the form $T = T_0 + T_1/\beta + \mathcal{O}(1/\beta^2)$ [42]. Substituting this series into (2.16) and equating like powers of $1/\beta$ yields a sequence of differential equations. If the sequence is cut at the

first order, we obtain

$$\mathcal{O}(1): \qquad 0 = \frac{1}{r^2}\frac{\partial}{\partial r}\left(r^2\frac{\partial T_0}{\partial r}\right), \qquad T_0(1,\tau) = 1, \qquad T_0(R,\tau) = T_m \tag{2.18}$$

$$\mathcal{O}(1/\beta): \qquad \frac{\partial T_0}{\partial \tau} = \frac{1}{r^2}\frac{\partial}{\partial r}\left(r^2\frac{\partial T_1}{\partial r}\right), \qquad T_1(1,\tau) = 0, \qquad T_1(R,\tau) = 0 \tag{2.19}$$

with respective solutions

$$T_0 = 1 + (T_m - 1)\frac{R}{r}\left(\frac{1-r}{1-R}\right) , \tag{2.20}$$

$$T_1 = \frac{(3R\mu_1 + T_m - 1)}{6(1-R)^2}\left\{\left[(3-r)r - \frac{2}{r}\right] - \frac{R}{r}\left(\frac{1-r}{1-R}\right)\left[(3-R)R - \frac{2}{R}\right]\right\}\frac{dR}{d\tau} , \tag{2.21}$$

where

$$\mu_1 = \frac{\Gamma(1-R)}{3R^2\left[1 + \frac{(1-c)}{\beta\delta T}\ln\left(T_m\delta T + 1\right)\right]} . \tag{2.22}$$

At this point, we already have an approximate solution for the temperature, $T \approx T_0 + T_1/\beta$. However, this solution contains the variables R and T_m which are still unknown. We obtain an equation for $R(\tau)$ by substituting for T in the Stefan condition (2.17)

$$\frac{dR}{d\tau} = \frac{(T_m - 1)}{R(1-R)}\left[1 + \frac{1}{\beta}\left\{\left(1 - c - \frac{1}{3R}\right)T_m + \frac{1}{3R} - \mu_1\right\}\right]^{-1} . \tag{2.23}$$

We obtain an equation for T_m by taking the time derivative of (2.13). This is,

$$\frac{dT_m}{d\tau} = \frac{3\mu_1}{1-R}\frac{dR}{d\tau}. \tag{2.24}$$

The equations (2.23) and (2.24) form a pair of coupled ordinary differential equations. This is a much simpler system to solve than the initial partial and ordinary differential equation system which applied over an unknown domain. Note that the initial condition for R is $R(0) = 1$ and the initial condition for T_m is obtained by substituting $R = 1$ in (2.13) and solving the subsequent nonlinear equation. We could make some analytical progress on the solution for R by using an expansion of the form $R \approx R_0 + R_1/\beta$ on equation (2.23), but this turns out to be rather complex whilst using any standard numerical tool, such as Matlab

routine ode15s, on (2.23)–(2.24) is straightforward.

Equations (2.23, 2.24) have two obvious singularities at $R = 0, 1$, where the velocity $R_\tau = \infty$. The initial singularity, when $R = 1$, is unphysical and a result of the boundary condition. The Stefan condition states that the velocity R_τ is proportional to the temperature gradient T_r. The temperature gradient $T_r \approx (T_m(t) - T(1,t))/(1-R)$ and since $T_m(0) \neq T(1,0)$ it will be infinite at $\tau = t = 0$, when $R = 1$. This singularity is typical for Stefan problems where the boundary temperature is fixed and could be avoided by applying a different condition, such as a heat flux or kinetic undercooling [25]. The second singularity, at $R = 0$ is a result of the physical system and not related to the initial or boundary conditions. The existence of a single singularity in the system may be inferred from Figure 2.1, the gradient $T_m \to -\infty$ as $R \to 0$ (but nowhere else). Note, this singularity could cause a problem with our perturbation solution, which requires the $\mathcal{O}(1/\beta)$ term to be much smaller than the leading order, hence our solution may break down as $R \to 0$. However, we have also made it clear that our solution must break down due to the failure of the Gibbs-Thomson relation and continuum theory in this limit so this issue is not a great mathematical concern.

The governing equations contain various parameters which control the behaviour to differing extents: the largest effect will be due to leading order terms. Equation (2.24) is simply the derivative of the Gibbs-Thomson relation (2.13) which, after neglecting $\mathcal{O}(1/\beta)$ terms, shows that $T_m \approx -\Gamma/R$. The leading order of equation (2.23) shows the R variation is proportional to $T_m - 1 = -1 - \Gamma/R$. The rate of decrease of the solid radius is therefore controlled primarily by $\Gamma = 2\sigma_{sl}T_m^*/(R_0\rho_l L_m \Delta T)$, that is, a particle will melt rapidly if it has high surface tension or bulk melt temperature or low density and latent heat. For any given material these parameters are fixed so the actual melting can only be controlled by the initial particle radius R_0 and the temperature change ΔT.

The one phase model is sometimes reduced by making assumptions on the parameter values. A common reduction involves equating the specific heats in each phase, $c_l = c_s$ (or $c = 1$ in our nondimensional notation) [120]. This assumption is convenient because it removes T_m from the Stefan condition (2.15) and reduces the generalized Gibbs–Thomson equation (2.13) to the standard, simpler version where $T_m \propto 1/R$. Wu *et al* [119] take $c = 1$

in the Gibbs-Thomson relation but $c \neq 1$ in the Stefan condition. In our case, setting $c = 1$ leads to $T_m = -\Gamma/R$ and equation (2.23) becomes

$$\frac{dR}{dt} = -\frac{R+\Gamma}{\beta R^2(1-R)}\left[\beta + \frac{(1+\Gamma)}{3R}\right]^{-1}. \tag{2.25}$$

This may be integrated to

$$-\beta(1-R^3) + a(1-R^2) - b(1-R) + b\Gamma \ln\left(\frac{\Gamma+1}{\Gamma+R}\right) = 3t\ , \tag{2.26}$$

where $a = (\Gamma+1)(3\beta-1)/2$ and $b = \Gamma^2(3\beta-1) + \Gamma(3\beta-2) - 1$. In the results section we will show calculations with $R_0 = 10,100\,\text{nm}$, which changes the value of Γ, for sufficiently large R_0 the curves with $c \neq 1$, $c = 1$ coincide.

A further reduction can be made by removing the Gibbs-Thomson effect from the model. In other words, considering a constant melt temperature $T_m = 0$, this is equivalent to setting $\Gamma = 0$ in (2.26). Then,

$$-\beta(1-R^3) + \frac{(3\beta-1)}{2}(1-R^2) - R + 1 = 3t. \tag{2.27}$$

This will also be examined in the results section.

In summary, we provide three different solution forms to the one-phase model (2.14)–(2.15). The solutions correspond to three levels of approximation: (i) The first and most general one is obtained by integrating (2.23)–(2.24) numerically, this takes into account the difference between the specific heats ($c \neq 1$) in the Stefan condition and the full expression for the Gibbs-Thomson equation; (ii) the second solution comes from (2.26) where we take $c = 1$, $\Gamma \neq 0$; (iii) the third is (2.27) where we have assumed $c = 1$ and $\Gamma = 0$. This last one, in fact, corresponds to the solution of the classical one–phase Stefan problem in the sphere, analysed by previous authors [3, 40].

2.4.2 Two–phase formulation

In the previous section we presented the one–phase solution that neglects the solid temperature. We now build on this solution to model the two–phase process specified by equations (2.10)–(2.13).

The same rescaling of the time variable, $t = \beta\tau$, can be applied to the equation for the temperature in the solid, equation (2.11), and θ expanded in terms of $1/\beta$. This, leads to

$$\mathcal{O}(1): \qquad 0 = \frac{1}{r^2}\frac{\partial}{\partial r}\left(r^2\frac{\partial\theta_0}{\partial r}\right), \qquad \left.\frac{\partial\theta_0}{\partial r}\right|_{r=0} = 0, \qquad \theta_0(R,\tau) = T_m \tag{2.28}$$

$$\mathcal{O}(1/\beta): \qquad \frac{\partial\theta_0}{\partial\tau} = \frac{k}{c}\frac{1}{r^2}\frac{\partial}{\partial r}\left(r^2\frac{\partial\theta_1}{\partial r}\right), \qquad \left.\frac{\partial\theta_1}{\partial r}\right|_{r=0} = 0, \qquad \theta_1(R,\tau) = 0 \tag{2.29}$$

with solution

$$\theta_0 = T_m, \qquad \theta_1 = -\frac{\mu_2}{2kR}(R^2 - r^2)\frac{dR}{d\tau}\ , \tag{2.30}$$

where

$$\mu_2 = \frac{c}{3R}\frac{\Gamma}{\left[1 + \frac{(1-c)}{\beta\delta T}\ln\left(T_m\delta T + 1\right)\right]}\ . \tag{2.31}$$

Note, since the leading order heat equation for θ_0 does not have a time derivative no initial condition is required. However, the one-phase reduction involves the assumption $\theta(r,t) = T_m(t)$, so if we wish to compare with the one-phase problem we require $\theta(r,0) = T_m(0)$ and indeed this is consistent with the boundary conditions given in (2.28).

The Stefan condition now leads to

$$\frac{dR}{d\tau} = \frac{(T_m - 1)}{R(1-R)}\left[1 + \frac{1}{\beta}\left\{\left(1 - c - \frac{2}{R}\right)T_m + \frac{2}{R} - \mu_1 - \mu_2\right\}\right]^{-1}. \tag{2.32}$$

The introduction of the solid temperature has modified equation (2.23) at first order by the term μ_2, which comes from the θ_1 expression. Since $\mu_2 > 0$ this term acts to speed up the melting process. In the following section we will see that the temperature in the solid does indeed contribute towards faster melting.

2.5 Results and Discussion

We now present a set of results corresponding to the solutions found in the previous section. First, we show the different solutions obtained for the one–phase model and compare them with numerical solutions using a method similar to that described in [66]. This is a semi–implicit finite difference scheme that discretizes implicitly for the temperature and explicitly for the moving front. The heat equation is converted into a planar equation with the transformation $T = u/r$ and the moving boundary is immobilized by means of the change of variable $\xi = (r - R)/(1 - R)$, to fix the domain. Second, we show the solution of the full two–phase model and compare it with that for the one–phase problem. Finally, we use the one and two–phase models to calculate the melting times for different initial particle sizes and external temperatures. We also show the temperature distribution in both phases as the melting proceeds.

The plots in Figure 2.3 show the position of the solid–liquid interface as a function of time for the one-phase problem with an inital dimensional radius $R_0 = 10\,\text{nm}$ and two different values of the Stefan number $\beta = 100$ and $\beta = 10$. The dimensional values may be retrieved by multiplying R by R_0 and t by the time-scale $\rho_l c_l R_0^2/k_l \approx 2.66\times10^{-12}$s. The solid and dashed lines represent the perturbation and numerical results respectively. Curve (i) corresponds to the solution of (2.23)–(2.24), curve (ii) corresponds to the solution of (2.26) resulting from setting $c_l = c_s$ (hence $c = 1$) and curve (iii) is the solution (2.27) obtained by setting $c = 1$, $\Gamma = 0$ (hence $T_m(t)$ is constant). As discussed earlier, the plots are cut-off at $R = 0.1$ which corresponds to a dimensional value $0.1R_0$, where $R_0 = 10\,\text{nm}$. Beyond this both the numerical and perturbation solutions of equations (2.23)–(2.24) break down due to the failure of the Gibbs-Thomson relation (as seen on the inset in Figure 2.1 there is no real value of T_m for $R < 1$nm). For large Stefan number it is clear that the asymptotics and numerics agree very well, with only a slight difference showing as $R \to 0$. Curves (i) and (ii) exhibit high velocities $R_t \to \infty$ both initially and as $R \to 0$. This behaviour is obvious from the factor $1/(R(1 - R))$ in equation (2.23). The rapid melting as $R \to 0$ has been predicted experimentally and depicted schematically in [48, Fig.1b] and also noted in [60]. Curve (ii),

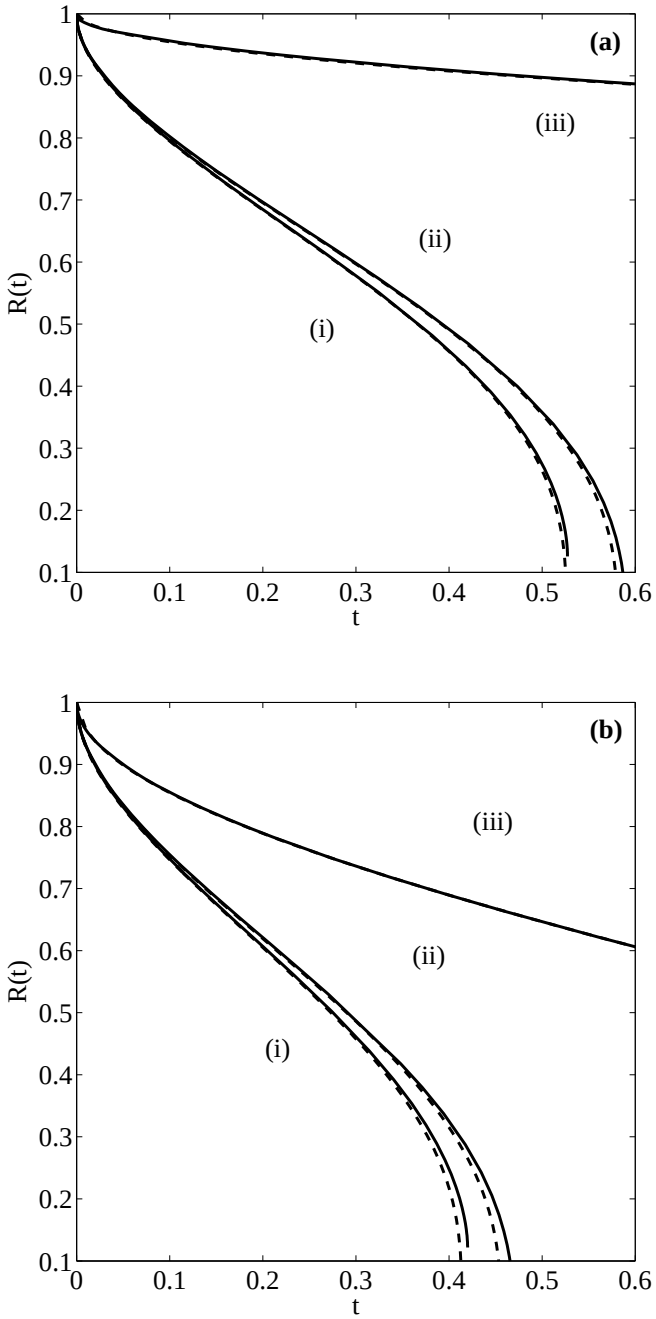

Figure 2.3: Position of the non–dimensional melting front $R(t)$ for a nanoparticle with initial dimensional radius $R_0 = 10\,\mathrm{nm}$, (a): $\beta = 100$ (b) $\beta = 10$. Curve (i) is the solution of (2.23)–(2.24), (ii) the solution of (2.26) and (iii) the solution of (2.27).

with $c = 1$, shows a melt time approximately 11% slower than that of curve (i). This is significantly greater than the error introduced by the perturbation (since we neglect terms of $\mathcal{O}(1/\beta^2)$ and $\beta = 100$, the perturbation errors are of $\mathcal{O}(10^{-2})\%$).

In Figure 2.4 we show the evolution of $R(t)$ for a nanoparticle with an initial radius of $R_0 = 100\,\text{nm}$ for $\beta = 100$ and $\beta = 10$, the time-scale $\rho_l c_l R_0^2/k_l \approx 2.66 \times 10^{-10}$. In this case, the solution breaks down when $R \approx 1\,\text{nm}/100\,\text{nm}$=0.01. In contrast to the previous figure we observe that the solutions (i) and (ii) are almost identical for most of the process, indicating the change in specific heat is not important (at least for the melting of gold) for sufficiently large particles. The difference between Figures 2.3 and 2.4 is the value of R_0 which changes from 10 to 100 nm. Earlier we pointed out that Γ is the main controlling parameter where $\Gamma \propto 1/R_0$. From the figures we can see that a large change in Γ does indeed result in a large change in melting times.

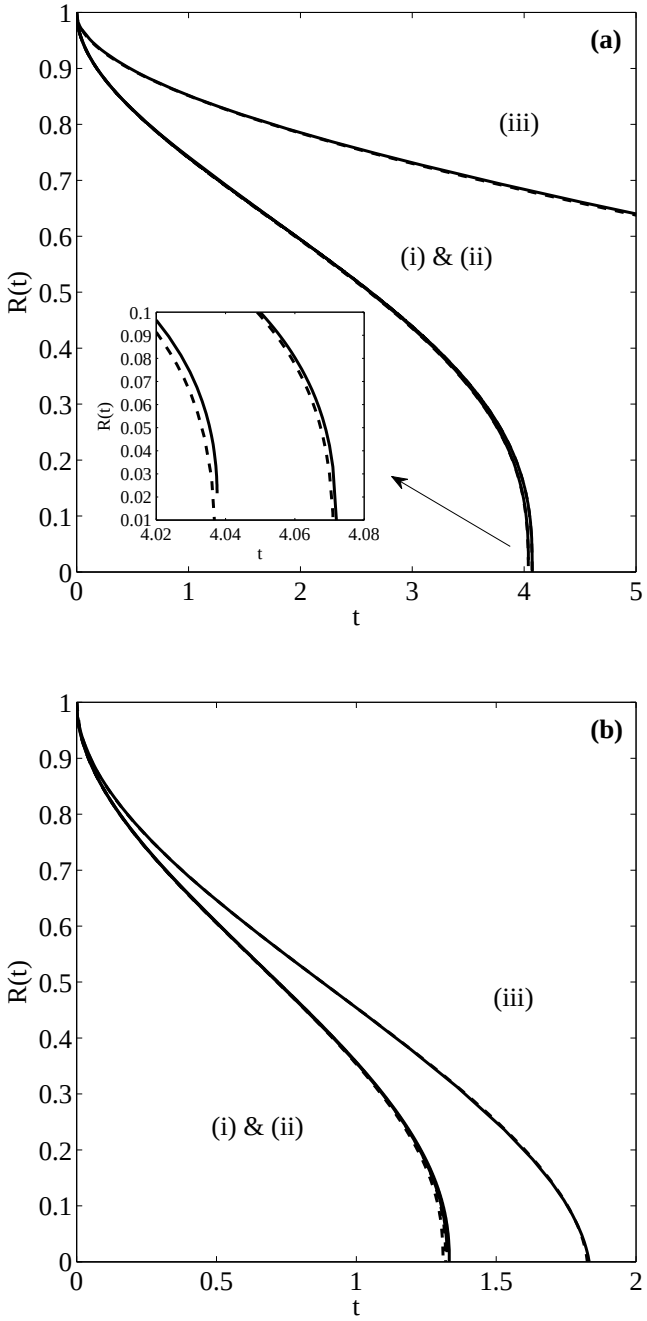

Figure 2.4: Position of the non–dimensional melting front $R(t)$ for a nanoparticle with initial radius $R_0 = 100\,\text{nm}$, (a): $\beta = 100$ (b) $\beta = 10$. Curve (i) is the solution of (2.23)–(2.24), (ii) the solution of (2.26) and (iii) the solution of (2.27).

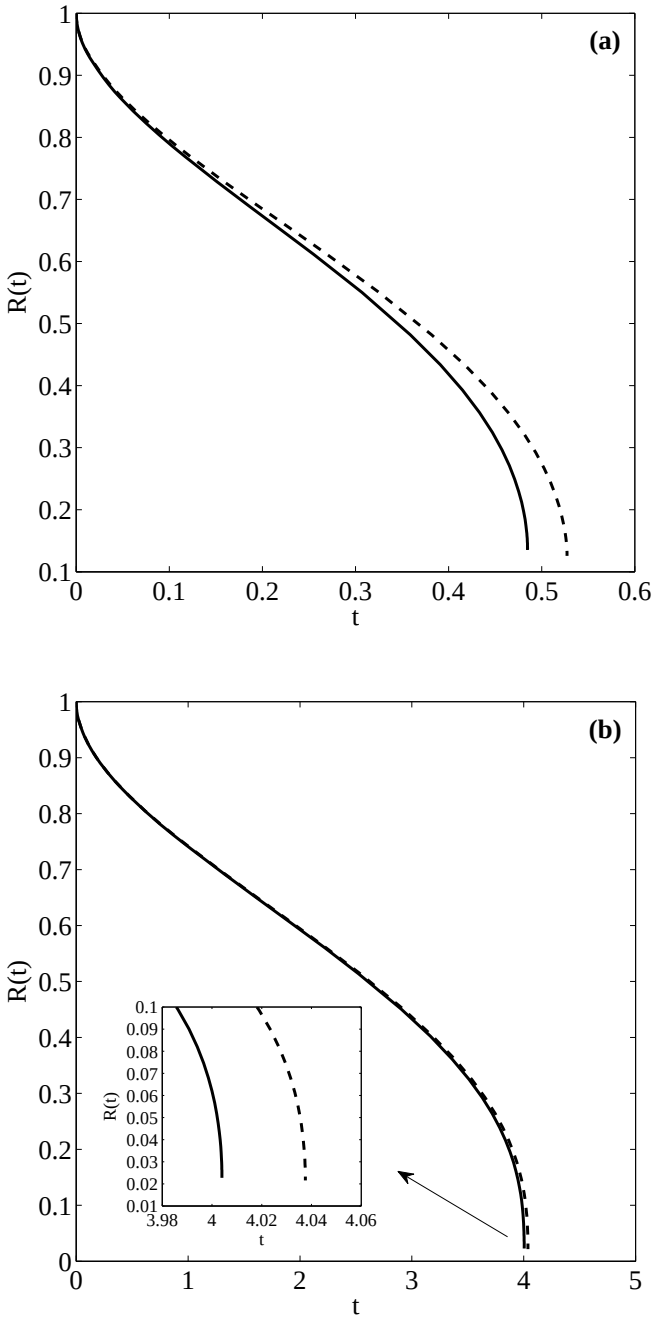

Figure 2.5: Comparison between one and two–phase solutions for $\beta = 100$, (a) $R_0 = 10\,\mathrm{nm}$ (b) $R_0 = 100\,\mathrm{nm}$.

Table 2.2: Melting times computed with the one–phase model.

	Melting times (s)		
	$R_0 = 10\,\text{nm}$	$R_0 = 100\,\text{nm}$	$R_0 = 500\,\text{nm}$
$\beta = 100$ ($T_H \approx 1341$ K)	$1.56 \cdot 10^{-12}$	$1.20 \cdot 10^{-9}$	$7.35 \cdot 10^{-8}$
$\beta = 10$ ($T_H \approx 1376$ K)	$1.25 \cdot 10^{-12}$	$0.39 \cdot 10^{-9}$	$1.25 \cdot 10^{-8}$
$\beta = 5$ ($T_H \approx 1415$ K)	$1.05 \cdot 10^{-12}$	$0.24 \cdot 10^{-9}$	$0.71 \cdot 10^{-8}$

Table 2.3: Melting times computed with the two–phase model.

	Melting times (s)		
	$R_0 = 10\,\text{nm}$	$R_0 = 100\,\text{nm}$	$R_0 = 500\,\text{nm}$
$\beta = 100$ ($T_H \approx 1341$ K)	$1.44 \cdot 10^{-12}$	$1.19 \cdot 10^{-9}$	$7.33 \cdot 10^{-8}$
$\beta = 10$ ($T_H \approx 1376$ K)	$1.15 \cdot 10^{-12}$	$0.39 \cdot 10^{-9}$	$1.25 \cdot 10^{-8}$
$\beta = 5$ ($T_H \approx 1415$ K)	$0.97 \cdot 10^{-12}$	$0.24 \cdot 10^{-9}$	$0.70 \cdot 10^{-8}$

Figure 2.5 displays a comparison of the one and two-phase formulations when $\beta = 100$. The difference between the formulations lies in the μ_2 term of the Stefan condition (2.32). Since $\mu_2 \propto \Gamma \propto 1/R_0$ we expect the greatest variation for small values of R_0. Figure 2.5a shows a comparison of results for $R_0 = 10\,\text{nm}$ and it is clear that there is a significant difference in the curves. However, in Figure 2.5b, where $R_0 = 100\,\text{nm}$ the curves are virtually identical (the blow-up shows the small percentage difference for small R). Consequently we may conclude that for a given material the variation in specific heat and the use of one or two phase formulations is only important for very small nanoparticles (large values of Γ). This conclusion on the one and two-phase formulation may be verified through Tables 2.2 and 2.3, which show melting times for multiple particle sizes and Stefan numbers. In all cases the melting times are relatively close, with the largest differences occurring with the smallest particles.

The results agree well with limited available experimental data. Our calculations show that when $R_0 = 10\,\text{nm}$ the melting time lies in the picosecond range, with $R_0 = 100\,\text{nm}$ the melting times go from a few to several hundred picoseconds, with $R_0 = 500\,\text{nm}$ melting times are well above the nanosecond scale. Pech *et al* [84] track the melting process of gold nanoparticles when they are heated by a laser beam with power 30 mW. They find that the

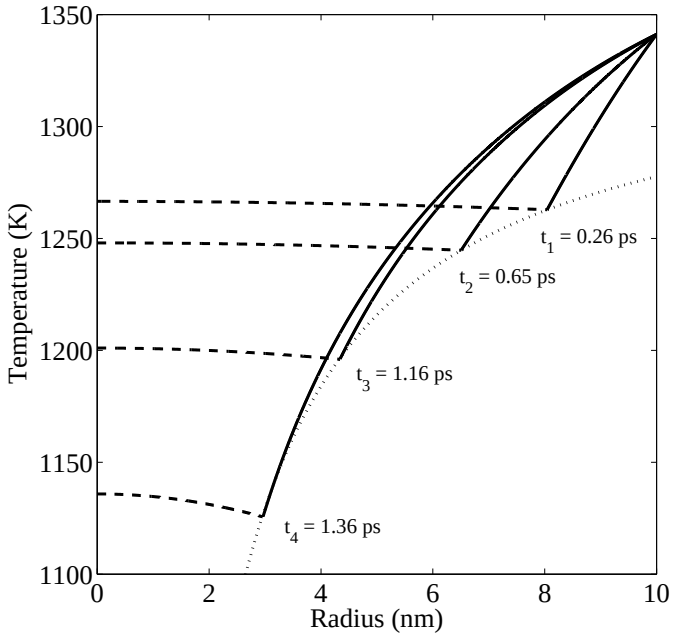

Figure 2.6: Blue is the solid phase, red the liquid phase and dashed the melting temperature. For $\beta = 100$ and $R_0 = 10\,\text{nm}$.

melting process is faster than 100 ps for particles with $R_0 = 50\,\text{nm}$. By assuming the same power and a regular spot laser beam of $4\,\mu\text{m}$ diameter we obtain a power per unit area of $2.39 \times 10^5\,\text{W/cm}^2$. Using this value in [33, Fig.1] the temperature increase at the nanoparticle surface is about $\Delta T \approx 40\,\text{K}$. In our model, this temperature increase corresponds to $\beta = 10$ and our predicted time to complete melting for a particle of this size is 73.3 ps. In [90] experimental observation of nanoparticle melting is carried out for particles with $R_0 = 2$ and 20 nm with melting times in the picosecond range.

Finally, in Figure 2.6, we present temperature distributions throughout the melting process for the problem of Figure 2.3a. Plots for different conditions all take a similar form, so we only present this single result and in this case we show the dimensional values. The dashed line represents the temperature in the solid phase ($0 < r < R(t)$), the solid line the temperature in the liquid phase ($R(t) < r < R_0$), they meet on the dotted line which represents the melt temperature $T_m(t)$. The final set of curves occur at $t = 1.36$ps. As $R \to 0$ the speed of melting increases and so the melting should be complete shortly after

this time. An interesting feature of this graph is that the temperature within the solid is greater than the melt temperature and this becomes more apparent as time increases. This presumably occurs because the melt temperature decreases faster than the solid can diffuse the temperature change at the boundary. So, unlike in standard Stefan problems, the temperature in the solid phase acts to speed up the melting. This high temperature was pointed out in [60] and attributed to superheating, where the solid is everywhere above the (variable) melt temperature. However other authors define superheating as a surface effect that refers to heating a solid above its bulk melting temperature [124, 97]. If we think of the melt temperature depression as representing the decrease in energy required for the solid particles to move to the liquid phase then it is clear that the bulk particles are not affected and so should not be described as superheated.

2.6 Conclusions

In this chapter we have presented a mathematical model for the melting of a spherical nanoparticle. The initial system of two partial differential equations coupled to the Gibbs-Thomson relation for the melt temperature and a Stefan condition to determine the domain was reduced to the solution of two first order ordinary differential equations. The approximate solution showed excellent agreement with the numerical solution of the full system.

The beauty of the reduced system is that it makes clear which parameters control the melting process. In this case the dominant parameter turned out to be $\Gamma = 2\sigma_{sl}T_m^*/R_0\rho_l L_m \Delta T$. From this we see the obvious feature that changing the particle size or the temperature driving the melting has a controlling influence. The non-dimensional grouping also indicates that, for example, increasing surface tension by a given factor is equivalent to decreasing the initial radius by the same factor.

The one-phase formulation and the system with $c_l = c_s$ was also examined, since these are standard simplifications. It was shown that for large values of Γ these formulations are inaccurate. However, as Γ decreased (from 6 to 0.6) the differences decreased and the simpler formulations proved sufficiently accurate.

An interesting feature of the two-phase solution is that the solid temperature is higher

than the melt temperature. This is not a feature of standard melting problems and presumably occurs because the melt temperature decreases faster than diffusion occurs in the solid. So, in contrast to melting on the macroscale, on the nanoscale the solid acts to speed up the melting process. This feature, coupled to the melting point depression leads to the abrupt melting that is observed experimentally.

All analysis was based on continuum theory, which obviously breaks down for sufficiently small particles. The generalised Gibbs-Thomson relation was also shown to break down, for gold this occurred around 1 nm. Hence all our results were cut off at this limit. For smaller particles, or to follow the melting process to its completion a non-continuum theory must be applied.

Chapter 3

The melting of nanoparticles with a density jump

F. Font, T.G. Myers, S.L. Mitchell. *A mathematical model for nanoparticle melting with density change* Microfluidics and Nanofluidics, DOI:10.1007/s10404-014-1423-x (May 2014)
Impact factor: 3.218

Abstract

The melting process of a spherical nanoparticle is analysed using a mathematical model derived from continuum theory. The standard model for macro-scale melting is modified to include melting point depression using the Gibbs-Thomson equation. The key difference between the current and previous work in the melting of nanoparticles is that the difference in densities between the solid and liquid phases is accounted for. This modifies the energy balance at the phase change interface to include a kinetic energy term, which then changes the form of the equation, it also requires an advection term in the heat equation for the liquid phase. Approximate analytical and numerical solutions are presented for the melting of particles in the range 10-100nm. It is shown that when the density difference is included in the model melting is significantly slower than when density is assumed constant throughout the process. This is attributed to the flowing liquid providing a sink term, namely kinetic

energy, in the energy balance. The difference in results is greatest for small particles, however, it is concluded that the varying density model will never reduce to the constant density model resulting in a difference of around 15% even at the macro-scale.

3.1 Introduction

There exists a large body of work concerning the mathematical modelling of phase change, which is often termed a Stefan problem. The original Stefan problem concerned the formation of sea ice. Since then the model has been applied to many different forms of phase change and geometries as well as topics in porous media flow and finance [82]. An analogous problem occurs in the growth of material from a saturated liquid, where concentration rather than temperature gradients drive the growth [19]. In the context of phase change, the vast majority of studies incorporate a number of restrictive assumptions, which are often made for mathematical convenience and limit the applicability of the results to highly idealised situations. Alexiades and Solomon [3, Chap. 1] provide a list of standard assumptions including constant latent heat, constant phase change temperature, a sharp phase change interface, constant thermal properties in each phase and a constant density which is equal in both phases. They state that this final assumption is perhaps the most unreasonable, indeed anyone with experience of burst water pipes will be aware of the true importance of density change. Consequently, in this chapter we will focus on the effect of density change. Our work is motivated by the melting of spherical nanoparticles however the model could be applied to more general situations of practical interest, such as pipe bursting, cryopreservation, phase change microvalves and metal casting, see [3, 28, 76, 77, 80].

In [3] freezing and melting with the incorporation of a density change is discussed. They state that most physical properties vary to some extent with temperature, but that at the phase change temperature there is often a sudden change. Although the value of the density may not change as much as other variables, its variation may lead to the most pronounced effects. They subsequently analyse phase change in Cartesian co-ordinates to show that the density jump introduces a non-standard term, proportional to the cube of the phase change velocity, into the Stefan condition. They discuss how neglecting this term can lead to over

or under estimation of the front velocity depending on the physical situation. However, they later neglect this term to permit exact similarity solutions. In [80] a similar approach is taken, again to find similarity solutions. In [13] the cubic term is neglected altogether and seek small time and similarity solutions for the freezing of a liquid layer and phase change in a porous half-space. In the following work we will demonstrate the importance of the cubic term, particularly near the beginning and end of the process.

At the nano-scale an important effect is that of melting point depression, which can lead to rapid melting as the particle size tends to zero. This may explain the sudden disappearance of particles discussed in [48]. The variation of the melt temperature with size is often represented by the Gibbs-Thomson equation, although there exist a number of other forms with the common feature that the temperature change is proportional to curvature [8, 48, 52, 78]. In the following work we will employ the classical Gibbs-Thomson relation

$$T_m = T_m^* \left(1 - \frac{2\sigma_{sl}\kappa}{\rho_s L_f}\right) , \tag{3.1}$$

where T_m^* is the bulk melting temperature, σ_{sl} the surface energy between the solid and the liquid, L_f the latent heat and ρ_s the density. The curvature of a sphere is $\kappa = 1/R$, where R is the particle radius. Note, if we take parameter values for gold, as given in Table 3.1, we find $T_m > 0$ when $R > 0.44$nm. Assuming our results only hold for $R > 2$nm we do not expect mathematical problems to arise due to using the above form of the Gibbs-Thomson relation.

In [60] small time and large Stefan number solutions are sought for a two-phase problem describing the melting of spherical nanoparticles subject to (3.1). In [29] the authors focus on the situation where the specific heats vary through the phase change. To account for this they apply a more general form of the Gibbs-Thomson relation. Their results show that melting point depression is extremely important in predicting the melt time of nanoparticles. They also investigate the effect of using the generalised Gibbs-Thomson relation as opposed to the above classical version. [119] had previously concluded that melting point depression could explain the rapid melting of nanoparticles. To simplify the mathematics their work used an approximation where the variation of specific heat was neglected in the generalised

Gibbs-Thomson relation (meaning (3.1) was valid) but retained in the remaining governing equations. In [29] it was shown that, when compared to using the generalised Gibbs-Thomson relation, this approach leads to differences on the order of 10% in melt times for 10 nm particles, whilst for 100 nm particles the difference is around 1%. In the following study we will see that allowing the density to vary can more than double the melt time of a 10 nm particle. Thus, in order to keep the analysis simple and focus on the density variation, we will assume the specific heats to be equal for both phases and model the melting point depression with (3.1).

The mathematical model to be developed in the following section will be based on continuum theory. Since our focus is on nanoscale phase change it is worth considering the validity of this theory. This issue is discussed in detail in [29]. To summarise, they state that comparison of molecular dynamics simulations, experiment and continuum theory have led to the conclusion that for fluid flow continuum theory may be accurate down to around 3 nm, for heat transfer and phase change 2 nm appears to be the lower limit, see [36, 112]. Consequently, we only expect our model to be valid for particles greater than 2nm. Note, the Gibbs-Thomson relation (3.1) requires $R > 2\sigma_{sl}/(\rho_s L_f)(\approx 0.4\text{nm for gold})$. So we may assume equation (3.1) to be accurate for physically realistic values of the continuum model.

In section 3.2 of this chapter we present a mathematical model that describes the melting of spherical nanoparticles including melting point depression and density change between phases. In section 3.3 we seek approximate solutions by means of a perturbation method. Then, we pinpoint the small time behaviour of the system and use it later on to initialize the numerical scheme described in section 3.4. Results are presented in section 3.5, comparing the numerical and approximate solutions. Finally, in section 3.6 we present the main conclusions of this study.

3.2 Mathematical model

We consider a solid sphere with radius R_0, initially at the melting temperature $T_m(R_0)$, which is given by the Gibbs-Thomson equation (3.1). The surface of the sphere is suddenly raised to temperature $T_H > T_m(R_0)$ which starts the melting process: a liquid phase grows

inwards from the surface of the particle until the solid disappears. We denote the moving solid-liquid interface by $R(t)$. Due to the density change the outer surface also moves, and it is designated as $R_b(t)$, where $R_b(0) = R_0$. A sketch of the model is presented in Figure 3.1.

To describe the melting process of the nanoparticle requires solving heat equations in the solid and liquid phases over the moving domains $0 < r < R(t)$ and $R(t) < r < R_b(t)$, respectively. The heat equation in the liquid is given by

$$\rho_l c_l \left(\frac{\partial T}{\partial t} + \nabla T \cdot \mathbf{v} \right) = k_l \nabla^2 T \,, \tag{3.2}$$

where T is the temperature, $\mathbf{v}$ is the velocity of the fluid caused by the density change, k_l the thermal conductivity and c_l the specific heat. Since the geometry is spherical and the temperature applied on the surface $R_b(t)$ is constant we may assume spherical symmetry. The velocity may be written as $\mathbf{v} = (v(r), 0, 0)$ and the heat equation becomes

$$\rho_l c_l \left(\frac{\partial T}{\partial t} + v \frac{\partial T}{\partial r} \right) = k_l \frac{1}{r^2} \frac{\partial}{\partial r} \left(r^2 \frac{\partial T}{\partial r} \right) \qquad \text{on} \qquad R(t) < r < R_b(t). \tag{3.3}$$

This is the standard heat equation with advection see [3, 80, 122] for example.

Under the assumption of incompressible flow the velocity $\mathbf{v}$ can be determined from the continuity equation $\nabla \cdot \mathbf{v} = 0$. In the present case,

$$\frac{1}{r^2} \frac{\partial}{\partial r} \left(r^2 v \right) = 0 \,, \tag{3.4}$$

leading to

$$v = \frac{c_0}{r^2} \,, \tag{3.5}$$

where c_0 is a constant of integration. Mass conservation requires

$$\frac{d}{dt} \left[\rho_s \frac{4}{3} \pi R^3 + \rho_l \frac{4}{3} \pi (R_b^3 - R^3) \right] = 0 \,, \tag{3.6}$$

this provides an equation for the velocity of the outer surface

$$\frac{dR_b}{dt} = -\frac{R^2}{R_b^2}\left(\frac{\rho_s}{\rho_l} - 1\right)\frac{dR}{dt}. \tag{3.7}$$

Noting that $v(R_b) = dR_b/dt$ provides an expression for c_0 in (3.5) and so the velocity

$$v = -\frac{R^2}{r^2}\left(\frac{\rho_s}{\rho_l} - 1\right)\frac{dR}{dt}. \tag{3.8}$$

The temperature in the solid phase, θ, is given by the one dimensional heat equation

$$\rho_s c_s \frac{\partial \theta}{\partial t} = k_s \frac{1}{r^2}\frac{\partial}{\partial r}\left(r^2 \frac{\partial \theta}{\partial r}\right) \qquad \text{on} \qquad 0 < r < R(t)\ . \tag{3.9}$$

To avoid having to solve a thermal problem before the melting begins we will take the initial solid temperature to be $\theta(r, 0) = T_m(0)$. The appropriate boundary conditions for equations (3.3) and (3.9) are

$$T(R_b, t) = T_H, \quad T(R, t) = \theta(R, t) = T_m(t), \quad \left.\frac{\partial \theta}{\partial r}\right|_{r=0} = 0, \tag{3.10}$$

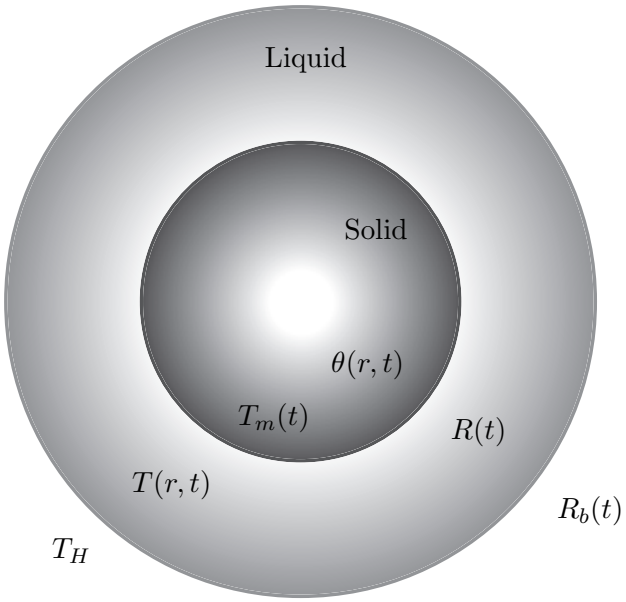

Figure 3.1: Sketch of the model, showing a solid sphere of radius $R(t)$ surrounded by a liquid layer with radius $R_b(t)$.

where $T_m(t)$ is given by equation (3.1).

Energy conservation across the surface $R(t)$ gives the Stefan condition

$$\rho_s \left[L_f + (c_l - c_s)(T_m - T_m^*) \right] \frac{dR}{dt} + \frac{\rho_s}{2} \left(1 - \frac{\rho_s}{\rho_l} \right)^2 \left(\frac{dR}{dt} \right)^3 = k_s \left. \frac{\partial \theta}{\partial r} \right|_{r=R} - k_l \left. \frac{\partial T}{\partial r} \right|_{r=R} . \tag{3.11}$$

A detailed derivation of the Cartesian version of this equation, with $\Delta c = 0$, is given in [3], we have simply generalised this to the spherical form.

Equation (3.11) contains a term that generally does not appear in the Stefan condition, namely the one involving R_t^3. This appears due to the kinetic energy which is a result of the density change forcing the fluid to move. Equation (3.8) shows the fluid velocity to be proportional to R_t, hence the kinetic energy is proportional to R_t^2, the rate of change of mass is also proportional to R_t, hence the cubic dependence. In general this term may appear to be of less importance than the standard first term on the left hand side, since the first term appears to be of order L_f greater than the cubic term (for fluids typically $L_f \sim 10^5$). However, it is well-known that the standard Stefan problem, with a fixed temperature boundary condition will have $R_t \to -\infty$ as $t \to 0$ and so the cubic term will dominate for at least a short period. The spherical Stefan problem has also been shown to have $R_t \to -\infty$ as the melting reaches completion [29, 60].

Equation (3.1), with $\kappa = 1/R(t)$, and equation (3.11) provide relations for the two unknowns $T_m(t)$, $R(t)$. The temperature gradients in (3.11) come from the solution of the liquid and solid heat equations. The radius is subject to the initial condition $R(0) = R_0$, while $T_m(0)$ is determined by setting $R = R_0$ in equation (3.1).

The above governing equations may be nondimensionalized by introducing the variables

$$\hat{T} = \frac{T - T_m^*}{T_H - T_m^*}, \quad \hat{\theta} = \frac{\theta - T_m^*}{T_H - T_m^*}, \quad \hat{r} = \frac{r}{R_0}, \quad \hat{t} = \frac{k_l}{\rho_l c_l R_0^2} t \ . \tag{3.12}$$

The nondimensional moving boundaries are $\hat{R} = R/R_0$ and $\hat{R}_b = R_b/R_0$. Dropping the hats,

the governing equations (3.3) and (3.9) become

$$\frac{\partial T}{\partial t} - (\rho - 1)\frac{R^2}{r^2}\frac{dR}{dt}\frac{\partial T}{\partial r} = \frac{1}{r^2}\frac{\partial}{\partial r}\left(r^2\frac{\partial T}{\partial r}\right), \qquad R < r < R_b \ , \tag{3.13}$$

$$\frac{\partial \theta}{\partial t} = \frac{k}{\rho}\frac{1}{r^2}\frac{\partial}{\partial r}\left(r^2\frac{\partial \theta}{\partial r}\right), \qquad 0 < r < R \ . \tag{3.14}$$

The Stefan condition is

$$\rho\left[\beta + (1-c)T_m\right]\frac{dR}{dt} + \gamma\left(\frac{dR}{dt}\right)^3 = k\frac{\partial \theta}{\partial r}\bigg|_{r=R} - \frac{\partial T}{\partial r}\bigg|_{r=R}, \tag{3.15}$$

and the boundary conditions (3.10) are

$$T(R_b, t) = 1, \quad T(R,t) = \theta(R,t) = -\frac{\Gamma}{R}, \quad \frac{\partial \theta}{\partial r}\bigg|_{r=0} = 0, \quad T(r,0) = -\Gamma, \tag{3.16}$$

and the initial condition for the melt front is $R(0) = 1$. The dimensionless parameters are defined by

$$\rho = \frac{\rho_s}{\rho_l}, \qquad k = \frac{k_s}{k_l}, \qquad \beta = \frac{L_f}{c_l \Delta T}, \qquad c = \frac{c_s}{c_l} \ , \tag{3.17}$$

$$\Gamma = \frac{2\sigma_{sl}T_m^*}{R_0 \rho_s L_f \Delta T}, \qquad \gamma = \frac{\alpha_l^3 \rho_s}{2R_0^2 k_l \Delta T}\left(\rho - 1\right)^2 \ , \tag{3.18}$$

where $\Delta T = T_H - T_m^*$ and $\alpha_l = k_l/\rho_l c_l$ is the liquid thermal diffusivity. Note that R_b and R are related by

$$R_b^3 = \rho - (\rho - 1)\, R^3 \ , \tag{3.19}$$

which is obtained by integrating equation (3.7) and applying the condition $R = R_b = 1$ at $t = 0$.

The problem parameters indicate the importance of the various terms. The density variation is represented by ρ, which also appears in γ. Setting $\rho = 1$ removes the advection term from the heat equation and the kinetic energy term from the Stefan condition. The importance of kinetic energy is indicated by γ. As well as depending on ρ, $\gamma \propto 1/R_0^2$,

that is the importance of the kinetic energy term increases quadratically as the particle size decreases. In [3] it is stated that, in general, the cubic term in the Stefan condition is expected to be negligible compared to the linear term. In the present study we will show that the kinetic energy term is dominant for particles below 100 nm radius. Further, due to the singularity in R_t at the beginning and end of the melt process the cubic term is important even for much larger particles.

The vast majority of studies of phase change neglect the density difference between phases, this is achieved by setting $\rho = 1$ (and hence $\gamma = 0$). In this limit the advection term disappears from (3.13) and the kinetic energy term disappears from equation (3.15), to provide the common form of Stefan problem. For a given material we may also look at the limit $\gamma \to 0$ by choosing a large particle, $R_0 \to \infty$ or a large temperature difference $\Delta T \to \infty$. In this situation the results do not converge to the results from the Stefan problem with $\rho = 1$, since firstly the advection term remains in the liquid heat equation and also γ multiplies R_t, so even though $\gamma \to 0$ the limit γR_t may not tend to zero when $R_t \to \infty$ and kinetic energy still has some small effect.

The ratio of specific heats is denoted $c = c_s/c_l$. In Table 3.1 we see that $c \approx 0.79$ for gold. A common assumption, at least in the mathematical community, is to set $c = 1$, which then permits the use of the classical Gibbs-Thomson equation (3.1) instead of the extended nonlinear form given in [29]. The effect of this approximation on nanoparticle melting has been investigated previously in [29, 60] and in particular it was shown that for large particles, with $R_0 = 100$ nm, setting $c = 1$ made a negligible difference to melt times, whereas for smaller particles, $R_0 = 10$ nm, a difference of the order 10% was observed. Since our present focus is on the effect of density change we will set $c = 1$ from now on, since this permits the use of the simpler version of the Gibbs-Thomson relation and considerably simplifies the analysis.

The ratio of conductivities is denoted $k = k_s/k_l$. This is also often set to unity, but leaving it as its correct value does not affect the solution process. However, it does play an important role when reducing the two-phase model to one-phase (i.e. neglecting the solid temperature) as is carried out in [29, 118]. The fact that $k_s > k_l$ is key to the energy

Table 3.1: Approximate thermodynamical parameter values for gold. The value of σ_{sl} is taken from [8].

Substance	T_m^* (K)	L_f (J/Kg)	c_l, c_s (J/Kg·K)	ρ_l, ρ_s (kg/m^3)	k_l, k_s (W/m·K)	σ_{sl} (N/m)
Gold	1337	6.37×10^4	163/129	$1.73\times10^4/1.93\times10^4$	106/317	0.27

conserving model of [74].

The parameter Γ indicates the effect of melting point depression. If $\Gamma = 0$ then the melt temperature is fixed. In general $\Gamma \propto 1/R_0$ so as the radius decreases Γ increases and melting point depression is more significant.

The Stefan number is denoted by β, for a specific material this varies due to the temperature scale of the process. For a small temperature variation the Stefan number is large and the melting process is slow. For a large temperature variation the melt process is fast (although slow and fast are rather relative on the nanoscale). Note, particularly within the engineering community, the Stefan number may be referred to as the inverse of our value, i.e. $\beta = c_l\Delta T/L_f$. With nanoparticles, any small increase above the melt temperature will be sufficient to completely melt the particle (once melting starts melting point depression begins and the process speeds up). Consequently it makes sense to work in the large β regime, which then allows us to use a perturbation solution method. This will be detailed in the following section, we will then compare the approximate solution with a full numerical solution which is described in section 3.4.

3.3 Perturbation solution

Analytical solutions allow us to understand the important factors within a physical process in a way that numerical solutions cannot. For this reason we now seek an approximate analytical solution, based on a large Stefan number.

The mathematical description of the problem is given by equations (3.13)-(3.15) with boundary conditions (3.16). Equation (3.1) relates the melt temperature to the radius $R(t)$. To make analytical progress we make use of a standard perturbation technique. As in [29], we

consider β to be large for our system (for gold heated 10 K above the bulk melt temperature $\beta \approx 40$) and define a new time scale $t = \beta\tau$. This permits us to assume expansions for the temperatures $\theta = \theta_0 + \theta_1/\beta + \mathcal{O}(1/\beta^2)$ and $T = T_0 + T_1/\beta + \mathcal{O}(1/\beta^2)$. Then, equations (3.13) and (3.14) can be expressed as a sequence of simpler problems. For example, the leading order problem (where all terms with a factor $1/\beta^n$, where $n \geq 1$, are neglected) is represented by the steady-state equations

$$0 = \frac{1}{r^2}\frac{\partial}{\partial r}\left(r^2\frac{\partial T_0}{\partial r}\right), \qquad 0 = \frac{1}{r^2}\frac{\partial}{\partial r}\left(r^2\frac{\partial \theta_0}{\partial r}\right), \tag{3.20}$$

with boundary conditions $T_0(R_b, \tau) = 1$, $T_0(R, \tau) = \theta_0(R, \tau) = -\Gamma/R$, and $\theta_{0r}(0, \tau) = 0$. The solution to this system is

$$\theta_0 = -\frac{\Gamma}{R}, \qquad T_0 = -\frac{\Gamma}{R} + \frac{R_b}{R}\frac{(r-R)}{r}\left(\frac{R+\Gamma}{R_b - R}\right). \tag{3.21}$$

The first order correction, which includes terms with a factor $1/\beta$, is described by

$$\frac{\partial T_0}{\partial \tau} - (\rho - 1)\frac{R^2}{r^2}\frac{dR}{d\tau}\frac{\partial T_0}{\partial r} = \frac{1}{r^2}\frac{\partial}{\partial r}\left(r^2\frac{\partial T_1}{\partial r}\right), \tag{3.22}$$

$$\frac{\partial \theta_0}{\partial \tau} = \frac{k}{\rho}\frac{1}{r^2}\frac{\partial}{\partial r}\left(r^2\frac{\partial \theta_1}{\partial r}\right), \tag{3.23}$$

with boundary conditions $T_1(R_b, \tau) = T_1(R, \tau) = \theta_1(R, \tau) = \theta_{1r}(0, \tau) = 0$. The appropriate solutions are

$$T_1 = \frac{(\Gamma + R_b)(R_b - r)(r - R)}{6(R_b - R)^2 r}\left\{\frac{3(\rho-1)R(\Gamma+R)(R_b-R)}{(\Gamma+R_b)r}\right. \tag{3.24}$$

$$\left. + \frac{(\rho-1)R(\Gamma+R)[3 - R(R_b + r + R)]}{R_b^2(\Gamma+R_b)} - r + 2R_b - R\right\} R_\tau, \tag{3.25}$$

$$\theta_1 = -\frac{\rho}{6k}\frac{\Gamma}{R^2}(R^2 - r^2)R_\tau. \tag{3.26}$$

Now, substituting $\theta \approx \theta_0 + \theta_1/\beta$ and $T \approx T_0 + T_1/\beta$ into the Stefan condition (3.15) with

the new time scale, we obtain the following equation

$$\frac{\gamma}{\beta^3}\left(\frac{dR}{d\tau}\right)^3 + \left\{\rho - \frac{\rho\Gamma}{\beta 3R} + \frac{(R+\Gamma)}{\beta 6R}\left[\frac{(\rho-1)(3R_b - R^2R_b - 2R^3)}{(R_b-R)} + \frac{2(\Gamma+R_b)}{(\Gamma+R)}\right]\right\}\frac{dR}{d\tau} + \frac{R_b}{R^2}\frac{(R+\Gamma)}{(R_b-R)} = 0 \ , \tag{3.27}$$

which is subject to the initial condition $R(0) = 1$. Note, since R_b can be expressed in terms of R via equation (3.19) this is a single ordinary differential equation for the unknown position $R(t)$. It is possible to also expand R and R_b, however this makes the calculation more complex and so we do not follow this route. So, the perturbation method has reduced the original problem, specified by two partial differential equations, a first order ordinary differential equation and an algebraic equation, to a single cubic first order ordinary differential equation. To solve this equation we may set $z = dR/d\tau$ so that it can be expressed as a cubic polynomial of the form $z^3 + k_1 z + k_2 = 0$. In all cases that we tested this equation had only one real root, $z_1 < 0$, we then integrated $dR/d\tau = z_1$ numerically.

For comparison, in the results section we will show solutions with no density jump between phases. This solution may be found by setting $\rho = 1$ in (3.27). This also determines $\gamma = 0$ and $R_b = 1$. In this case equation (3.27) reduces to

$$\left(1 + \frac{1}{3\beta R}\right)\frac{dR}{d\tau} + \frac{\Gamma + R}{R^2(1-R)} = 0, \qquad R(0) = 1 \ , \tag{3.28}$$

with solution

$$-\beta(1-R^3) + a(1-R^2) - b(1-R) + b\Gamma \ln\left(\frac{\Gamma+1}{\Gamma+R}\right) = 3\beta\tau \ , \tag{3.29}$$

where $a = [3\beta(\Gamma+1) - 1]/2$ and $b = (\Gamma+1)(3\beta\Gamma - 1)$. In section 3.5 we will compare the solutions of (3.27) with (3.29) for different parameter values and see how the melting times are affected by neglecting the density jump between phases.

A classical difficulty with the numerical solution of Stefan problems occurs because at $t = 0$ one of the phases may not exist, thus the initial conditions are problematic, see [66] (this issue occurs for any value of β). For this reason it is often beneficial to carry out a

small time analysis of the system to determine the initial behaviour. To achieve this we rescale time as $t = \delta\hat{\tau}$, where $\delta \ll 1$. It is also useful to rescale the space variable r as $\eta = (r - R)/(R_b - R)$ on $R < r < R_b$ and as $\xi = r/R$ on $0 < r < R$. This transforms (3.15) into

$$(R_b - R)\left[\rho\beta\left(\frac{dR}{d(\delta\hat{\tau})}\right) + \gamma\left(\frac{dR}{d(\delta\hat{\tau})}\right)^3\right] = k\frac{(R_b - R)}{R}\left.\frac{\partial\theta}{\partial\xi}\right|_{\xi=1} - \left.\frac{\partial T}{\partial\eta}\right|_{\eta=0} . \tag{3.30}$$

The initial condition, $R(0) = 1$, indicates that for small times R should take the form

$$R = 1 - \lambda(\delta\hat{\tau})^p , \tag{3.31}$$

where p, λ are constant. Equation (3.19) indicates $(R_b - R) \approx \lambda(\delta\hat{\tau})^p$ and equation (3.30) may now be written as

$$-\lambda(\delta\hat{\tau})^p\left[\rho\beta\lambda p(\delta\hat{\tau})^{p-1} + \gamma(\lambda p)^3(\delta\hat{\tau})^{3p-3}\right] = k\lambda(\delta\hat{\tau})^p\left.\frac{\partial\theta}{\partial\xi}\right|_{\xi=1} - \left.\frac{\partial T}{\partial\eta}\right|_{\eta=0} . \tag{3.32}$$

The difficulty now lies in choosing the appropriate value of p. From a physical standpoint we know that the melting is driven by the temperature gradient in the liquid, T_η. This causes the motion R_t and so one, or both of the terms on the left hand side must balance the T_η term. Since $\delta \ll 1$ this requires one of the powers $2p - 1$ or $4p - 3$ to be zero (and hence the δ term is unity). In other words $p = 1/2$ or $p = 3/4$. In the case of no density jump, $\gamma = 0$, then there is only one possibility, namely $p = 1/2$. However, when $\gamma \neq 0$ the second term is largest and so we must choose $p = 3/4$. This means that for small times the radius decreases as

$$R \approx \begin{cases} 1 - \lambda_1 t^{3/4} & \text{if } \gamma \neq 0 , \\ 1 - \lambda_2 t^{1/2} & \text{if } \gamma = 0 . \end{cases} \tag{3.33}$$

The corresponding velocities take the form $R_t \sim t^{-1/4}, t^{-1/2}$ for $\gamma \neq 0$ and $\gamma = 0$ respectively. Both solution forms indicate an infinite velocity as $t \to 0$, but the decrease in radius is faster with no density change (which then results in faster melting). Note, we have not yet determined the constants λ_1, λ_2, this will be dealt with in the following section.

3.4 Numerical solution method

The full problem requires the solution of the heat equations in the liquid and solid over an a priori unknown domain which is determined by the Stefan condition. The solution may be achieved via a finite difference scheme after applying a number of transformations.

Firstly, the temperature variables are changed to $v = r\theta$ and $u = rT$. This is a standard transformation which converts the spherical heat equation into the planar equivalent. The variables $\eta = (r - R)/(R_b - R)$ and $\xi = r/R$ which were defined earlier to obtain the perturbation solution may be used to immobilize the boundaries of u and v, respectively. This leads to the following governing equations

$$\frac{\partial v}{\partial t} = \frac{R_t}{R}\xi\frac{\partial v}{\partial \xi} + k\frac{1}{R^2}\frac{\partial^2 v}{\partial \xi^2} \qquad \text{on} \qquad 0 < \xi < 1 \ , \tag{3.34}$$

and

$$\begin{aligned}(R_b - R)^2\frac{\partial u}{\partial t} =& \frac{\partial^2 u}{\partial \eta^2} - \frac{(\rho - 1)(R_b - R)^2R^2}{[R + \eta(R_b - R)]^3}R_t u \\ &+ (R_b - R)\left\{\left[1 + \frac{(\rho - 1)R^2}{[R + \eta(R_b - R)]^2} - \eta\right]R_t + \eta R_{bt}\right\}\frac{\partial u}{\partial \eta} \ ,\end{aligned} \tag{3.35}$$

on $0 < \eta < 1$. These two equations are subject to the boundary conditions $v(0,t) = 0$, $v(1,t) = u(0,t) = -\Gamma$ and $u(R_b,t) = R_b$. The initial conditions will be discussed below. The Stefan condition may now be written as

$$\rho\beta R^2\frac{dR}{dt} + \gamma R^2\left(\frac{dR}{dt}\right)^3 = k\frac{\partial v}{\partial \xi}\bigg|_{\xi=1} - \frac{R}{(R_b - R)}\frac{\partial u}{\partial \eta}\bigg|_{\eta=0} + (k-1)\Gamma \ , \tag{3.36}$$

where $R(0) = 1$.

A semi-implicit scheme may now be employed on the system, discretizing implicitly for u, v and explicitly for R, R_t in (3.34)-(3.35). The discrete forms of the partial derivatives are

$$\frac{\partial v}{\partial t} = \frac{v_i^{n+1} - v_i^n}{\Delta t}, \qquad \frac{\partial v}{\partial \xi} = \frac{v_{i+1}^{n+1} - v_{i-1}^{n+1}}{2\Delta\xi}, \qquad \frac{\partial^2 v}{\partial \xi^2} = \frac{v_{i+1}^{n+1} - 2v_i^{n+1} + v_{i-1}^{n+1}}{\Delta\xi^2} \ , \tag{3.37}$$

where $i = 1, \ldots, I$ and $n = 1, \ldots, N$, and analogously for u. Using these derivative definitions equations (3.34)-(3.35) can be expressed as a matrix system which are solved at each time step n. The position of the melt front is obtained from (3.36) using the time derivative

$$\frac{dR}{dt} = \frac{R^{n+1} - R^n}{\Delta t} \ , \tag{3.38}$$

and a three point backward difference for the partial derivatives.

As mentioned earlier, the initial condition can be problematic. There are two reasons for this: firstly the liquid phase does not even exist at $t = 0$, secondly there is a discontinuity between the imposed boundary condition $u(1, t) = 1$ and the initial condition $u(r, 0) = -\Gamma$ which results in an infinite velocity at $t = 0$. So, in order to specify a numerical scheme that does not immediately blow up conditions must be determined for some small time $t > 0$, where a liquid phase exists and the velocity may be large, but not infinite. This may be achieved utilising the limiting cases discussed in the previous section. Substituting (3.33) into (3.35) and (3.36) and allowing $t \to 0$ leads to the following boundary value problem for temperature in the liquid when $\gamma \neq 0$

$$\frac{d^2u}{d\eta^2} = 0, \quad u(0) = -\Gamma, \quad u(1) = 1, \quad \left(\frac{3}{4}\right)^3 \lambda_1^4 \rho = \left.\frac{du}{d\eta}\right|_{\eta=0} . \tag{3.39}$$

This has the solution

$$u = (\Gamma + 1)\eta - \Gamma, \qquad \lambda_1 = \left(\frac{4}{3}\right)^{3/4} \left(\frac{\Gamma + 1}{\rho}\right)^{1/4} . \tag{3.40}$$

Note, the above expression determines λ_1 for equation (3.33).

In the case $\gamma = 0$ we obtain

$$\frac{d^2u}{d\eta^2} - \frac{\lambda_2^2}{2}(1 - \eta)\frac{du}{d\eta} = 0, \quad u(0) = -\Gamma, \quad u(1) = 1, \quad \beta\frac{\lambda_2^2}{2} = \left.\frac{du}{d\eta}\right|_{\eta=0} . \tag{3.41}$$

Although more complex than the previous case, this is a standard thermal problem with

solution

$$u = 1 - (1+\Gamma)\frac{\mathrm{erf}\,(\lambda_2(1-\eta)/2)}{\mathrm{erf}\,(\lambda_2/2)}\ , \tag{3.42}$$

where λ_2 satisfies the transcendental equation

$$\frac{1}{2}\sqrt{\pi}\,\beta\,\lambda_2\,e^{\lambda_2^2/4}\ \mathrm{erf}\ (\lambda_2/2) = 1+\Gamma. \tag{3.43}$$

The numerical scheme may now be started at some small time $t > 0$ using equations (3.40) and (3.42)-(3.43) to provide the appropriate temperatures and so avoiding the possible singular behaviour at $t = 0$.

3.5 Results and discussion

In this section we present a set of results for the melting of a spherical nanoparticle. We use data appropriate for gold (as shown in Table 3.1) since this is a very common material for nanoparticles. The density change between solid and liquid gold is within the range of many materials, so it provides typical results.

In Figure 3.2 we plot the evolution of the solid-liquid interface, $R(t)$, for a nanoparticle with initial dimensional radius 100 nm and $\beta = 100$ (which corresponds to relatively slow melting). Two pairs of curves are shown, one for the case $\rho = 1$, the other using the correct value for gold, $\rho \approx 1.116$. The solid lines represent the solution of the equations derived from the perturbation analysis, i.e. the solution for $\rho = 1$ given by (3.29), the other for $\rho = 1.116$ given by (3.27), the dashed line is the numerical solution. In both cases the perturbation solution is very close to the numerical solution, indicating a full numerical analysis is not necessary. It is quite clear that the two sets of solutions lead to very different melt times. When $\rho = 1$ the melt process lasts until $t \approx 4$, with the correct change in density the process lasts until $t \approx 4.7$, an approximately 15% increase. Note, we define the melt time as being the time when our calculation stops (in this case $R \approx 0.004$, below this value the Gibbs-Thomson relation (3.1) predicts a negative melt temperature). As stated in the introduction, the continuum model only holds down to around $R = 2$nm. In fact we expect

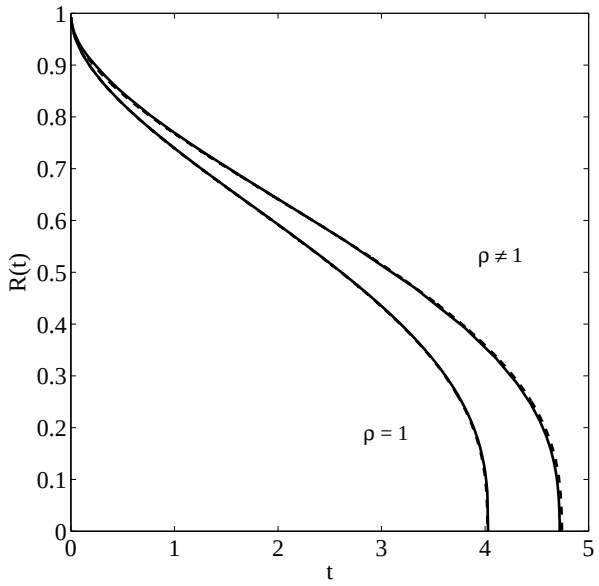

Figure 3.2: Evolution of the nondimensional melting front $R(t)$ for the two cases of study $\rho = 1.116$ and $\rho = 1$, for $\beta = 100$ and $R_0 = 100$ nm. Solid line represents perturbation solution, dashed lines the numerical solution.

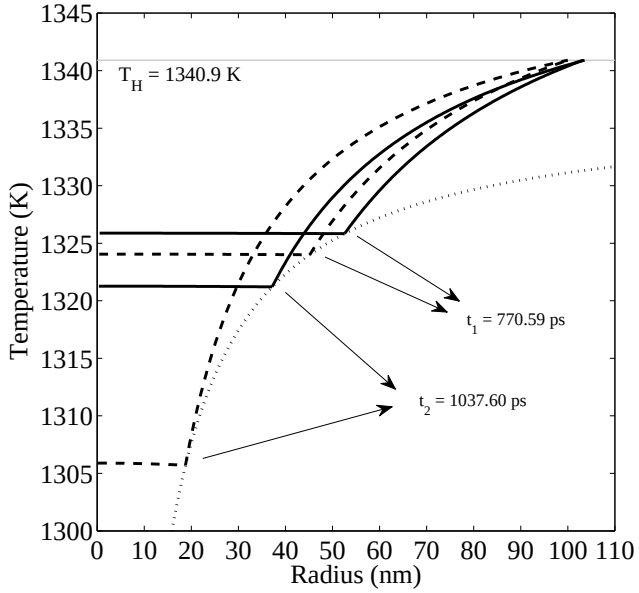

Figure 3.3: Dimensional temperature profiles for curves of Figure 3.2. The solid line represents temperature for $\rho = 1.116$, the dashed line $\rho = 1$ and dotted line shows the melt temperature variation.

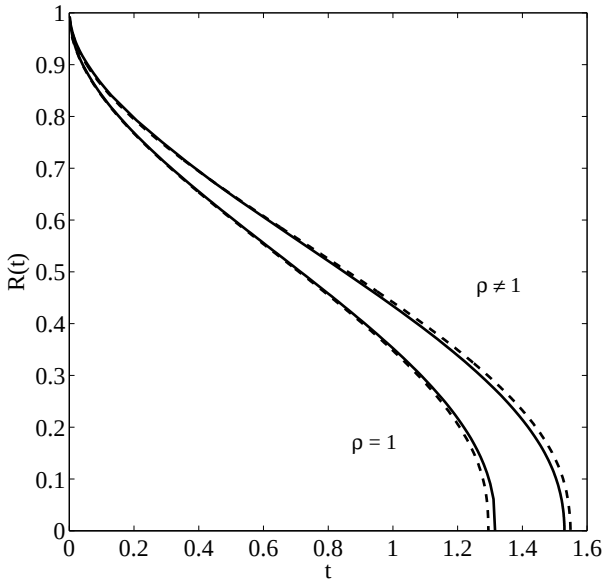

Figure 3.4: Evolution of the nondimensional melting front $R(t)$ for $\rho = 1$ and $\rho = 1.116$, for $\beta = 10$ and $R_0 = 100$ nm.

complete melting (or dissipation of the particle) to occur somewhere between 2 and 0 nm but given that as $R \to 0$ the melt velocity $R_t \to -\infty$ an estimate based on our final value will be very accurate. (If we actually stop the calculation at $R = 2/100$ we find a melt time 0.05% below that predicted by stopping at $R = 0.004$.) Both sets of curves show a melt velocity $R_t \to -\infty$ in the final stages of melting. We associate this with the sudden melting of nanoparticles as $R \to 0$, observed experimentally in [48] and already discussed and analyzed in previous theoretical studies [5, 29, 60].

In Figure 3.3 we present the dimensional temperature profiles corresponding to the curves in Fig. 3.2. We choose the dimensional form to better show the temperature variation and typical times. The curves all come from the numerical solution: the solid line represents the case where $\rho \approx 1.116$ while the dashed line is $\rho = 1$. The dotted line shows the evolution of the melt temperature as the radius decreases. Temperature profiles are shown for two times, $t = 770.59, 1037.6$ps. The dashed lines range between 0 and 100nm while the solid lines have a moving right hand boundary ($R_b = R_b(t)$) and so end at $R_b > R_0$.

In Figure 3.4 we present two sets of results for the same initial radius, but now $\beta = 10$. Since $\beta \propto 1/\Delta T$ we expect faster melting than in the previous example and this is obviously

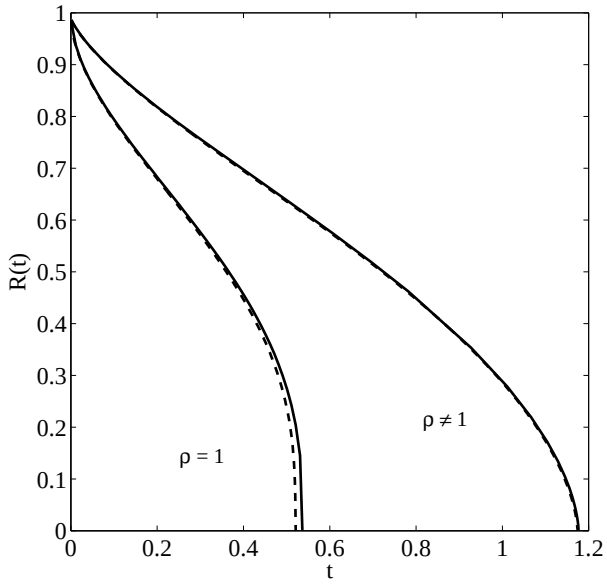

Figure 3.5: Evolution of the nondimensional melting front $R(t)$ for $\rho = 1.116$ and $\rho = 1$, for $\beta = 100$ and $R_0 = 10$ nm. Solid line represents perturbation solution, dashed lines the numerical solution.

the case. Since the perturbation expansion is based on $1/\beta$ it is no surprise that the dashed line is slightly further from the solid line than in Figure 3.2, however the accuracy is still good. Again there is a rapid decrease in radius during the final moments and so we expect the final melting time to be very accurate, whether measured at $R = 2/100$ or closer to $R = 0$.

Figures 3.5–3.7 show results for a particle with initial radius $R_0 = 10$nm. All features are qualitatively similar to those of the 100nm particle figures, with an obvious reduction in melt times. In the case of Fig. 3.5, where $\beta = 100$, ending the calculation close to $R = 0$ or at $R = 2/10$ results in a 7% difference in melt times. Choosing $\rho = 1$ rather than the true value will give a more than 55% decrease in melt time. In Fig. 3.7, where $\beta = 10$, the decrease is greater than 60%. Fig. 3.6 shows the temperature profiles corresponding to Fig 3.5. An interesting feature is that it is clear the temperature in the solid is greater than the melt temperature and so the solid acts to increase the melt rate (this is also the case in Fig. 3.3, but less obvious). In standard situations, where T_m is constant, the solid acts to slow down melting.

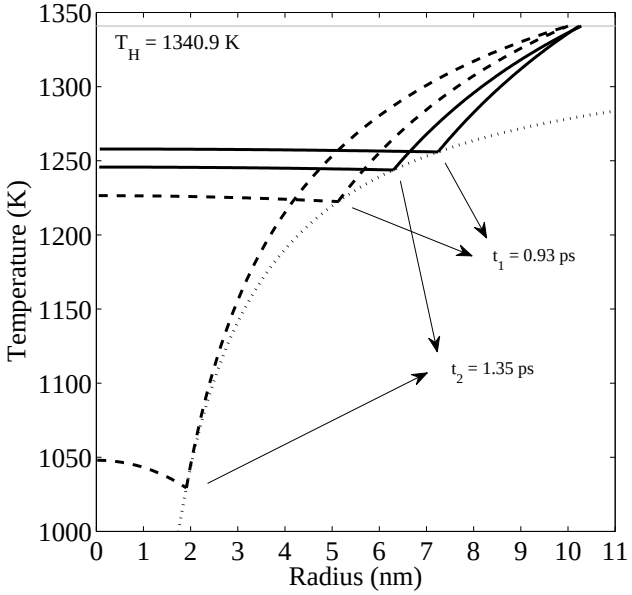

Figure 3.6: Dimensional temperature profiles for curves of Figure 3.5. The solid line represents temperature for $\rho = 1.116$, the dashed line $\rho = 1$ and dotted line shows the melt temperature variation.

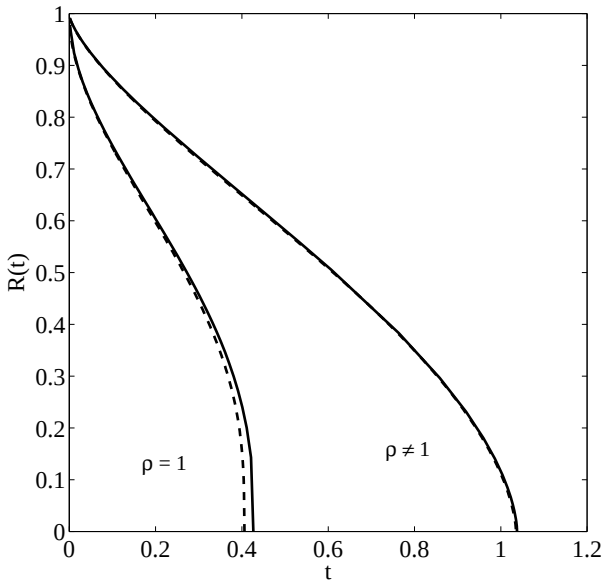

Figure 3.7: Evolution of the nondimensional melting front $R(t)$ for $\rho = 1.116$ and $\rho = 1$, for $\beta = 10$ and $R_0 = 10$ nm. Solid line represents perturbation solution, dashed lines the numerical solution.

In Tables 3.2 and 3.3 we present dimensional melting times for particle radii 10, 50, 100 nm and $\beta = 5, 10, 100$ for $\rho = 1$ and $\rho = 1.116$ respectively. The dimensional times are obtained by multiplying the nondimensional melting time by the time scale $\rho_l c_l R_0^2/k_l$. By comparing the two tables we see that for a particle with $R_0 = 10$ nm, the computed melting times for the case $\rho = 1$ are between 56% (for $\beta = 100$) and 65% (for $\beta = 5$) faster than for the ones corresponding to $\rho = 1.116$. In the second column ($R_0 = 50$ nm), the melting times for the case $\rho = 1$ are between the 16% and 23% faster than those for $\rho = 1.116$. Finally, the third column ($R_0 = 100$ nm) shows differences between the two cases of 15% and 16%. Results for larger particles show that the difference settles at approximately 15%. This difference in melt times carries through to the macro-scale, indicating the importance of incorporating density variation within more standard Stefan problems.

Table 3.2: Melting times for the case $\rho = 1$. Results for gold.

	Melting times (s)		
	$R_0 = 10$ nm	$R_0 = 50$ nm	$R_0 = 100$ nm
$\beta = 100$ ($T_H \approx 1341$ K)	$1.38{\cdot}10^{-12}$	$1.55{\cdot}10^{-10}$	$1.07{\cdot}10^{-9}$
$\beta = 10$ ($T_H \approx 1376$ K)	$1.08{\cdot}10^{-12}$	$0.69{\cdot}10^{-10}$	$0.34{\cdot}10^{-9}$
$\beta = 5$ ($T_H \approx 1415$ K)	$0.89{\cdot}10^{-12}$	$0.45{\cdot}10^{-10}$	$0.21{\cdot}10^{-9}$

Table 3.3: Melting times for the case $\rho = 1.116$. Results for gold.

	Melting times (s)		
	$R_0 = 10$ nm	$R_0 = 50$ nm	$R_0 = 100$ nm
$\beta = 100$ ($T_H \approx 1341$ K)	$3.12{\cdot}10^{-12}$	$1.84{\cdot}10^{-10}$	$1.26{\cdot}10^{-9}$
$\beta = 10$ ($T_H \approx 1376$ K)	$2.75{\cdot}10^{-12}$	$0.85{\cdot}10^{-10}$	$0.41{\cdot}10^{-9}$
$\beta = 5$ ($T_H \approx 1415$ K)	$2.49{\cdot}10^{-12}$	$0.58{\cdot}10^{-10}$	$0.25{\cdot}10^{-9}$

The physical mechanism behind the slower melting when $\rho = 1.116$ is easily explained by considering the energy in the system. Melting occurs due to heat being input at the boundary R_b. When $\rho = 1$ this energy goes to heating up the material and driving the phase change. However, when $\rho = 1.116$ the fluid must move due to the expansion (or contraction depending on the material) caused by the phase change. This provides another energy sink, namely kinetic energy, which then results in less energy available to melt the material. Mathematically we can see from equation (3.33) that when $\rho = 1$ the initial melt rate $R_t \propto t^{-1/2}$ is much greater than when $\rho = 1.116$, $R_t \propto t^{-1/4}$.

In Figure 3.8 we demonstrate the relative strength of the two terms constituting the left hand side of equation (3.15), which represent latent heat release and kinetic energy, for the cases where $R_0 = 10, 100$ nm and $\beta = 10$. The dashed line shows the result for $R_0 = 10$ nm. Since its value is close to or greater than unity throughout the melt process this signifies the cubic term is generally dominant. When $R_0 = 100$ nm the cubic term is negligible for most of the process, but the peaks at the beginning and end mean that it still plays an important role there. Decreasing γ further will push the position of the peaks towards the initial and final times, but will never remove them. Consequently kinetic energy will always play some role in the energy balance provided $\gamma \neq 0$.

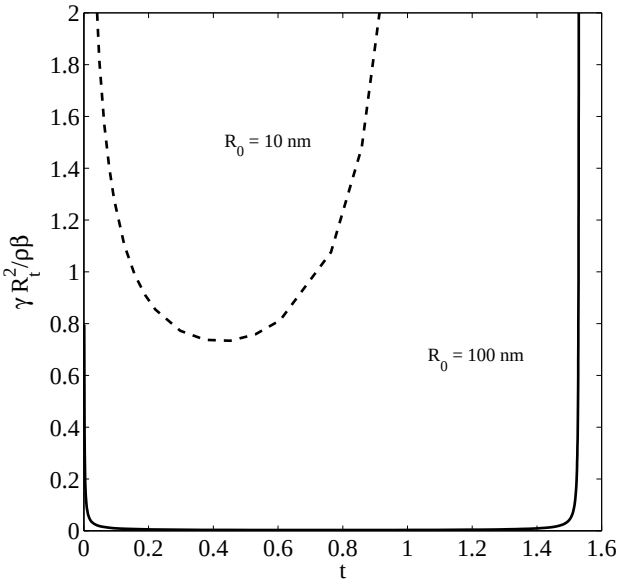

Figure 3.8: Relative importance of the term γR_t^3 against $\rho\beta R_t$ for $\beta = 10$, for nanoparticles with radius $R_0 = 100$ nm (solid line) and $R_0 = 10$ nm (dashed line).

With no experimental results which exactly describe our theoretical models we must rely on similar studies to provide estimates and at least quantitative agreement. For instance, in [84] the melting of gold nanoparticles is studied experimentally by time resolved x-ray scattering when heated up by a laser beam. They find that the time to complete melting is less than 100 ps for nanoparticles with $R_0 = 50$ nm. In [90] the melting of 2 and 20 nm gold nanoparticles is studied, finding melting times on the picosecond scale. Our results show indeed the right order of magnitude, however we are not aware of the existence of any experimental studies that could further validate the accuracy of our results.

3.6 Conclusions

The main aim of this chapter was to determine whether the standard modelling assumption, that the density remains constant throughout the phase change, is valid in the context of nanoparticle melting. Our results clearly show that as the particle radius decreases the effect of the density change becomes increasingly important. We presented results for the melting

of gold and found that melt times for a particle with initial radius 10 nm were more than doubled when the density ratio was changed from $\rho = 1$ to $\rho \approx 1.116$. This increase in melt time may be attributed to the fact that with $\rho = 1$ the liquid phase remains stationary so all energy input into the system is converted to heat or to drive the phase change. If $\rho = 1.116$ then the liquid is forced to move which requires kinetic energy and means less energy is available for the phase change.

We therefore conclude that any mathematical model of nanoparticle melting should incorporate density variation. In fact our results show an even stronger conclusion, namely that in general the density variation should be included in phase change models regardless of size. In the case studied in the present chapter the difference in melt times (neglecting or including density variation) tended to a limit of approximately 15% as the particle size increased.

Chapter 4

Solidification of supercooled melts

F. Font, S.L. Mitchell, T.G. Myers. *One-dimensional solidification of supercooled melts*
International Journal of Heat and Mass Transfer, 62, 411-421 (2013)
Impact factor: 2.315

Abstract

In this chapter a one-phase supercooled Stefan problem, with a nonlinear relation between the phase change temperature and front velocity, is analysed. The model with the standard linear approximation, valid for small supercooling, is first examined asymptotically. The nonlinear case is more difficult to analyse and only two simple asymptotic results are found. Then, we apply an accurate Heat Balance Integral Method to make further progress. Finally, we compare the results found against numerical solutions. The results show that for large supercooling the linear model may be highly inaccurate and even qualitatively incorrect. Similarly as the Stefan number $\beta \to 1^+$ the classic Neumann solution which exists down to $\beta = 1$ is far from the linear and nonlinear supercooled solutions and can significantly overpredict the solidification rate.

4.1 Introduction

Supercooled liquids can solidify much more rapidly than a non-supercooled liquid and when rapid solidification occurs the liquid may not have time to form its usual crystalline structure. Materials made from supercooled melts can therefore have markedly different properties to the standard form of the material. A material formed from a supercooled liquid, usually called a glassy or amorphous solid, can present greater corrosion resistance, toughness, strength, hardness and elasticity than common materials: amorphous metal alloys can be twice as strong and three times more elastic than steel. Such materials are currently used in medicine, defence and aerospace equipment, electronics and sports [109, 95, 111]. Recent advances in the production and use of amorphous solids provides the motivation for this theoretical study on the solidification of a supercooled liquid.

Theoretical investigations of Stefan problems have focussed primarily on the situation where the phase change temperature is constant. However, there are various applications where this temperature changes from its standard value (the heterogenoeus nucleation temperature) and may even vary with time. One method to reduce the freezing point is to increase the ambient pressure. This method is exploited in the food industry, whereby the sample is cooled well below the normal freezing temperature by applying a high pressure. The pressure is then released and almost instantaneous freezing occurs. This permits the freezing of certain products that normally spoil when frozen more slowly. The technique is also used in cryopreservation [54]. Pressure may also vary due to surface tension effects at a curved interface. Hence freezing fronts with high curvature may exhibit a variable phase change temperature. Another mechanism for varying the phase change temperature occurs when a liquid is supercooled or undercooled (we will use both terms in the following work), that is, the liquid is cooled below the heterogeneous nucleation temperature. In this situation the liquid molecules have little energy which affects their mobility and hence their ability to move to the solid interface [4, 19].

In this chapter we focus on the final mechanism, where the liquid is supercooled. In the standard Stefan problem the phase change temperature is specified as a constant, say

T_m, and the speed of the phase change front is related to the temperature gradient in the surrounding phases. When modelling the solidification of a supercooled liquid, the phase change temperature is unknown and so a further equation is required, which relates the speed of the front to the degree of supercooling. If we denote the temperature at which the phase change occurs as T_I and $s(t)$ as the position of the front then a typical form for the relation between the front velocity, s_t, and the degree of supercooling is shown in Figure 4.1. The left hand plot represents the copper solidification process, the right hand plot represents salol (which occurs at a slow rate and so provides relatively simple experiments). Both curves have the same qualitative form. For a small degree of supercooling, *i.e.* for copper $T_m - T_I < 250$ K, the speed of the front increases as the supercooling increases. This behaviour seems physically sensible, the cooler the sample the more rapid the freezing. However, for larger supercooling the process slows down as the molecules become more 'sluggish' due to a lack of energy. The maximum solidification rate for copper is around 2.9m/s, for salol it is around 4.4 $\times 10^{-5}$m/s (making salol a more popular choice for experimental studies).

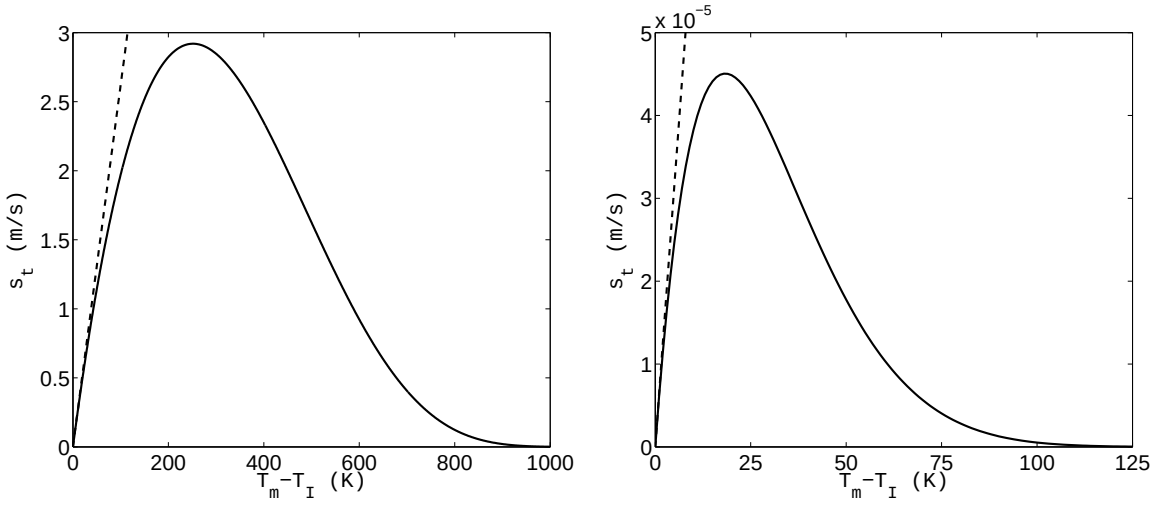

Figure 4.1: Representation of the solidification speed of copper (left) and salol (right) as a function of the supercooling. The solid line represents the full expression for s_t, the dashed line the linear approximation.

Using a statistical mechanics argument, it is shown in Ashby & Jones [4, Chap. 6] that

the solidification rate may be approximated by

$$s_t = \frac{d\Delta h}{6hT_m} e^{-\frac{q}{kT_I}} (T_m - T_I) \ , \tag{4.1}$$

where d is the molecular diameter, h the Planck constant, q the activation energy and k the Boltzmann constant. The parameter Δh is the product of the latent heat and the molecular weight divided by Avogadro's number (for salol $\Delta h \approx 2.14 \times 10^{-1}$ kg/mol, for Cu $\Delta h \approx 6.35 \times 10^{-2}$ kg/mol. A linearised version of eq. (4.1) is often dealt with in the literature, [15, 23, 25, 58, 62],

$$T_I(t) = T_m - \phi s_t \ , \tag{4.2}$$

where $\phi = 6hT_m e^{\frac{q}{kT_m}}/(d\Delta h)$. This expression for ϕ provides one interpretation of the usual kinetic undercooling coefficient described, for example, in [19, 15, 25]. The solid lines in Figure 4.1 were obtained by plotting eq. (4.1) using the parameter values of Table 4.1, the dashed lines come from eq. (4.2).

The classical Neumann solution to the Stefan problem with fixed boundary and constant far field temperature requires setting $\phi = 0$ in (4.2). With the Neumann solution the interface velocity increases as the Stefan number β decreases: as $\beta \to 1^+$ the velocity tends to infinity and the Neumann solution breaks down (where the Stefan number is the ratio of latent to sensible heat). In order to obtain solutions for Stefan numbers $\beta \leq 1$, numerous authors have adopted the linear profile, with $\phi \neq 0$, which removes the infinite boundary velocity. Incorporating the effects of the linear interfacial kinetics into the Stefan problem, by using (4.2), results in different solution behaviour depending on the value of β: for $\beta > 1$ the velocity $s_t \propto t^{-1/2}$ (as occurs with the Neumann solution), when $\beta = 1$ it changes to $s_t \propto t^{-1/3}$ and for $\beta < 1$, s_t is constant (and the temperature is a travelling wave solution), see [19]. The short time solution given in [15] has s_t constant at leading order with a first order correction of $t^{1/2}$, valid for all β.

In the following work we will study the one-phase solidification process subject to arbitrary supercooling and so employ eq. (4.1) to determine the interface temperature T_I. In section 4.3 we make a similarity substitution to simplify the governing equations and then

look for approximate small and large time solutions. In section 4.3.2 we investigate the linear supercooled model to reproduce all the different behaviours mentioned above (which are usually generated via different analytical techniques). In section 4.3.3 we find a small time solution, valid for all β, and a large time solution valid for $\beta < 1$. We are not aware of any such analysis on the nonlinear model in the literature. In section 4.4 we describe an accurate Heat Balance Integral Method (HBIM) and show how the resultant equations can reproduce all the behaviours predicted for linear supercooling. Further, using this method we can find the same range of behaviour for nonlinear supercooling at large times. In section 4.5 we present results for the asymptotic and HBIM models and compare them with a numerical solution.

4.2 Mathematical model

We consider a one-dimensional supercooled liquid initially occupying $x \geq 0$, with solidification starting at the point $(x,\, t) = (0,\, 0)$. An appropriate one-phase Stefan problem is then specified by

$$\frac{\partial T}{\partial t} = \alpha_l \frac{\partial^2 T}{\partial x^2} \ , \qquad s < x < \infty \ , \tag{4.3}$$

$$T = T_I(t) \ , \qquad \rho_l L_m s_t = -k_l \frac{\partial T}{\partial x} \ , \qquad \text{at } x = s \ , \tag{4.4}$$

$$T \to T_\infty \ , \qquad \text{as } x \to \infty \ , \tag{4.5}$$

$$T(x, 0) = T_\infty \ , \qquad s(0) = 0 \ , \tag{4.6}$$

where $T_\infty < T_m$. The parameters $\alpha_l, \rho_l, L_m, k_l$ represent the thermal diffusivity, density, latent heat and conductivity of the liquid, respectively. Typical parameter values are presented in Table 4.1. The interface temperature is related to the interface velocity by eq. (4.1). The linearised version is given by (4.2) and setting $\phi = 0$ in this equation brings us back to the standard condition that the interface temperature takes the constant value T_m. Note, the system (4.3)-(4.6) in fact loses energy. In [25] this issue is discussed in detail and an energy conserving form is presented which is valid in the limit $k_s/k_l \to 0$. However, this limit is

Substance	T_m (K) ($\times 10^3$)	L_m (J/kg) ($\times 10^5$)	c_l (J/kg·K) ($\times 10^3$)	ρ_l (kg/m^3) ($\times 10^3$)	k_l (W/m·K)	q (J) ($\times 10^{-20}$)	d (m) ($\times 10^{-9}$)
Copper	1.36	2.09	0.53	8.02	157.18	6.71	0.23
Salol	0.316	0.90	1.58	1.18	0.18	6.61	1.00

Table 4.1: Approximate thermodynamical parameter values for Cu and Salol, taken from [4, 9, 24, 61].

physically unrealistic and in [74] the reduction in the limit $k_s/k_l \to \infty$ is determined. Results there are shown for the two limiting cases and the basic one-phase reduction of (4.3)-(4.6) which are then compared against the numerics for the full two-phase problem. It is shown that the reduction (4.3)-(4.6) gives a reasonable approximation and is in fact more accurate than the energy conserving form with $k_s/k_l \to 0$. So, since (4.3)-(4.6) is the most common form we retain it for this paper.

The system (4.3)-(4.6) may be nondimensionalised with

$$\hat{T} = \frac{T - T_m}{\Delta T} , \qquad \hat{t} = \frac{t}{\mathcal{T}} , \qquad \hat{x} = \frac{x}{L} , \qquad \hat{s} = \frac{s}{L} , \qquad \hat{T}_I = \frac{T_I - T_m}{\Delta T} , \tag{4.7}$$

where $\mathcal{T} = L^2/\alpha_l$ and $L = \phi\alpha_l/\Delta T$. The temperature scale is $\Delta T = T_m - T_\infty$. The length-scale is determined from eq. (4.1), however if $T_I = T_m$ there is no natural length-scale and it must be left arbitrary. Dropping the hat notation the governing equations are now

$$\frac{\partial T}{\partial t} = \frac{\partial^2 T}{\partial x^2} , \qquad s < x < \infty , \tag{4.8}$$

$$T = T_I(t) , \qquad \beta s_t = -\frac{\partial T}{\partial x} , \qquad \text{at } x = s , \tag{4.9}$$

$$T \to -1 , \qquad \text{as } x \to \infty , \tag{4.10}$$

$$T(x, 0) = -1 , \qquad s(0) = 0 , \tag{4.11}$$

where $\beta = L_m/(c_l\Delta T)$. The nondimensional interface temperature T_I is determined from

$$s_t = -T_I \exp\left(\frac{QT_I}{P + T_I}\right) , \tag{4.12}$$

where $Q = q/(kT_m)$ and $P = T_m/\Delta T$. The case of no supercooling is retrieved by setting

$T_I(t) = 0$ in (4.9) and then (4.12) is not used, small supercooling requires ΔT to be small such that $P \to \infty$ and the exponential term of (4.12) may be set to unity, then $s_t = -T_I(t)$. Otherwise, the full expression in (4.12) is used to determine T_I.

When $T_I(t)$ is not identically zero then we require an initial value (and also one for s_t). Noting that $T(x,0) = -1$ and $T_I(t) = T(s,t)$ then $s(0) = 0$ indicates that $T_I(0) = T(0,0) = -1$. An initial (finite) value for s_t may then be found by substituting $T_I(0) = -1$ into eq. (4.12). The linearised version simply leads to $s_t(0) = 1$. In the case $T_I \equiv 0$ then as $t \to 0$ the discontinuity in temperature due to the conflicting conditions $T(0,0) = 0, T(x,0) = -1$ cannot be avoided. This indicates that the front velocity $s_t = -T_x(s,t)$ is infinite at $t = 0$ (this will become clear in subsequent sections).

Before proceeding further, it is convenient to immobilise the boundary by setting

$$y = x - s \ , \qquad T(x,t) = F(y,t) \ . \tag{4.13}$$

Then the system (4.8)-(4.11) becomes

$$\frac{\partial^2 F}{\partial y^2} = \frac{\partial F}{\partial t} - s_t \frac{\partial F}{\partial y} \ , \qquad 0 < y < \infty \ , \tag{4.14}$$

$$F = T_I(t) \ , \quad \beta s_t = -\frac{\partial F}{\partial y} \ , \qquad \text{at } y = 0 \ , \tag{4.15}$$

$$F \to -1 \ , \qquad \text{as } y \to \infty \ , \tag{4.16}$$

$$F(y,0) = -1 \ , \qquad s(0) = 0 \ . \tag{4.17}$$

In the following we will analyse this system further.

4.3 Asymptotic analysis

Most exact solutions to Stefan problems, where they exist, can be obtained by similarity methods. Hence, we begin by looking for similarity solutions to the system (4.14)-(4.17) and so define

$$\eta = \frac{y}{t^\alpha} \ , \qquad F(y,t) = G(\eta) \ . \tag{4.18}$$

The governing equations (4.14)-(4.16) are now

$$G'' = -\Big(\alpha\eta t^{2\alpha-1} + t^{\alpha}s_t\Big)G' \ , \qquad 0 < \eta < \infty \ , \tag{4.19}$$

$$G(0) = T_I(t) \ , \qquad G|_{\eta\to\infty} \to -1 \ , \qquad \beta t^{\alpha}s_t = -G'(0) \ , \tag{4.20}$$

with $s(0) = 0$, and primes denote differentiation with respect to η. Denoting $\nu = -G'(0)/\beta \geq 0$ we use the Stefan condition to eliminate $t^{\alpha}s_t$ from (4.19) and so the model becomes

$$G'' = -\Big(\alpha\eta t^{2\alpha-1} + \nu\Big)G' \ , \qquad 0 < \eta < \infty \ , \tag{4.21}$$

$$G(0) = T_I(t) \ , \qquad G|_{\eta\to\infty} \to -1 \ , \qquad t^{\alpha}s_t = \nu \ , \qquad s(0) = 0 \ . \tag{4.22}$$

Since $G = G(\eta)$ this system is strictly only valid when the t dependence is removed from the equations involving G. In (4.21) this is achieved by setting $\alpha = 0$ or $1/2$ but then we must also take into account the boundary condition $G(0) = T_I(t)$.

4.3.1 No kinetic undercooling

The classical formulation for the one-phase supercooled Stefan problem with no kinetic undercooling is obtained by setting $T_I(t) = 0$ [19]. In this case we choose $\alpha = 1/2$ and so the governing eqs (4.21)-(4.22) are now

$$G'' = -\left(\frac{\eta}{2} + \nu\right)G' \ , \qquad 0 < \eta < \infty \ , \tag{4.23}$$

$$G(0) = 0 \ , \quad t^{1/2}s_t = \nu \ , \qquad G|_{\eta\to\infty} \to -1 \ . \tag{4.24}$$

Integrating the Stefan condition gives $s = 2\nu\sqrt{t}$ and the solution for G is

$$G(\eta) = -1 + \frac{\operatorname{erfc}\left(\eta/2 + \nu\right))}{\operatorname{erfc}\left(\nu\right)} \ , \qquad s = 2\nu\sqrt{t} \ . \tag{4.25}$$

The definition of $\nu = -G'(0)/\beta$ then leads to the transcendental equation

$$\beta\sqrt{\pi}\nu \operatorname{erfc}(\nu)e^{\nu^2} = 1 \ . \tag{4.26}$$

In the original variables the solution is

$$T = -1 + \frac{\operatorname{erfc}\left(x/(2\sqrt{t})\right)}{\operatorname{erfc}\left(\nu\right)} \ , \qquad s = 2\nu\sqrt{t} \ , \qquad s_t = \frac{\nu}{\sqrt{t}} \ , \tag{4.27}$$

together with (4.26) this defines the well-known Neumann solution[19]. The values of ν and hence the velocity of the phase change front are therefore dependent on $\beta = L_m/(c_l\Delta T)$. As mentioned earlier, this solution has infinite velocity at $t = 0$ (since $s_t \propto 1/\sqrt{t}$). Eq. (4.26) determines $\nu(\beta)$, it has a unique solution for $\beta > 1$ but when $\beta \leq 1$ no solution exists; as $\beta \to 1^+$, $\nu \to \infty$ and the front velocity is ∞ for all time.

4.3.2 Linear kinetic undercooling

Small time solutions

As discussed in section 4.2, without kinetic undercooling the initial boundary temperature is fixed, $T(0,0) = 0$, thus forcing an initial infinite temperature gradient. With kinetic undercooling $T(0,0) = T_I(0) \approx -1$ permits a finite temperature gradient. This indicates the need for different scalings at small times.

Let us now consider the governing eqs (4.14)-(4.17). Noting that $F(y,0) = -1$ we look for a small time similarity solution close to $F = -1$ and so re-define the function $G(\eta)$ as

$$\eta = \frac{y}{t^{1/2}} \ , \qquad F(y,t) = -1 + t^{1/2}G(\eta) \ . \tag{4.28}$$

This transforms eqs (4.14)-(4.17) into

$$G'' = \frac{1}{2}G - \frac{\eta}{2}G' - t^{1/2}s_tG' \ , \qquad 0 < \eta < \infty \ , \tag{4.29}$$

$$-1 + t^{1/2}G(0) = -s_t \ , \quad \beta s_t = -G'(0) \ , \qquad G|_{\eta\to\infty} \to 0 \ . \tag{4.30}$$

The factor $t^{1/2}$ in front of $G(\eta)$ in (4.28) is chosen to balance the Stefan condition in (4.30) and then it follows that $s \propto t$. This leaves time in the governing eq. (4.29) and the boundary condition (4.30a): for this reason we make the small time substitution $t = \epsilon\tau$, $s = \epsilon r$, where

ϵ is an artificial small parameter [12, 51], to find

$$G'' = \frac{1}{2}G - \frac{\eta}{2}G' - \epsilon^{1/2}\tau^{1/2}r_\tau G' \ , \qquad 0 < \eta < \infty \ , \tag{4.31}$$

$$-1 + \epsilon^{1/2}\tau^{1/2}G(0) = -r_\tau \ , \quad r_\tau = \nu \ , \qquad G|_{\eta\to\infty} \to 0 \ . \tag{4.32}$$

This form motivates a perturbation series with $G(\eta) = G_0(\eta) + \mathcal{O}(\epsilon^{1/2})$ and $r(\tau) = r_0(\tau) + \epsilon^{1/2}r_1(\tau) + \mathcal{O}(\epsilon)$, i.e. the leading order form for G is independent of τ but this is not necessarily true for r. The leading order problem is then

$$G_0'' = \frac{1}{2}G_0 - \frac{\eta}{2}G_0' \ , \qquad 0 < \eta < \infty \ , \tag{4.33}$$

$$1 = r_{0\tau} \ , \quad r_{0\tau} = \nu \ , \qquad G_0|_{\eta\to\infty} = 0 \ . \tag{4.34}$$

Combining the first two boundary conditions in (4.34) shows that $\nu = 1$ and this provides the second boundary condition for G_0, namely $G_0'(0) = -\beta$ (since $\nu = -G'(0)/\beta$). The solution is then

$$G_0(\eta) = \beta\left[\frac{2}{\sqrt{\pi}}e^{-\eta^2/4} - \eta\,\mathrm{erfc}\left(\frac{\eta}{2}\right)\right] \ , \qquad r_0(\tau) = \tau \ . \tag{4.35}$$

Although the self-similarity assumption in (4.28) does not permit us to solve for the temperature at first order, eq. (4.32a) indicates that

$$r_{1\tau} = -\tau^{1/2}G_0(0) \qquad \Rightarrow \qquad r_1 = -\frac{4\beta\tau^{3/2}}{3\sqrt{\pi}} \ ,$$

where we have used the value $G_0(0) = 2\beta/\sqrt{\pi}$. Writing this solution back in the original variables gives

$$T(x,t) \approx -1 + \beta\left[2\sqrt{\frac{t}{\pi}}\exp\left(-\frac{(x-s)^2}{4t}\right) - (x-s)\mathrm{erfc}\left(\frac{x-s}{2\sqrt{t}}\right)\right] \ , \tag{4.36}$$

$$s \approx t\left[1 - \frac{4\beta}{3\sqrt{\pi}}\sqrt{t}\right] \ , \qquad s_t \approx 1 - \frac{2\beta}{\sqrt{\pi}}\sqrt{t}\,. \tag{4.37}$$

Recall that the temperature is accurate only to leading order whilst the position of the front

is accurate to first order. Note, we will see the condition $s_t \to 1$ as $t \to 0$ arising below for various other cases.

Large time solutions

For sufficiently small times, the solution of the previous section holds for any value of β (although restrictions are imposed due to the linearisation of the relation $s_t(T_I)$, this is discussed in section 4.3.3). The large time solution, on the other hand, takes different forms depending on whether β is greater, less than or equal to 1.

Case $\beta < 1$: In this case we choose $\alpha = 0$, in (4.18), and the governing eqs (4.21)-(4.22) reduce to

$$G'' = -\nu G' \ , \qquad 0 < \eta < \infty \ , \tag{4.38}$$

$$G(0) = -s_t \ , \qquad G|_{\eta\to\infty} \to -1 \ , \qquad s_t = \nu \ , \qquad s(0) = 0 \ . \tag{4.39}$$

Note, now $\eta = y = x - s$, which indicates a travelling wave solution. The travelling wave formulation differs from the other forms of similarity solution. In general the similarity transformation $\eta = y/t^\alpha$ with $\alpha \neq 0$ allows the far-field and initial conditions to be combined, that is $\eta \to \infty$ when $x \to \infty$ or $t \to 0$. When $\alpha = 0$, the limit $t \to 0$ requires $s \to 0$ and since $0 \leq x \leq s$ the co-ordinate $\eta = x - s \to 0$. So in this case the initial condition must coincide with the left hand boundary condition. Since initially the temperature is everywhere at $T(x,t) = G(\eta) = -1$, the condition $G(0) = -s_t$ then requires $s_t = 1$.

The Stefan condition integrates immediately to give $s(t) = \nu t$ and this may be used to remove the time dependence in the boundary condition $G(0) = \nu$. Integrating the governing eq. (4.38) and applying the boundary conditions in (4.39) leads to

$$G = -1 + (1 - \nu)e^{-\nu\eta} \ . \tag{4.40}$$

To determine the value of ν we now use the above solution and the definition $\nu = -G'(0)/\beta$

to show that $\nu = 1 - \beta$ and hence

$$G = -1 + \beta e^{-\eta(1-\beta)} \ , \qquad s = (1-\beta)t \ , \tag{4.41}$$

which is obviously a travelling wave. Since the front propagates in the positive η direction, $s_t > 0$, the solution is restricted to values $\beta < 1$.

The travelling wave solution describes a constant shape that propagates with time: the temperature and temperature gradient are constant at the moving front $G(0) = -1 + \beta$, $G_\eta(0) = -\beta(1-\beta)$. However, we noted above that for $T_I(t) \neq 0$ the initial condition is $s_t(0) = 1$ but here we have $s_t(0) = 1 - \beta \neq 1$: in other words, we do not satisfy the initial condition. The travelling wave solution is commonly quoted as an exact solution to Stefan problems but in this case it may only be considered as a large time solution and this will become clear when we compare against the numerics. With this in mind we should not apply $s(0) = 0$ and the results in the original variables are

$$T = -1 + \beta e^{-(1-\beta)(x-s)} \ , \qquad s = (1-\beta)t + C_0 \ , \qquad s_t = (1-\beta) \ . \tag{4.42}$$

Case $\beta > 1$: For $\beta > 1$ we can make progress by applying a large time substitution $t = \tau/\epsilon$ to (4.21)-(4.22) but now with $\alpha = 1/2$. The Stefan condition (4.22b) then implies scaling $s = r/\epsilon^{1/2}$ and the governing equations are

$$G'' = -\left(\nu + \frac{\eta}{2}\right) G' \ , \qquad 0 < \eta < \infty \ , \tag{4.43}$$

$$G(0) = -\epsilon^{1/2} r_\tau \ , \quad \tau^{1/2} r_\tau = \nu \ , \qquad G|_{\eta\to\infty} = -1 \ . \tag{4.44}$$

Note, in the previous example we simply solved for G and then found we could not apply the initial condition $s(0) = 0$, hence suggesting a large time solution. Here we begin under the assumption of large time and so do not impose $s(0) = 0$. The Stefan condition then immediately leads to $r = 2\nu\sqrt{\tau} + c_0$, where c_0 is an integration constant. The small parameter in the boundary condition suggests a series solution $G = G_0 + \mathcal{O}(\epsilon^{1/2})$. The leading order problem is then simply the $\alpha = 1/2$ case without kinetic undercooling (4.25)-(4.26) but the

initial condition no longer applies. Viewed from another angle *we can interpret the no kinetic undercooling problem as a large time leading order approximation to the kinetic undercooling problem.* The first order problem has a time-dependent boundary condition and so, as for the small time solution in section 4.3.2, only the leading order problem is consistent with the current similarity transformation.

Writing the solution back in the original variables gives

$$T \approx -1 + \frac{\operatorname{erfc}\left(x/(2\sqrt{t}) - C_1\right)}{\operatorname{erfc}\left(\nu\right)} \ , \qquad s \approx 2\nu\sqrt{t} + C_1 \ , \qquad s_t \approx \frac{\nu}{\sqrt{t}} \ . \tag{4.45}$$

Case $\beta = 1$: It is clear that this intermediate case cannot be found from the arguments given above and the analysis turns out to be more delicate. We therefore study it in more detail.

Instead of the similarity transformation given in (4.18) we define

$$\eta = \frac{y}{t^\alpha} \ , \qquad F(y,t) = G(\eta,t) \ . \tag{4.46}$$

The governing eqs (4.14)-(4.16) are now

$$\frac{\partial^2 G}{\partial \eta^2} = t^{2\alpha}\frac{\partial G}{\partial t} - \left(\alpha\eta t^{2\alpha-1} + t^\alpha s_t\right)\frac{\partial G}{\partial \eta} \ , \qquad 0 < \eta < \infty \ , \tag{4.47}$$

$$G\big|_{\eta=0} = -s_t \ , \qquad G|_{\eta\to\infty} \to -1 \ , \qquad t^\alpha s_t = -\left.\frac{\partial G}{\partial \eta}\right|_{\eta=0} \ , \tag{4.48}$$

again we do not impose $s(0) = 0$.

We apply a large time substitution

$$t = \frac{\tau}{\epsilon} \ , \qquad s = \frac{r}{\epsilon^\gamma} \ , \qquad G(\eta,t) = H(\eta,\tau) \ , \tag{4.49}$$

to equations (4.47)-(4.48), for the moment leaving the exponents α, γ unknown. Then the Stefan condition in (4.48) becomes

$$\tau^\alpha r_\tau = \epsilon^{\alpha+\gamma-1}\left.\frac{\partial H}{\partial \eta}\right|_{\eta=0} \ ,$$

and so we must have $\gamma = 1-\alpha$ for the front to move (at leading order). Hence, the governing equations are

$$\frac{\partial^2 H}{\partial \eta^2} = \tau^{2\alpha}\epsilon^{1-2\alpha}\frac{\partial H}{\partial \tau} - \left(\alpha\eta\tau^{2\alpha-1}\epsilon^{1-2\alpha} + \tau^{\alpha}r_{\tau}\right)\frac{\partial H}{\partial \eta}\ , \qquad 0<\eta<\infty\ , \tag{4.50}$$

$$H\big|_{\eta=0} = -\epsilon^{\alpha}r_{\tau}\ , \qquad H|_{\eta\to\infty}\to -1\ , \qquad \tau^{\alpha}r_{\tau} = -\frac{\partial H}{\partial \eta}\bigg|_{\eta=0}\ . \tag{4.51}$$

From examining (4.50) and (4.51a) it is clear that we require $0<\alpha<1/2$, in order that $\epsilon^{1-2\alpha}$, $\epsilon^{\alpha}\to 0$ as $\epsilon\to 0$. We now introduce expansions

$$H(\eta,\tau) = H_0(\eta) + \epsilon^{1-2\alpha}\tau^{\theta}H_1(\eta) + \dots\ , \qquad r(\tau) = r_0(\tau) + \epsilon^{1-2\alpha}r_1(\tau) + \dots\ , \tag{4.52}$$

where again θ is left unspecified. Substituting these expansions into (4.50)-(4.51) gives the leading order problem

$$H_0''(\eta) = -\nu_0 H_0'(\eta)\ , \qquad 0<\eta<\infty\ , \tag{4.53}$$

$$H_0(0) = 0\ , \qquad H_0|_{\eta\to\infty}\to -1\ , \qquad \tau^{\alpha}r_{0\tau} = \nu_0\ , \tag{4.54}$$

where $\nu_0 = -H_0'(0)$. This has solution

$$H_0(\eta) = -1 + e^{-\nu_0\eta}\ , \qquad r_0 = \frac{\nu_0}{1-\alpha}\tau^{1-\alpha} + c_0\ , \qquad \beta = 1\ . \tag{4.55}$$

Note, the definition of $\nu_0 = -H_0'(0)$ is automatically satisfied and provides no information. We must then look to the higher order terms to determine ν_0. Neglecting the leading order terms in the boundary condition for $H|_{\eta=0}$ leads to the balance $\epsilon^{1-2\alpha}\tau^{\theta}H_1(0) = -\epsilon^{\alpha}r_{0\tau}$. To make the terms balance we choose $\alpha = 1/3$. Thus the $\mathcal{O}(\epsilon^{1/3})$ problem is

$$\tau^{\theta}H_1''(\eta) = -\frac{\eta}{3}\tau^{-1/3}H_0'(\eta) - \nu_0\tau^{\theta}H_1'(\eta) - \tau^{1/3}r_{1\tau}H_0'(\eta)\ , \qquad 0<\eta<\infty\ , \tag{4.56}$$

$$\tau^{\theta}H_1(0) = -r_{0\tau}\ , \qquad H_1|_{\eta\to\infty}\to 0\ , \qquad \tau^{1/3}r_{1\tau} = -\tau^{\theta}H_1'(0)\ . \tag{4.57}$$

To remove τ from the equations requires setting $\theta = -1/3$. Thus (4.56)-(4.57) reduce to

$$H_1''(\eta) = -\frac{\eta}{3}H_0'(\eta) - \nu_0 H_1'(\eta) - \nu_1 H_0'(\eta) \ , \qquad 0 < \eta < \infty \ , \tag{4.58}$$

$$H_1(0) = -\nu_0 \ , \quad \tau^{2/3} r_{1\tau} = \nu_1 \ , \qquad H_1|_{\eta\to\infty} \to 0 \ , \tag{4.59}$$

where $\nu_1 = -H_1'(0)$. The solution to this system is

$$H_1 = -\frac{1}{6\nu_0^2}\left[2 + 6\nu_0^2\nu_1\eta + 2\nu_0\eta + \nu_0^2\eta^2\right]e^{-\nu_0\eta} \ . \tag{4.60}$$

Substituting for $H_1(0)$ into (4.59a) gives an equation to determine ν_0

$$\nu_0 = \left(\frac{1}{3}\right)^{1/3} \ . \tag{4.61}$$

Finally we may write down the position of the moving front

$$r_0 = \left(\frac{9}{8}\right)^{1/3} \tau^{2/3} + c_0 \ . \tag{4.62}$$

Note, the dependence $r \sim \tau^{2/3}$ is quoted in [19, 15, 58, 62] (without the multiplicative constant). Finally, in the original notation we have

$$T \approx -1 + \exp\left(\frac{x-s}{(3t)^{1/3}}\right) \ , \qquad s \approx \left(\frac{9}{8}\right)^{1/3} t^{2/3} + C_2 \ , \qquad s_t \approx (3t)^{-1/3} \ . \tag{4.63}$$

4.3.3 Nonlinear kinetic undercooling

Theoretically, the Neumann solution holds for any $\beta > 1$. Adopting the linear approximation to the $s_t(T_I)$ relation permits the solution domain to be extended to include $\beta \leq 1$. Taking the values for L_m, c_l for salol given in Table 4.1 indicates $\beta \to 1$ as $\Delta T \to 57$K and this is where the Neumann solution predicts the velocity tends to infinity. However, if we look again at Figure 4.1b) it is clear that the velocity is in fact significantly below its maximum value of 4.5×10^{-5}m/s. Further, the linear model is only valid for $\Delta T < 10$K, that is for $\beta > 5.7$. For copper a similar argument indicates the linear model holds for $\beta > 3.95$. Consequently,

for relatively large values of β neither the Neumann or linear approximations will provide physically realistic solutions and we must deal with the full nonlinear relation (4.12).

Key to the similarity solutions of the previous section was the ability to remove the time dependence from the conditions at $x = s(t)$. The nonlinear relation (4.12) makes this a much more difficult task and so in this section we limit our analysis to small time and travelling wave solutions. In the subsequent section we will then introduce an accurate form of heat balance integral method which permits approximate solutions for further cases.

Small time solutions

Using the previous definitions of η, G as given in section 4.3.2 we obtain eqs (4.29)-(4.30) with the only difference being that in the boundary condition (4.30a) we replace the right hand side with T_I. This relation is then used in eq. (4.12) to give

$$s_t = \left[1 - t^{1/2}G(0)\right] \exp\left\{ \frac{Q\left[-1 + t^{1/2}G(0)\right]}{P + \left[-1 + t^{1/2}G(0)\right]} \right\}. \tag{4.64}$$

We now make the small time substitution $t = \epsilon\tau$, $s = \epsilon r$, and expand the exponential term using a Taylor series expansion. This brings us to the leading order problem specified by eqs (4.33,4.34) but with the condition $r_{0\tau} = 1$ replaced by

$$r_{0\tau} = \exp\left(-\frac{Q}{P-1}\right). \tag{4.65}$$

This has solution

$$G_0 = \beta \exp\left(-\frac{Q}{P-1}\right)\left[\frac{2}{\sqrt{\pi}}e^{-\eta^2/4} - \eta \mathrm{erfc}\left(\frac{\eta}{2}\right)\right], \qquad r_0 = \tau \exp\left(-\frac{Q}{P-1}\right). \tag{4.66}$$

As before we cannot find G_1 but can determine an expression for r_1, namely

$$r_1 = -\exp\left(-\frac{2Q}{P-1}\right)\left[1 - \frac{QP}{(P-1)^2}\right]\tau^{3/2}\frac{4\beta}{3\sqrt{\pi}}. \tag{4.67}$$

Writing the solution back in the original variables leads to

$$T \approx -1 + t^{1/2}\beta \exp\left(-\frac{Q}{P-1}\right)\left[\frac{2}{\sqrt{\pi}}e^{-\frac{(x-s)^2}{4t}} - \left(\frac{x-s}{t^{1/2}}\right)\operatorname{erfc}\left(\frac{x-s}{2t^{1/2}}\right)\right] , \tag{4.68}$$

$$s \approx \exp\left(-\frac{Q}{P-1}\right) t\left\{1 - \exp\left(-\frac{Q}{P-1}\right)\left[1 - \frac{QP}{(P-1)^2}\right]\frac{4\beta}{3\sqrt{\pi}}t^{1/2}\right\} , \tag{4.69}$$

$$s_t \approx \exp\left(-\frac{Q}{P-1}\right)\left\{1 - \exp\left(-\frac{Q}{P-1}\right)\left[1 - \frac{QP}{(P-1)^2}\right]\frac{2\beta}{\sqrt{\pi}}t^{1/2}\right\} . \tag{4.70}$$

Large time solutions

Case $\beta < 1$: The travelling wave analysis in section 4.3.2 easily translates to the current problem. We find

$$G = -1 + (1 + T_I)e^{-\nu\eta} , \tag{4.71}$$

where $T_I = \beta - 1$. The wave speed ν, which varies with T_I, follows from substituting $s_t = \nu$ into eq. (4.12)

$$\nu = s_t = (1-\beta)\exp\left(\frac{Q(\beta-1)}{P+\beta-1}\right). \tag{4.72}$$

The temperature in the original variables is

$$T = -1 + \beta\exp(-\nu(x-s)) , \tag{4.73}$$

and the position and velocity of the freezing front are

$$s = (1-\beta)\exp\left(\frac{Q(\beta-1)}{P+\beta-1}\right)t + C_0 , \qquad s_t = (1-\beta)\exp\left(\frac{Q(\beta-1)}{P+\beta-1}\right). \tag{4.74}$$

As in the linear case, the above travelling wave solution is restricted to values $\beta < 1$ and, since it cannot satisfy the initial condition, should be considered a large time approximation.

4.4 Solution with the HBIM

The Heat Balance Integral Method (HBIM) introduced by Goodman [32] is a well-known approximate method for solving Stefan problems. The basic idea behind the method is to

approximate the temperature profile, usually with a polynomial, over some distance $\delta(t)$ known as the heat penetration depth. The heat equation is then integrated to determine a simple ordinary differential equation for δ. The solution of this equation, coupled with the Stefan condition then determines the temperature and position $s(t)$. The popularity of the HBIM is mainly due to its simplicity. However, in its original form there are a number of drawbacks, primarily a lack of accuracy for certain problems but also the rather arbitrary choice of approximating function, see [64] for a more detailed description of the method and problems. Recently a number of variants of the HBIM have been developed which address the issues and have led to simple solution methods that, over physically realistic parameter ranges, have proved more accurate than second order perturbation solutions [63, 65, 70, 71]. For the current study we will use the HBIM to permit us to make further analytical progress in the case of large supercooling.

For the one-phase semi-infinite problem with large supercooling the HBIM proceeds as follows. For $t > 0$ the temperature decreases from $T(s,t) = T_I$ to -1 as $x \to \infty$. With the HBIM the temperature profile is specified over a finite distance $x \in [s, \delta]$, where the 'heat penetration depth' δ is defined as the position beyond which the temperature rise is negligible. This leads to the boundary conditions $T(\delta,t) = -1$, $T_x(\delta,t) = 0$ and $\delta(0) = 0$. The simplest polynomial profile satisfying these conditions, along with $T(s,t) = T_I(t)$, is given by the function

$$T = -1 + (1 + T_I)\left(\frac{\delta - x}{\delta - s}\right)^n . \tag{4.75}$$

In the original HBIM the value $n = 2$ was employed, although other values have been used in later studies (often motivated by numerical solutions), see [64]. For now we leave it unspecified. The heat balance integral is determined by integrating the heat eq. (4.8) over the spatial domain, leading to

$$\frac{\mathrm{d}}{\mathrm{d}t}\int_s^\delta T\,\mathrm{d}x - T\big|_{x=\delta}\delta_t + T\big|_{x=s}s_t = T_x\big|_{x=\delta} - T_x\big|_{x=s} . \tag{4.76}$$

Substituting the expression for T from (4.75) gives

$$\frac{\mathrm{d}}{\mathrm{d}t}\left[\frac{(T_I-n)(\delta-s)}{n+1}\right]+\delta_t+T_I s_t=\frac{n(1+T_I)}{\delta-s}\ . \tag{4.77}$$

This involves the unknowns, $\delta(t)$, $s(t)$. A further equation comes from the Stefan condition

$$\beta s_t=\frac{n(1+T_I)}{\delta-s}\ , \tag{4.78}$$

and the system is closed with eq. (4.12). The exponent n is also unknown and this is determined through Myers' method, described in [70, 71]. If we define $f(x,t)=T_t-T_{xx}$, then the HBIM may be specified through the integral $\int_s^\delta f\,dx=0$. The modification suggested in [70, 71] was to choose n to minimise the least-squares error $E_n=\int_s^\delta f^2\,dx$. This leads to significant improvements in the accuracy of the HBIM as well as providing an error measure that does not require knowledge of an exact or numerical solution. For certain problems, for example when the boundary conditions are time-dependent, n may vary with time. To keep the method simple n is then set to its initial value, since this is where the greatest error E_n usually occurs. A subsequent refinement to this method, called the Combined Integral Method (CIM), was developed by Mitchell & Myers [65, 73] which provides a more consistent way to deal with cases where n is time-dependent.

The standard HBIM is often criticized due to a lack of accuracy. To indicate the accuracy of these new methods we point out that in [73] the CIM, second order large β and leading order small β perturbation solutions are compared against the exact solution for a two-phase supercooled Stefan problem. For $\beta\in[0.012,51.5]$ the CIM is the most accurate method with a percentage error in the front velocity in the range $[0.1,0.4]\%$. In the range $\beta\in[1,51.5]$ the error for the 2nd order perturbation varies almost linearly between 100 and 0.4% (for $\beta<1$ the error is off the graph). Over the whole range plotted in [73, Fig. 5], $\beta\in[10^{-4},10^2]$, the CIM error is a decreasing function of β with a maximum when $\beta=10^{-4}$ of around 0.44%. Given that the polynomial exponents only depend on β we expect Myers' method to be even more accurate than the CIM and so in the following, for simplicity, we will restrict n to be independent of time and so use Myers' method.

4.4.1 Linear kinetic undercooling

For the case of linear kinetic undercooling, $T_I(t) = -s_t$, and so we can use the Stefan condition (4.78) to eliminate δ from (4.77) and so derive an equation depending solely on $s(t)$. Assuming n is constant we obtain the second order ODE

$$s_{tt} = \frac{(n+1)\beta s_t^3(1-\beta-s_t)}{n(1-s_t^2)} \ . \tag{4.79}$$

Hence the HBIM has reduced the initial Stefan problem to one of solving a single ODE for s. This is obviously a much simpler prospect than solving the full Stefan problem. Once s is known the interface temperature is determined by $T_I = -s_t$, δ is given by eq. (4.77) and the temperature profile follows from (4.75). As discussed earlier the initial conditions are $s(0) = 0, s_t(0) = 1$. Eq. (4.79) is easily solved using the Matlab routine `ode15s`. In this case, the error minimisation process leads to $n \approx 3.57$. The condition $s_t(0) = 1$ leads to an initial singularity in acceleration. Motivated by the previous small time solution we assume a form $s_t = 1 + Bt^\alpha$ when $t \ll 1$ which leads to $s_t = 1 - \sqrt{\beta^2(n+1)/n}\, t^{1/2}$ and hence $s = t - (2/3)\sqrt{\beta^2(n+1)/n}\, t^{3/2}$. These forms are then used as the initial conditions for the numerical calculation starting at some time $t = t_0 \ll 1$.

Note, this is not the first time that an HBIM has been applied to kinetic undercooling problems. Charach & Zaltzman [15] studied the linear case employing the error function profile

$$T = -1 + (1 + T_I)\text{erfc}\left[c(x-s)\right] \ , \tag{4.80}$$

where c is an unknown time-dependent coefficient to be determined. This form was motivated by the $T_I = 0$ case of eq. (4.27). The solutions obtained in this manner exhibit the same large time behaviours discussed earlier although by comparing to the numerical results we found this profile to be significantly less accurate than that using Myers' method. It also requires c to be determined and $c(0)$ turns out to be infinite. For these reasons we do not show this solution on any plots.

4.4.2 Nonlinear kinetic undercooling

For the case of large supercooling the appropriate expression for $T_I(t)$ is obtained from eq. (4.12). Eliminating δ from (4.77) by means of the Stefan condition (4.78) we obtain

$$\frac{2(1+T_I)}{s_t}\frac{dT_I}{dt} - \frac{(1+T_I)^2}{s_t^2}s_{tt} = \frac{(n+1)\beta(\beta-1-T_I)}{n}s_t \ . \tag{4.81}$$

The above equation suggests making the change of variable $y = s_t$, which leads to

$$\frac{\mathrm{d}T_I}{dt} = \frac{(1+T_I)}{2y}\frac{\mathrm{d}y}{dt} + \frac{(n+1)\beta(\beta-1-T_I)y^2}{2n(1+T_I)} \ . \tag{4.82}$$

A second equation can be obtained by taking the time derivative of (4.12)

$$\frac{\mathrm{d}y}{dt} = -\exp\left(\frac{Q\,T_I}{P+T_I}\right)\left[1+\frac{QP\,T_I}{(P+T_I)^2}\right]\frac{\mathrm{d}T_I}{dt} \ . \tag{4.83}$$

Eqs (4.82) and (4.83), together with the definition $y = s_t$, constitute a system of three nonlinear first order ODEs that can be easily solved with the Matlab routine `ode15s`. The initial conditions for this system are $T_I(x,0) = -1$, $y(0) = \exp(-Q/(P-1))$ and $s(0) = 0$. Again, the exponent n is determined by minimizing E_n for $t \approx 0$ giving $n \approx 3.61$.

4.4.3 Asympotic analysis within the HBIM formulation

Linear kinetic undercooling

Applying a large time subsitution allows us to examine the solution behaviour analytically and in particular make comparison with earlier solution forms. Firstly, we write $t = \tau/\epsilon$ and $s = r/\epsilon^\gamma$ and eq. (4.79) becomes

$$\epsilon^{2-\gamma}r_{\tau\tau} = \frac{(n+1)\beta\epsilon^{3(1-\gamma)}r_\tau^3(1-\beta-\epsilon^{1-\gamma}r_\tau)}{n(1-\epsilon^{2(1-\gamma)}r_\tau^2)} \ . \tag{4.84}$$

The obvious balance comes from setting $2-\gamma = 3(1-\gamma)$, which gives $\gamma = 1/2$, and so (4.84) reduces to

$$r_{\tau\tau} \approx \frac{(n+1)\beta(1-\beta)r_\tau^3}{n} \qquad \Rightarrow \qquad r_\tau^{-2} \approx \frac{2(n+1)\beta(\beta-1)\tau}{n} + c_0 \ . \tag{4.85}$$

To ensure $r_\tau > 0$ requires $\beta > 1$. Since all solutions with $\beta \geq 1$ have $s_t \to 0$ (or equivalently $T_I \to 0$) as $t \to 0$ the constant $c_0 = 0$. This indicates $s_t \approx \sqrt{n/(2(n+1)\beta(\beta-1)t)}$ and is consistent with the large time solution given in section 4.3.2 for $\beta > 1$.

A second balance comes from setting $\gamma = 1$ in (4.84). Then the right hand side is dominant and so $r_\tau = 1-\beta$, giving $s_t = 1-\beta$ (and so requiring $\beta < 1$). This is consistent with the travelling wave solution, valid for $\beta < 1$, found in section 4.3.2.

A third reduction is obtained by first setting $\beta = 1$ in eq. (4.84)

$$\epsilon^{2-\gamma} r_{\tau\tau} = -\frac{(n+1)\epsilon^{4(1-\gamma)} r_\tau^4}{n(1-\epsilon^{2(1-\gamma)} r_\tau^2)} \ . \tag{4.86}$$

Then balancing both sides gives $2-\gamma = 4(1-\gamma)$, or $\gamma = 2/3$, leading to

$$r_{\tau\tau} \approx -\frac{(n+1)r_\tau^4}{n} \qquad \Rightarrow \qquad r_\tau \approx \left(\frac{3(n+1)\tau}{n}\right)^{-1/3} \ . \tag{4.87}$$

Thus

$$s_t \approx \left(\frac{3(n+1)t}{n}\right)^{-1/3} \qquad \Rightarrow \qquad s \approx \left(\frac{9n}{8(n+1)}\right)^{1/3} t^{2/3} \ . \tag{4.88}$$

Again the constants of integration have been set to zero to achieve the appropriate behaviour as $t \to \infty$. This is the behaviour predicted by the large time, $\beta = 1$ analysis of section 4.3.2.

From the above we see that the HBIM formulation allows us to easily capture the three forms of solution behaviour determined in section 4.3.2.

Nonlinear kinetic undercooling

As in the previous section we may make analytical progress in the large time limit by setting $t = \tau/\epsilon$, $s = r/\epsilon^{\gamma}$ and also $T_I = \epsilon^{\theta} U$, where γ, $\theta \geq 0$. Eq. (4.12) then becomes

$$\epsilon^{1-\gamma} r_{\tau} = -\epsilon^{\theta} U \exp\left(\frac{Q\,\epsilon^{\theta} U}{P + \epsilon^{\theta} U}\right). \tag{4.89}$$

This equation clearly shows that for the front to move $\theta = 1 - \gamma$. Eq. (4.81) becomes

$$\epsilon \frac{2(1+\epsilon^{1-\gamma}U)}{r_{\tau}} \frac{dU}{d\tau} - \epsilon^{\gamma} \frac{(1+\epsilon^{1-\gamma}U)^2}{r_{\tau}^2} r_{\tau\tau} = \epsilon^{1-\gamma} \frac{(n+1)\beta(\beta - 1 - \epsilon^{1-\gamma}U)}{n} r_{\tau}\ . \tag{4.90}$$

We note that the first term in (4.90) will never be dominant for any value of $\gamma \in [0, 1]$. So, in fact,

$$-\epsilon^{\gamma} \frac{(1+\epsilon^{1-\gamma}U)^2}{r_{\tau}^2} r_{\tau\tau} \approx \epsilon^{1-\gamma} \frac{(n+1)\beta(\beta - 1 - \epsilon^{1-\gamma}U)}{n} r_{\tau}, \quad \forall\ \ \gamma. \tag{4.91}$$

Moreover, we realize that the exponential in (4.89) affects the leading order term only when $\gamma = 1$, otherwise $r_{\tau} = -U + \mathcal{O}(\epsilon^{1-\gamma})$, *i.e.* the linear case is retrieved, and so we find the same balances as in the previous section. First, for $\gamma = 1/2$ (4.91) reduces to (4.85) valid for $\beta > 1$ ($s_t \sim t^{-1/2}$). Second, setting $\beta = 1$, we find that $\gamma = 2/3$ and (4.91) reduces to (4.88) ($s_t \sim t^{-1/3}$). Finally, for $\gamma = 1$ the right hand side of (4.91) is dominant and we find $U = T_I = \beta - 1$. Then s_t is described by the travelling wave solution (4.72) which requires $\beta < 1$. There is also the possibility of setting $\gamma = 0$ but this implies $T_I = \epsilon U \ll 1$ which is not consistent with the specification of large supercooling.

Discussion

The equations obtained through the HBIM formulation for the linear case are easily analysed to determine the three time dependencies found at large times by previous authors. In the nonlinear case the asymptotic analysis may no longer be applied, however the HBIM formulation indicates the three same solution forms. When $\beta \geq 1$, as $t \to \infty$ the velocity $s_t \to 0$ and so $T_I \to 0$. Consequently we should expect the linear and nonlinear cases to coincide. The numerics of the following section confirms this. When $\beta < 1$ the value of s_t is

constant and differs for the linear and nonlinear cases.

4.5 Results

We now present a set of results for the various scenarios discussed in section 4.3 and section 4.4. The asymptotic and HBIM results are compared with a numerical scheme similar to that developed by Mitchell & Vynnycky [66, 67]. This uses the Keller box scheme, which is a second order accurate finite-difference method, and has been successfully applied to several moving boundary problems. The boundary immobilisation transformation at the end of section 4.2, along with a small time analysis, ensures that the correct starting solution is used in the numerical scheme. In all examples we use parameter values for copper, hence $Q \approx 3.5811$. The value of β and P depend on ΔT hence the plots with $\beta = 0.7, 1, 1.5$ correspond to $P \approx 2.417, 3.453, 5.179$ respectively.

For clarity we present the results in three subsections: in the first we compare numerics, HBIM and asymptotic solutions for the case of linear kinetic undercooling, then repeat this for nonlinear undercooling, and finally we compare results obtained through the two undercooling models and the classical Neumann solution.

4.5.1 Linear kinetic undercooling

In Figure 4.2 we compare the results of the numerical solution (solid line), the HBIM (dashed) defined by eq. (4.79) and the small and large time asymptotics (dash-dot) for the case $\beta = 1$. The value of the exponent used in the HBIM was $n = 3.57$ which was determined by minimising the least-squares error. The left-hand figure shows the solutions for $t \in [0, 0.1]$. In this range the numerical and HBIM solutions are virtually indistinguishable whilst the small time asymptotic solution is only accurate for the very initial stage. The asymptotic solution does have a time restriction since the leading order term must be significantly greater than the first order. In fact a more rigorous bound is imposed by the restriction that $s_t > 0$ thus requiring $t < \pi/(4\beta^2)$ and so the smaller the value of β the longer the solution is valid (although recall β is restricted such that the linear undercooling relation is valid). The right hand figure shows a comparison of the numerics, HBIM solution and large time asymptotics

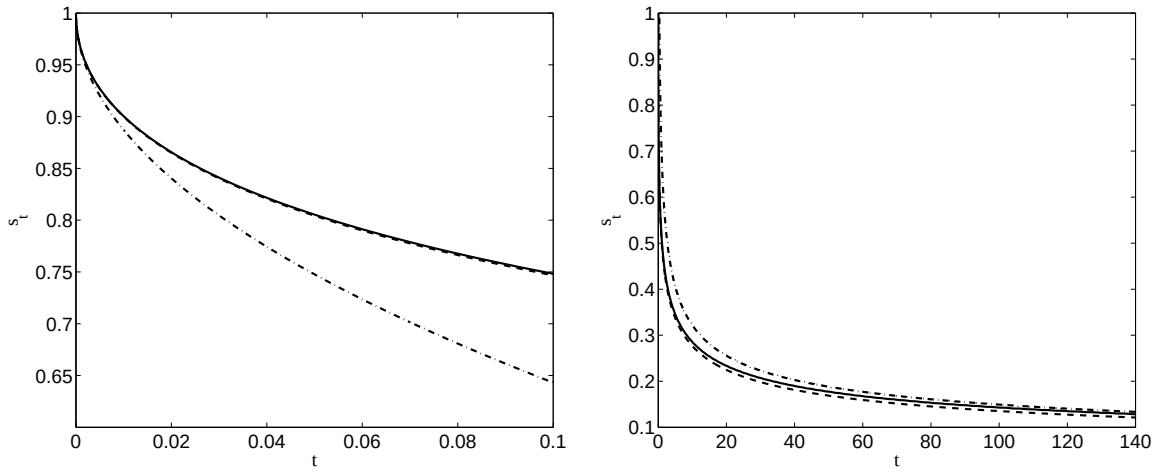

Figure 4.2: Linear kinetic undercooling with a) $t \in [0, 0.1]$, b) $t \in [0, 140]$. The sets of curves denote the numerical solution (solid line), HBIM (dashed) and small and large time asymptotics (dash-dotted) results for the interface velocity when $\beta = 1$.

carried on until $t = 140$. Again the HBIM is close to the numerics for all of the range. The large time asymptotic solution improves as t increases and for t approximately greater than 80 becomes more accurate than the HBIM.

Figure 4.3 displays two sets of results demonstrating the two other forms of behaviour, with $\beta < 1$ and $\beta > 1$. The left hand figure is for $\beta = 0.7$. For large times the solution is a travelling wave. The large time asymptotic result is therefore a straight line corresponding to the wave speed $s_t = 1 - \beta = 0.3$. As mentioned in section 4.3.2, the travelling wave does not match the initial conditions, which the HBIM and numerics correctly capture, and so must be classified as a large time solution. Even at $t = 100$ the travelling wave speed is around 3% below the numerical solution.

For $\beta > 1$ the large time asymptotic solution (at leading order) reduces to the no kinetic undercooling (or Neumann) solution. The velocity is represented by (4.45c) and it is shown in the right hand plot in Figure 4.3 for $\beta = 1.5$ together with numerical and HBIM results (which again are virtually indistinguishable). At $t = 100$ the difference between numerics and asymptotics is around 10%. However, if we increase β to 2 the error at $t = 100$ reduces to 4%.

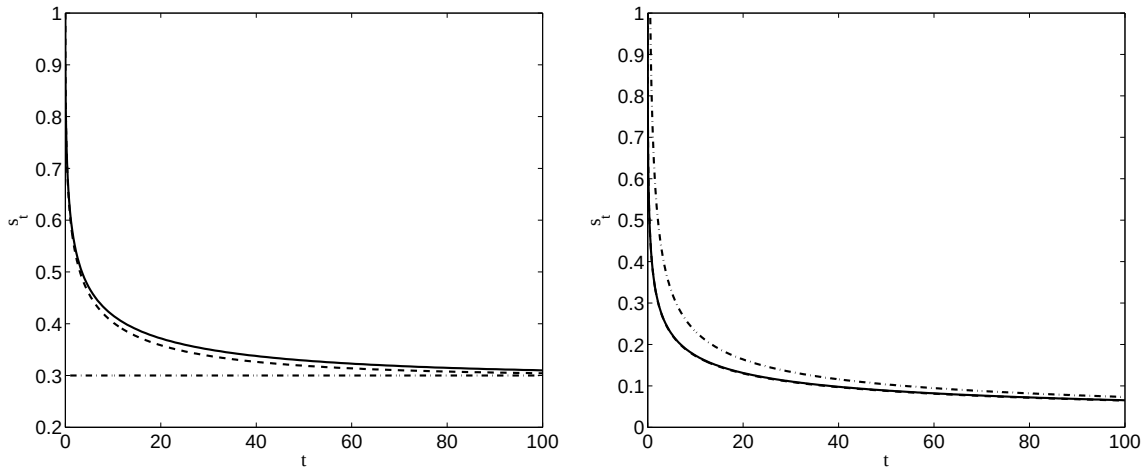

Figure 4.3: Linear kinetic undercooling with $t \in [0, 100]$ and a) $\beta = 0.7$, b) $\beta = 1.5$. The sets of curves denote the numerical solution (solid line), HBIM (dashed) and large time asymptotics (dash-dotted) results for the interface velocity.

4.5.2 Nonlinear kinetic undercooling

In Figures 4.4 and 4.5 we demonstrate different solution behaviours for the nonlinear kinetic undercooling case. In contrast to the linear examples we do not have large time asymptotic solutions for $\beta \leq 1$ and only show HBIM and numerical solutions for those cases. The HBIM solution is obtained by integrating (4.82)–(4.83) using Matlab routine `ode15s`.

The left hand plot in Figure 4.4 shows the small time behaviour with $\beta = 1$, when $t \in [0, 0.1]$. Again the HBIM (with $n = 3.57$) appears to be very accurate, whilst the asymptotic solution slowly loses accuracy. As before this is bounded by a time restriction, $t \ll \pi/4\beta^2 \exp[2Q/(1-P)][1 - QP/(P-1)^2]^2$. Decreasing β would improve the accuracy of the asymptotic solution. The HBIM solution has the initial value $s_t = \exp(-Q/(P-1))$, which in this case gives $s_t(0) \approx 0.232$. An important difference between this solution and the zero and linear undercooling cases is that the speed now increases with time. Referring to Figure 4.1, this indicates that this value of Stefan number requires $T_m - T_I$ such that we begin to the right of the peak in the $s_t(\Delta T)$ curve. As time proceeds and T_I approaches T_m we will move to the left and so observe an initial increase in s_t followed by a decrease as we pass the peak. This behaviour is apparent in the right hand plot of Figure 4.4, which shows the

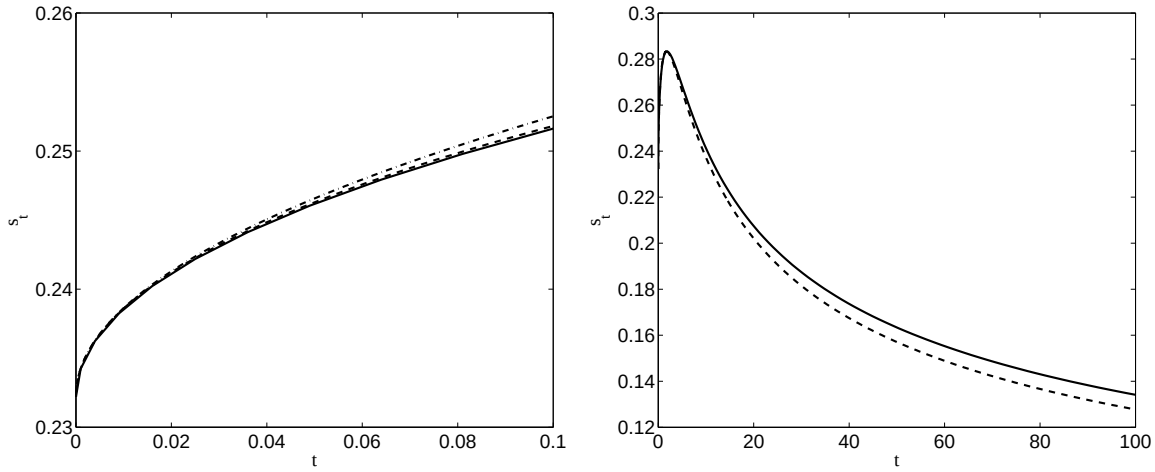

Figure 4.4: Nonlinear kinetic undercooling with a) $t \in [0, 0.1]$, b) $t \in [0, 100]$. The sets of curves denote the numerical solution (solid line), HBIM (dashed) and small time asymptotics (dash-dotted) results for the interface velocity when $\beta = 1$.

numerical and HBIM solution for $t \in [0, 100]$. For $t \in [0, 5]$ (approximately) s_t increases to a maximum of just above 0.28 and then slowly decreases with the $t^{-1/3}$ behaviour predicted in section 4.4.3.

Figure 4.5 displays results for $\beta = 0.7, 1.5$ for $t \in [0, 300], [0, 40]$ respectively. The left hand figure shows that the HBIM is always close to the numerical solution and that the travelling wave result is only achieved after a very large time. Even after $t = 300$ the large time asymptotic solution is 4% below the numerical solution. This approach to the travelling wave is much slower than in the linear case. The HBIM and numerical results, as in Figure 4.4, show an initial growth in s_t followed by a decrease for $t > 30$, again this may be attributed to starting from the right of the peak in the $s_t(\Delta T)$ graph and then moving to the left, across the peak as t increases. The right hand figure contains the HBIM and numerical solutions for $\beta = 1.5$. Obviously the curves are very close to each other. The larger value of β indicates a lower value of ΔT than in the left hand plot and this means the degree of undercooling is always such that we remain to the left of the peak on the $s_t(\Delta T)$ graph. Consequently s_t is a decreasing function of time and, as shown in section 4.4.3, $s_t \propto t^{-1/2}$.

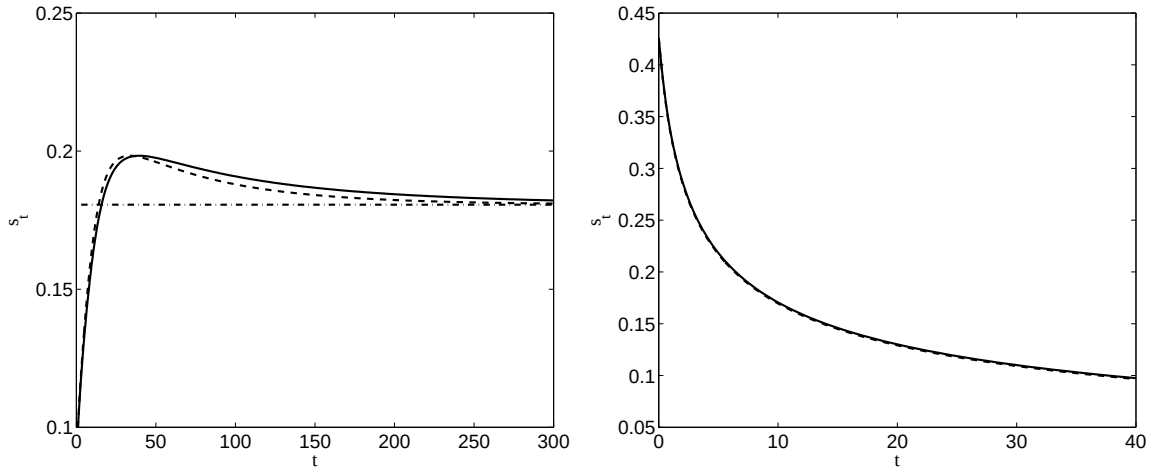

Figure 4.5: Nonlinear kinetic undercooling with a) $\beta = 0.7$, $t \in [0, 100]$ and b) $\beta = 1.5$, $t \in [0, 40]$. The sets of curves denote the numerical (solid line) HBIM (dashed) and, when $\beta = 0.7$, asymptotic (dash-dot) solutions for the interface velocity.

At the end of section 4.4 it was mentioned that the two solution forms, with $\beta \geq 1$, must approach the linear kinetic undercooling forms since $T_I = -s_t \to 0$. Comparing Figures 4.2 and 4.4 shows the large time solutions for $\beta = 1$ do coincide, similarly with the results when $\beta = 1.5$ shown in the right side of Figures 4.3 and 4.5. However, when $\beta < 1$ then $T_I = 1 - \beta$ does not approach T_m and so linear and nonlinear results for $\beta = 0.7$, shown in the left side of Figures 4.3 and 4.5, have different limits, $s_t = 0.3$ and $s_t \approx 0.18$ respectively.

4.5.3 Comparison of linear and nonlinear undercooling

In Figure 4.6 we show plots of the velocity s_t for $t \in [0, 100]$ and the temperature T at $t = 1$ for the case $\beta = 1.1$. This β value was chosen to permit the inclusion of the Neumann solution. On the plots the solid line represents the numerical solution of the nonlinear problem, the dashed line that of the linear case and the dot-dash line the Neumann solution.

The left hand plot shows the velocities s_t. The Neumann solution breaks down at $\beta = 1$, however, it is clear from the curves that even for $\beta = 1.1$ it is far from the solutions with undercooling. This indicates that, although the Neumann solution is accepted as valid down to $\beta = 1$, it may be highly inaccurate and inappropriate for describing the solidification of a

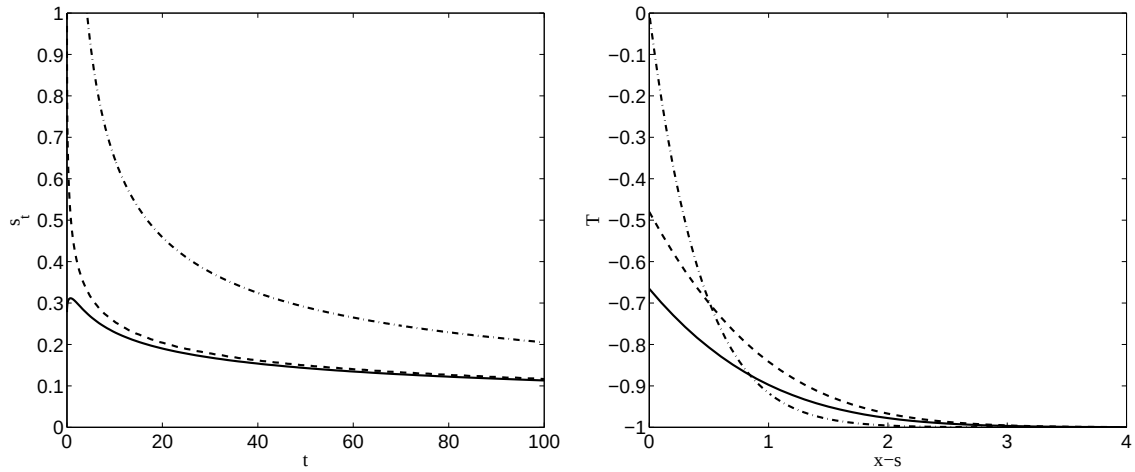

Figure 4.6: Comparison of velocities and temperatures (at $t = 1$) predicted by the nonlinear (solid line), linear (dashed line) and Neumann (dot-dash) solutions for $\beta = 1.1$.

supercooled liquid. The choice $\beta = 1.1$ means that we operate to the left of the peak in the $s_t(\Delta T)$ graph, where the linear approximation is close to the nonlinear curve. Consequently, the corresponding velocities shown on Figure 4.6 converge quite rapidly. However, for small times the linear case has much higher velocities which would result in a significantly higher prediction for s than when using the nonlinear relation. Decreasing the value of β causes the s_t curves to diverge further.

The right hand plot shows the temperature profiles at $t = 1$ as a function of the fixed boundary co-ordinate $y = x - s$. The Neumann solution (dash-dotted line) has a constant temperature $T = 0$ at $x = s$ for all times, while the nonlinear (solid) and linear (dashed) solutions present a variable temperature at $x = s$ that tends to 0 as time increases. The differences observed between the temperature profiles become smaller for larger times and the solutions look almost the same at $t = 100$.

4.6 Conclusions

In this chapter we have investigated the one-phase one-dimensional Stefan problem with a nonlinear relation between the phase change temperature and solidification rate. In the limits of zero and linear (small) supercooling we reproduced the asymptotic behaviour found

in previous studies. The asymptotics for the nonlinear regime proved more difficult and then our analysis was limited to small time solutions for arbitrary Stefan number and a travelling wave solution at large time (valid for $\beta < 1$). A recent extension to the Heat Balance Integral Method was then applied to the system to reduce the problem to a single ordinary differential equation for the case of linear supercooling and two ordinary differential equations for the nonlinear case. Asymptotic techniques could then be applied to the ordinary differential equations to reproduce the various asymptotic behaviours found in the linear system. For the nonlinear system it turned out that the same behaviour could be found at large times and, given the proximity of the HBIM solution to numerical results we conclude that this reflects the behaviour of the full system.

Whilst asymptotic analysis is a popular method to analyse the solution form in various limits it may only be valid over a very small range. In contrast the HBIM solution was very close to the numerical solution and in general proved more accurate than the small and large time asymptotics. In the nonlinear case, where the asymptotic solutions were not available for all cases the HBIM equations could still be analysed to predict the solution behaviour. This indicates that the new accurate version of the HBIM is a useful tool in analysing this type of problem.

An interesting point concerns the Neumann solution. Although this solution exists for supercooled fluids (such that $\beta \to 1^+$) it can be highly inaccurate. In our final set of results we compared solutions for $\beta = 1.1$. The Neumann solution has $s_t(0) = \infty$, with linear supercooling $s_t(0) = 1$ and with the nonlinear relation $s_t(0) = e^{-Q/(P-1)}$, which for the current study on copper gave $s_t(0) \approx 0.278$. For large times the linear and nonlinear velocities converged (although the initial discrepancy may lead to a large difference in the position of the front) whilst the Neumann solution had s_t approximately 50% higher even at $t = 100$. Increasing the value of β caused the three solution sets to converge. Perhaps the main conclusion of this study is that for practical purposes when attempting to predict realistic solidification rates for $\beta < 1$ and even for values slightly greater than unity the nonlinear relation should be employed. Even though the Neumann solution exists it should not be trusted to predict solidification rates of supercooled liquids for values of β close to

unity.

Chapter 5

Energy conservation in the Stefan problem with supercooling

T.G. Myers, S.L. Mitchell, F. Font. *Energy conservation in the one-phase supercooled Stefan problem*
International Communications on Heat and Mass Transfer, 39, 1522-1225 (2012)
Impact factor: 2.208

Abstract

A one-phase reduction of the one-dimensional two-phase supercooled Stefan problem is developed. The standard reduction, employed by countless authors, does not conserve energy and a recent energy conserving form is valid in the limit of small ratio of solid to liquid conductivity. The present model assumes this ratio to be large and conserves energy for physically realistic parameter values. Results for three one-phase formulations are compared to the two-phase model for parameter values appropriate to supercooled salol (similar values apply to copper and gold) and water. The present model shows excellent agreement with the full two-phase model.

5.1 Introduction

When a solid forms from a liquid at the heterogeneous nucleation temperature the freezing process is relatively slow and the liquid molecules have time to rearrange into a standard crystalline configuration. However, a supercooled (or undercooled) liquid is in an unstable state, ready to solidify rapidly as soon as the opportunity arises. The solidification process may be so rapid that the liquid molecules have no time to rearrange themselves into the usual crystal structure and instead form an unorganised or amorphous solid structure that is reminiscent of the liquid phase. For this reason solids formed from a supercooled liquid have been referred to as *liquids on pause* [79]. The different molecular arrangement means that such solids may have very different properties to the normal solid phase. Amorphous metal alloys, formed by supercooling below the glass transition temperature can be twice as strong and three times more elastic than steel [79]. Numerous applications for materials formed from a supercooled liquid, such as in sport and electronic equipment, medical and aerospace, are discussed in the article of Telford [109].

The practical importance of solids formed from a supercooled liquid motivates the need for the theoretical understanding of the associated phase change process. Although the two-phase problem is well defined, it may be difficult to solve, given that it involves two partial differential equations on an *a priori* unknown, moving domain. The associated one-phase problem is a significantly less challenging prospect, particularly when dealing with complex geometries. However it has been shown that the standard one-phase reduction does not conserve energy [25]. In this chapter we examine the one-phase reduction of the one-dimensional Stefan problem. It is shown that the energy conserving form of [25] although mathematically correct is not appropriate for physically realistic problems and so we propose an alternative reduction which shows excellent agreement with the full two-phase model.

5.2 Mathematical models

One of the most basic formulations of the two-phase supercooled Stefan problem in non-dimensional form consists in the heat equations

$$\frac{\partial \theta}{\partial t} = \frac{k}{c}\frac{\partial^2 \theta}{\partial x^2} \qquad 0 < x < s(t)\,, \qquad\qquad \frac{\partial T}{\partial t} = \frac{\partial^2 T}{\partial x^2} \qquad s(t) < x < \infty\,, \tag{5.1}$$

with boundary conditions

$$T(s,t) = \theta(s,t) = T_I(t)\,, \qquad T|_{x\to\infty} \to -1\,, \qquad T(x,0) = -1\,, \tag{5.2}$$

and the Stefan condition

$$[\beta - (1-c)s_t]\, s_t = \left(k\frac{\partial \theta}{\partial x} - \frac{\partial T}{\partial x}\right)\Big|_{x=s}\,, \qquad s(0) = 0\,, \tag{5.3}$$

where T, θ represent the liquid and solid temperatures, $k = k_s/k_l$ the thermal conductivity ratio, c the specific heat ratio, $\beta = L_m/(c_l \Delta T)$ the Stefan number, L_m the latent heat and ΔT the degree of supercooling. The above system describes the phase change process of a supercooled semi-infinite material which solidifies from the boundary $x = 0$. The phase change boundary is at $x = s(t)$, where $s(0) = 0$. The variable $T_I(t)$ represents the temperature at the phase change interface. If solidification occurs at the heterogeneous nucleation temperature we choose $T_I(t) = 0$. With supercooling a non-linear relation exists between T_I and s_t [4, 11]. For small levels of supercooling it is standard to choose a linear approximation $T_I(t) = -s_t$. This is often referred to as a *linear kinetic undercooling model*. For simplicity we will use the linear approximation throughout this chapter although the methodology translates immediately to the non-linear case. The above formulation involves the assumption that the density change between liquid and solid phases is small and so may be neglected compared to other physical changes, such as the jump in specific heat. We augment this system with the initial condition $\theta(x,0) = \theta_i$ and a boundary condition $\theta_x(0,t) = 0$: for a standard one-phase problem these extra conditions are unnecessary but

they are required when looking for a reduction from a two-phase model. Note, we choose the boundary condition at $x = 0$ to match that of [15] and also because it is appropriate when working in cylindrical and spherical co-ordinates, but other boundary conditions will work in the arguments below.

The standard one-phase Stefan problem is retrieved from the system (5.1)-(5.3) by simply ignoring the θ equation and setting $k = 0$ in the Stefan condition, consequently

$$\frac{\partial T}{\partial t} = \frac{\partial^2 T}{\partial x^2} \qquad s < x < \infty \,, \tag{5.4}$$

with boundary conditions

$$T(s,t) = -s_t \,, \qquad T|_{x\to\infty} \to -1 \,, \qquad T(x,0) = -1 \,, \tag{5.5}$$

and the Stefan condition

$$[\beta - (1-c)s_t]\, s_t = -\left.\frac{\partial T}{\partial x}\right|_{x=s} , \qquad s(0) = 0 \,. \tag{5.6}$$

In fact this is often further reduced by choosing $c = 1$. It is well-known that if supercooling is neglected, *i.e.* $T_I(t) = 0$, and $c = 1$, then the well-known Neumann solution may be applied to (5.4)-(5.6), but this breaks down as $\beta \to 1^+$. Applying the linear kinetic undercooling temperature $T_I(t) = -s_t$ prevents this breakdown and so permits solutions for arbitrary undercooling.

Evans and King [25] point out that the above reduction does not conserve energy since the limit $\theta \to 0$ involves a singular perturbation of the two-phase system. Physically the issue is obvious: the reduction is based on setting θ constant, without the undercooling term the boundary condition determines $\theta = T_I \equiv 0$ and so the (non-dimensional) constant is zero and this satisfies the heat equation and boundary condition at $x = s$ for all time. With kinetic undercooling the temperature at $x = s$ varies with time, so $\theta(s,t)$ is a function of time and the assumption of constant θ is no longer valid.

To determine a consistent one-phase model, Evans and King [25] investigate the limit

$k \to 0$ which is equivalent to neglecting θ in the Stefan condition. The heat equation in the solid then indicates $\theta_t \to 0$ and so $\theta \approx \theta(x) = \theta_i$, (after imposing the initial condition). However, this contradicts the condition $\theta(s,t) = -s_t \neq \theta_i$ and so indicates the need for a boundary layer. To analyse this boundary layer a new co-ordinate is introduced, $x = s(t) - k\hat{x}$ (where $k \ll 1$), which transforms (5.1b) to

$$s_t \frac{\partial \theta}{\partial \hat{x}} + k \frac{\partial \theta}{\partial t} = \frac{1}{c} \frac{\partial^2 \theta}{\partial \hat{x}^2} \,. \tag{5.7}$$

Neglecting the small term involving k allows the equation to be integrated and applying $\theta \to \theta_i$ as $\hat{x} \to \infty$ gives

$$\frac{1}{c} \frac{\partial \theta}{\partial \hat{x}} = s_t(\theta - \theta_i) \,. \tag{5.8}$$

Noting that $\theta_{\hat{x}} = -k\theta_x$ we may use (5.8) to replace the solid temperature gradient in the Stefan condition (5.3) and applying $\theta(s,t) = -s_t$ gives

$$\left[\beta - s_t - c\theta_i\right] s_t = -\frac{\partial T}{\partial x} \,. \tag{5.9}$$

The correct reduction of the two-phase Stefan problem *in the limit* $k \to 0$ is therefore specified by equations (5.4)-(5.5), with the Stefan condition given by (5.9). The properties and behaviour of systems of this form, with appropriate modification for different physical situations have been studied for example in [118, 47].

Heat conduction occurs on the microscopic scale due to the transfer of kinetic energy from hot, rapidly vibrating atoms or molecules to their cooler, more slowly vibrating neighbours. In solids the close, fixed arrangement of atoms means that conduction is more efficient than in fluids, which have a larger distance between atoms. Consequently, in general, the conductivity of a solid is greater than that of its corresponding liquid phase, for example with water and ice $k = k_s/k_l \approx 4$, for solid and molten gold $k \approx 3$. Hence the limit $k \to 0$ has limited applicability and for practical Stefan problems it would seem more appropriate to study the large k limit.

Now we let $k \to \infty$ and the heat equation (5.1b) reduces to $\theta_{xx} \approx 0$, so to leading order $\theta = c_0(t) + c_1(t)x = -s_t$ (after applying the boundary conditions). So far this seems a reasonable result, large k indicates heat travels rapidly through the solid (compared to the travel time in the liquid) which then equilibrates to the boundary temperature almost instantaneously. However, in the Stefan condition we have the term $k\theta_x$, which is zero to leading order (since $\theta = -s_t(t)$), but since the coefficient k is large it is possible that the first order term plays an important role. If we write $\theta = \theta_0 + (1/k)\theta_1 + \mathcal{O}(1/k^2)$ then the leading and first order heat equations are

$$\frac{\partial^2 \theta_0}{\partial x^2} = 0\,, \qquad\qquad c\frac{\partial \theta_0}{\partial t} = \frac{\partial^2 \theta_1}{\partial x^2}\,. \tag{5.10}$$

The appropriate temperatures are $\theta_0 = -s_t$ and $\theta_1 = -cs_{tt}(x^2 - s^2)/2$. The Stefan condition becomes

$$[\beta - (1-c)s_t]\, s_t = k\left(\frac{\partial \theta_0}{\partial x} + \frac{1}{k}\frac{\partial \theta_1}{\partial x} + \mathcal{O}(1/k^2)\right)\bigg|_{x=s} - \left.\frac{\partial T}{\partial x}\right|_{x=s}\,. \tag{5.11}$$

Substituting for θ_1 in (5.11) we find that the one-phase Stefan problem in the limit of large k is then specified by equations (5.4)-(5.5) and the Stefan condition

$$css_{tt} + [\beta - (1-c)s_t]\, s_t = -\left.\frac{\partial T}{\partial x}\right|_{x=s}\,. \tag{5.12}$$

The inclusion of the derivative s_{tt} requires an extra initial condition. In the absence of supercooling, $T_I = 0$, hence $T(s,t) = T_I$ indicates $T(0,0) = 0$. For $x > 0$ we have $T(x,0) = -1$, hence the temperature gradient

$$T_x(x,0)|_{x\to 0} = \lim_{h\to 0}\frac{T(h,0) - T(0,0)}{h} = \lim_{h\to 0}\left(\frac{-1-0}{h}\right) = -\infty\,. \tag{5.13}$$

In the one phase problem the front velocity is a function of the temperature gradient with the result that without kineic undercooling the above initial infinite gradient indicates $s_t(0) = \infty$. This may be seen, for example, in the well-known Neumann solution where $s_t \sim 1/\sqrt{t}$. The singularity is an obvious consequence of the unphysical nature of the boundary condition:

choosing $T = -1$ for all $x > 0$ and $T = 0$ at a single point $x = 0$ is not consistent with an equation based on continuum theory. Kinetic undercooling provides a mechanism for removing the unphysical behaviour. The only way to avoid the singularity is if $T(0,0) = \lim_{h\to 0}(T(h,0) + \mathcal{O}(h)) = \lim_{h\to 0}(-1 + \mathcal{O}(h)) = -1$. In physical terms we may think of an undercooled melt at temperature $T = -1$ everywhere when some infinitesimally small amount of energy is input at the boundary resulting in $T(0,0) = -1+\mathcal{O}(h)$: this is sufficient to set off the solidification process (and it is well-known that *'working with undercooled liquids is a bit like juggling mousetraps: they're prone to suddenly "snap" and ruin the trick'* [79]). Since $T_I(0) = T(0,0) = -1$ we find that in the case of linear undercooling the additional boundary condition required to close the Stefan problem is

$$s_t(0) = -T_I(0) = 1\,. \tag{5.14}$$

This argument also helps us with the one-phase formulation of equation (5.9) which requires an initial solid temperature, θ_i (despite the solid phase not entering the one-phase problem). Since the initial 'kick' to start solidification may be infinitesimal, and for t sufficiently close to zero an infinitesimally small amount of latent heat has been released, the only physically sensible value for the solid temperature is $\theta_i = -1$. These initial conditions on θ_i and s_t are obtained more formally through a short time asymptotic analysis in [14].

5.3 Energy conservation

The non-dimensional thermal energy in the two-phase system is given by

$$E = \int_0^s c\,\theta\,dx + \int_s^\infty T\,dx\,. \tag{5.15}$$

During the phase change the molecular rearrangement also releases (or uses) energy, namely the latent heat. So the rate of change of thermal energy, E_t, must balance the rate at which

energy is produced by the phase change, βs_t. Differentiating the above equation we find

$$\frac{dE}{dt} = \int_0^s c\frac{\partial \theta}{\partial t}\, dx + c\,\theta(s,t)\frac{ds}{dt} + \int_s^\infty \frac{\partial T}{\partial t}\, dx - T(s,t)\frac{ds}{dt}\,. \tag{5.16}$$

The heat equations in (5.1) allow the time derivatives to be replaced with x derivatives in the integrals, which may then be evaluated immediately. Noting that $\theta(s,t) = T(s,t) = -s_t$ then (5.16) becomes

$$\frac{dE}{dt} = k\frac{\partial \theta}{\partial x}\bigg|_{x=0} + \left(k\frac{\partial \theta}{\partial x} - \frac{\partial T}{\partial x}\right)\bigg|_{x=s} + \frac{\partial T}{\partial x}\bigg|_{x=\infty} + (1-c)\left(\frac{ds}{dt}\right)^2\,. \tag{5.17}$$

The temperature gradients at $x = s$ may be removed via the Stefan condition (5.3). The insulated boundary condition of the current study requires $\theta_x(0,t) = 0$, and as $x \to \infty$ the gradient $T_x \to 0$, so we are left with

$$\frac{dE}{dt} = \left[\beta - (1-c)\frac{ds}{dt}\right]\frac{ds}{dt} + (1-c)\left(\frac{ds}{dt}\right)^2 = \beta\frac{ds}{dt}\,. \tag{5.18}$$

So the rate of change of thermal energy balances the latent heat release and the two-phase formulation conserves energy. Note, the argument follows in the same way for different boundary conditions, for example if we choose a constant flux $k\theta_x(0,t) = q$ then the rate of change of thermal energy balances the latent heat release plus the heat input at the boundary.

The energy balance for the standard one-phase problem specified by equations (5.4)-(5.5) can be obtained from the above argument by neglecting all θ terms in (5.16) (or equivalently setting $c = k = 0$ in (5.17)) and applying the Stefan condition (5.6) to replace $T_x(s,t)$

$$\frac{dE}{dt} = \left[\beta - (1-c)\frac{ds}{dt}\right]\frac{ds}{dt} + \left(\frac{ds}{dt}\right)^2 \neq \beta\frac{ds}{dt}\,. \tag{5.19}$$

This demonstrates that energy is not conserved in this formulation. The equivalent expression in limit $k \to 0$ is obtained by replacing $\theta_x(s,t)$ via (5.8) and applying the Stefan

condition (5.9) to replace $T_x(s,t)$ to equation (5.17) to obtain

$$\frac{dE}{dt} = c\frac{ds}{dt}\left(\frac{ds}{dt} + \theta_i\right) + \left[\beta - \frac{ds}{dt} - c\theta_i\right]\frac{ds}{dt} + (1-c)\left(\frac{ds}{dt}\right)^2 = \beta\frac{ds}{dt}\,. \tag{5.20}$$

Finally the one-phase limit with $k \to \infty$ is determined using the definition of θ_1 to give $k\theta_x(s,t) = -css_{tt}$ and $T_x(s,t)$ comes from the Stefan condition (5.12) to give

$$\frac{dE}{dt} = -cs\frac{d^2s}{dt^2} + \left(cs\frac{d^2s}{dt^2} + \left[\beta - (1-c)\frac{ds}{dt}\right]\frac{ds}{dt}\right) + (1-c)\left(\frac{ds}{dt}\right)^2 = \beta\frac{ds}{dt}\,. \tag{5.21}$$

Hence the large and small k formulations also conserve energy.

5.4 Results

We now present two sets of results for the solidification of salol and water. The results were computed numerically using the boundary immobilisation method and Keller box finite difference technique used in [66, 67]. The $k \to 0$ result was rather unexpected so the computations were verified using an accurate heat balance method, as described in [70, 71]. This provided solutions typically within 0.5% of the numerics. As discussed above, the $k \to 0$ formulation requires a value for the solid temperature θ_i. At the end of §5.2 we demonstrated that $\theta_i = -1$. We also tried $\theta_i = 0$ but this did not improve the correspondence.

In Figure 5.1 we compare the position of the phase change front for the three one-phase formulations against the two-phase solution using parameter values appropriate for salol and with two values of β. Salol was chosen since it was the material with the lowest value of $k \approx 1.4$ for which we had all the necessary data, see [4]. The values of β correspond to dimensional temperatures of 234.8, 272.4K (the heterogeneous phase change temperature $T_m \approx 314.7$K), the value of $c = c_s/c_l = 0.73$. The solid line in the figure represents the two-phase model, the dotted line the standard one-phase model of equations (5.4)-(5.6), this is bounded by the two limiting cases which conserve energy using the Stefan conditions (5.9) for $k \to 0$ (dot-dash line) and (5.12) for $k \to \infty$ (dashed line). Even in this case, where k is relatively small we find that the large k solution is extremely close to the two-phase model

while the limit $k \to 0$ shows an approximately 40% difference to the two-phase solution. It is also surprising that this latter energy conserving form is further from the two-phase solution than the form that does not conserve energy. The two sets of plots are for small values of β (in particular we wished to show results with $\beta < 1$ and $\beta > 1$). In the limit of large β the curves all coincide but for the $k \to 0$ case the convergence is slow: for $\beta = 40$ the $k \to \infty$ result is within 0.005% of the 2 phase result, the $k \to 0$ solution is within 1.8%.

In Figure 5.2 we show results for a water-ice system where $k \approx 4, c \approx 0.49$. This has a significantly lower c value than salol and a higher k value. The values $\beta = 0.7, 1.3$ correspond to temperatures 158.9, 211.5 (where $T_m \approx 273$K), see [20]. With the larger k value we can observe that the two-phase formulation and the large k one-phase approximation are almost indistinguishable. The $k \to 0$ formulation differs by approximately 30% and again the result obtained by simply neglecting θ is more accurate than this latter energy conserving form.

In addition to the results shown above we also carried out the same calculations for molten and solid copper, $k \approx 2.4, c \approx 0.72$ and gold $k \approx 3, c \approx 0.79$. In both cases the value of c is similar to that of salol and so the copper results were virtually identical to those of salol, whilst the gold results showed a very slight decrease in the velocity s_t.

5.5 Conclusions

In summary, our simulations show that the one-phase reduction with large k can provide an excellent agreement with the two-phase problem for a wide range of physically realistic parameter values and supercooling. The small k formulation of [25] whilst mathematically correct is highly inaccurate for practical problems and surprisingly significantly less accurate than the non-energy conserving form. Only in the limit of large Stefan number do the solutions coincide (and in this case the supercooled formulation is unnecessary). We therefore propose that an accurate approximation to the two-phase one-dimensional Stefan problem is obtained by the simpler one-phase approximation specified by equations (5.4)-(5.5) and the Stefan condition (5.12). Using standard notation the dimensional form consists in the

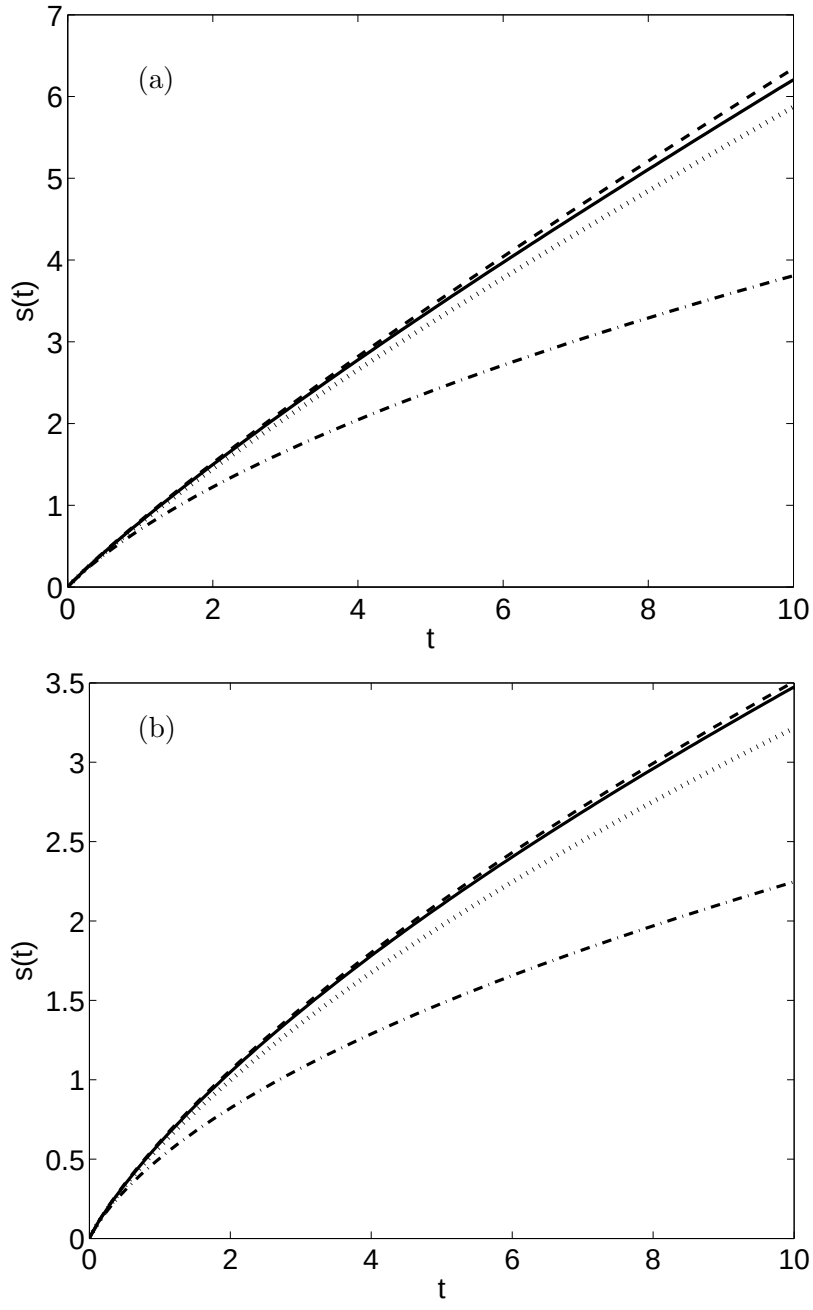

Figure 5.1: Variation of $s(t)$ for salol, $k \approx 1.4, c = 0.73$ and (a) $\beta = 0.7$, (b) $\beta = 1.3$.

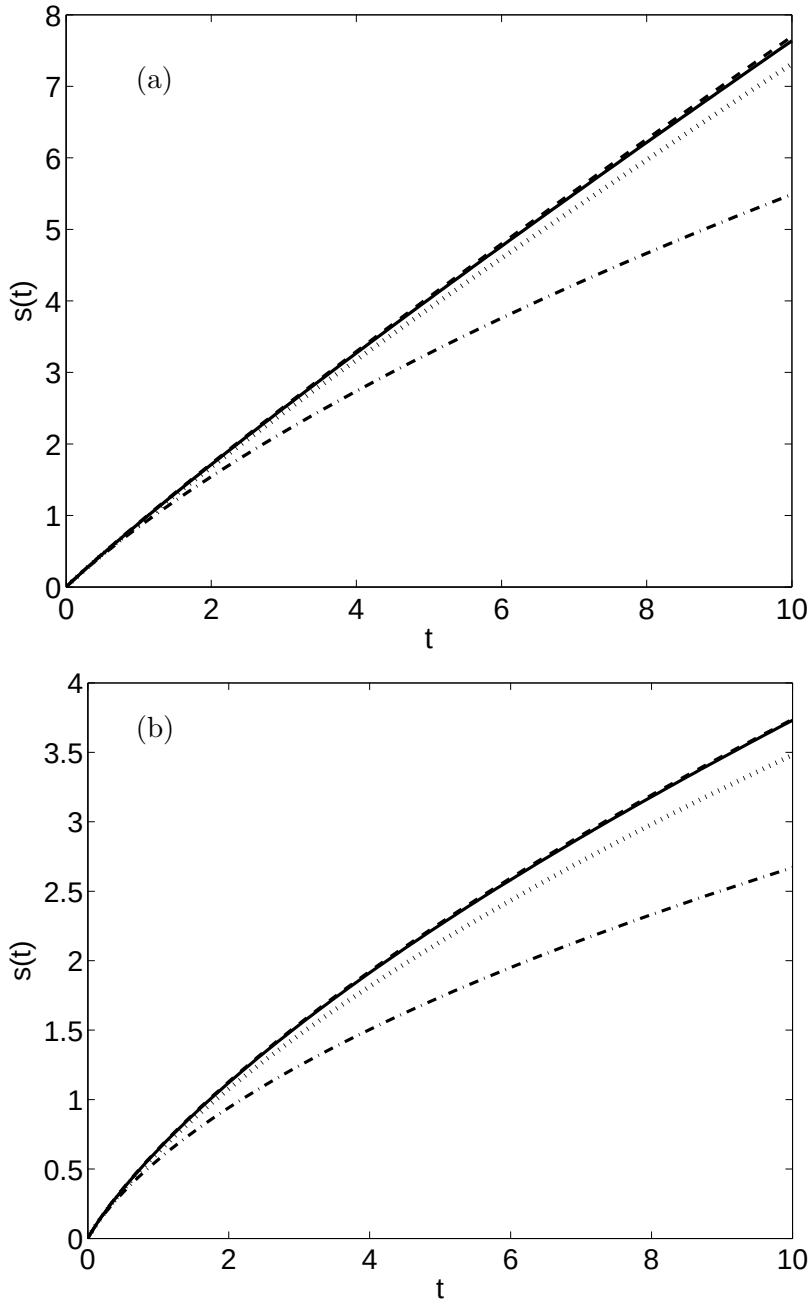

Figure 5.2: Variation of $s(t)$ for water, $k \approx 4, c \approx 0.49$ and (a) $\beta = 0.7$, (b) $\beta = 1.3$.

heat equation

$$\frac{\partial T}{\partial t} = \frac{k_l}{\rho_l c_l}\frac{\partial^2 T}{\partial x^2} \qquad s(t) < x < \infty\,, \tag{5.22}$$

with boundary conditions

$$T(s,t) = T_m - \phi s_t\,, \qquad T|_{x\to\infty} \to T_\infty\,, \qquad T(x,0) = T_\infty\,, \tag{5.23}$$

and the Stefan condition

$$\rho_l c_s \phi s s_{tt} + \rho_l \left[L_m - (c_l - c_s)\phi s_t\right] s_t = -k_l \left.\frac{\partial T}{\partial x}\right|_{x=s}\,, \qquad s(0) = 0\,, \qquad s_t(0) = 1\,, \tag{5.24}$$

where the constant ϕ is the kinetic undercooling coefficient used in the linear relation $T_I(s_t) \approx T_m - \phi s_t$. Similar reductions can no doubt be obtained for related problems and a similar analysis may be easily applied to the nonlinear undercooling case.

Chapter 6

On the one phase reduction of the Stefan problem

T.G. Myers, F. Font. *On the one-phase reduction of the Stefan problem*
Submitted to International Communications on Heat and Mass Transfer (May 2014)
Impact factor: 2.208

Abstract

The one-phase reduction of the Stefan problem, where the phase change temperature is a variable, is analysed. It is shown that problems encountered in previous analyses may be traced back to an incorrectly formulated Stefan condition. Energy conserving reductions for Cartesian, cylindrically and spherically symmetric problems are presented and compared with solutions to the two-phase problem.

6.1 Introduction

The Stefan problem where the phase change temperature is fixed is a classical example of a moving boundary problem and has been well-studied for more than 100 years. However, with the advent of a number of new technologies, the situation where a material's phase

change temperature differs from the standard value is becoming increasingly important. For example, materials made from supercooled liquids are currently used in medicine, defence and aerospace equipment, electronics and sports [28, 109]. The phase change temperature of supercooled liquids can vary because the liquid molecules have lower energy than when solidifying under normal circumstances and this affects their ability to move to the solid interface. Nanoparticles have a vast array of applications in medicine, environmental remediation, materials and energy [29]. A key factor in understanding the melting of nanoparticles is the large decrease in melt temperature with decreasing size, for example a 2 nm radius gold nanoparticle will melt at approximately 500K below the bulk melt temperature [8]. In this case the high curvature of the melt interface leads to a large value for the surface tension induced stress which then reduces the melt temperature.

In order to simplify the mathematical description of the phase change process it is common to neglect one of the material phases, to produce the *one-phase Stefan problem*. When the melt temperature is the standard (or homogeneous) phase change temperature, here denoted T_m^*, then the one-phase problem is usually well-defined. However, when the phase change temperature is variable then difficulties arise (for example, energy may not be conserved) [25, 74, 118]. The issue with the one-phase formulation has been investigated by looking at asymptotic limits of low thermal conductivity in the solid (compared to that in the liquid) [25] and large conductivity in the solid [74].

In this chapter we will demonstrate that problems with the one-phase reduction may arise due to inconsistent assumptions concerning the temperature in the neglected phase. If the reduction is carried out consistently then there is no problem with the energy conservation. The one-phase reduction is invoked to simplify the analysis, another standard simplification involves assuming constant thermal properties throughout the process. If we consider the ratio of the thermal conductivity of water to ice $k = k_s/k_l \approx 4$ and the specific heat ratio $c = c_s/c_l \approx 0.5$ then it is clear that this assumption can lead to significant errors. Consequently in the following we will work with different (constant) values in each phase. The density also varies, usually to a lesser extent than conductivity and specific heat [3]. If we include density change in our analysis then the governing equations become more complex, with the

addition of advection and kinetic energy, see [30]. Consequently, to keep down the number of terms in the equations and so simplify the arguments we will focus on the situation where the density, ρ, is constant throughout the process. However, the arguments may be easily adapted to include it using the equations described in [30].

6.2 Governing equations for phase change

We will now derive the Stefan condition and heat equations for a one-dimensional Cartesian problem via an energy balance. For simplicity we examine the case of fixed density and so avoid the velocity terms caused by the shrinkage or expansion of the material.

The governing equations for the Stefan problem may be obtained from the energy conservation equation

$$\frac{\partial}{\partial t}\left[\rho I^*\right] = -\nabla \cdot \mathbf{q}^* \,, \tag{6.1}$$

where ρ is the density, I^* the internal energy and the conductive heat flux $\mathbf{q}^* = -k\nabla T^*$. This simply states that internal energy varies with time due to heat movement through the boundary. The star superscript indicates dimensional variables. The internal energy/unit mass is

$$I_s^* \quad = c_s(\theta^* - T_m^*) \,, \qquad\qquad I_l^* = c_l(T^* - T_m^*) + L_f \,, \tag{6.2}$$

where subscripts s, l denote solid and liquid, θ^*, T^* denote the respective temperatures. The heat equations may be obtained from the energy balance by simply substituting for I^* and $\mathbf{q}^*$ in (6.1)

$$\frac{\partial}{\partial t^*}\left[\rho c_s(\theta^* - T_m^*)\right] \;=\; \frac{\partial}{\partial x}\left(k_s \frac{\partial \theta^*}{\partial x^*}\right) \,, \tag{6.3}$$

$$\frac{\partial}{\partial t^*}\left[\rho(c_l(T^* - T_m^*) + L_f)\right] \;=\; \frac{\partial}{\partial x}\left(k_l \frac{\partial T^*}{\partial x^*}\right) . \tag{6.4}$$

Noting that all thermal properties and T_m^* are constant within each phase leads to the

familiar form

$$\rho c_s \frac{\partial \theta^*}{\partial t^*} = k_s \frac{\partial^2 \theta^*}{\partial x^{*2}} , \qquad \rho c_l \frac{\partial T^*}{\partial t^*} = k_l \frac{\partial^2 T^*}{\partial x^{*2}} . \tag{6.5}$$

The Stefan condition may also be obtained from the conservation equation (6.1) via the Rankine-Hugoniot condition

$$\frac{\partial f}{\partial t} + \nabla \cdot \mathbf{g} = 0 \quad \Rightarrow \quad [f]_-^+ s_t = [\mathbf{g} \cdot \mathbf{n}]_-^+ , \tag{6.6}$$

where $\mathbf{n}$ is the unit normal (in this case it is simply $\hat{\mathbf{x}}$) and $f, \mathbf{g}$ are functions evaluated on either side of the discontinuity, $x^* = s^*(t^*)$. For the case where a fluid initially occupying $x^* \geq 0$ is solidified from the boundary $x^* = 0$ we take the $^+$ superscript to indicate fluid, $x^* > s^*$, and $^-$ to indicate solid, $x^* < s^*$. Comparing the energy balance (6.1) to the Rankine-Hugoniot condition shows $f = \rho I^*$, $\mathbf{g} = \mathbf{q}^*$, and the Stefan condition follows from the second of equations (6.6)

$$\begin{aligned} \rho \left[(c_l (T^*(s^*, t^*) - T_m^*) + L_f) - c_s (\theta^*(s^*, t^*) - T_m^*) \right] s_{t^*}^* = \\ - k_l \left. \frac{\partial T^*}{\partial x^*} \right|_{x^* = s^*} + k_s \left. \frac{\partial \theta^*}{\partial x^*} \right|_{x^* = s^*} . \end{aligned} \tag{6.7}$$

The spherical and cylindrically symmetric versions are obtained from

$$\begin{aligned} \frac{\partial}{\partial t^*} \left[\rho c_s (\theta^* - T_m^*) \right] &= \nabla \cdot (k_s \nabla \theta^*) , \\ \frac{\partial}{\partial t^*} \left[\rho (c_l (T^* - T_m^*) + L_f) \right] &= \nabla \cdot (k_l \nabla T^*) , \end{aligned} \tag{6.8}$$

and

$$\begin{aligned} \rho \left[(c_l (T^*(s^*, t^*) - T_m^*) + L_f) - c_s (\theta^*(s^*, t^*) - T_m^*) \right] s_{t^*}^* = \\ - k_l \left. \frac{\partial T^*}{\partial r^*} \right|_{r^* = R^*} + k_s \left. \frac{\partial \theta^*}{\partial r^*} \right|_{r^* = R^*} , \end{aligned} \tag{6.9}$$

where the phase change front is now located at $r^* = R^*$ and temperatures depend on r^*, t^*.

6.3 Stefan problem with melting point depression

The standard two-phase, one-dimensional Cartesian Stefan problem with melting point depression is typically specified by heat equations in the solid and liquid phases and the following Stefan condition

$$\rho\left[(c_l - c_s)\left(T_I^*(t) - T_m^*\right) + L_f\right] s_{t^*}^* = -k_l \left.\frac{\partial T^*}{\partial x^*}\right|_{x^*=s^*} + k_s \left.\frac{\partial \theta^*}{\partial x^*}\right|_{x^*=s^*}, \tag{6.10}$$

where $T_I^*(t)$ is the interface temperature, see [3, 15, 25, 29, 60, 74, 119, 118]. The variation of $T_I^*(t)$ may be described by a number of relations. For supercooling models an exponential relation between T_I^* and $s_{t^*}^*$ holds. This is frequently linearised for small departures from the bulk phase change temperature so $T_I^* - T_m^* \propto s_{t^*}^*$ [19, 28]. With high curvature some form of Gibbs-Thomson relation is typically used [29, 28].

In order to follow previous asymptotic reductions we will now formulate the non-dimensional version of the problem via the following scales,

$$\theta = \frac{\theta^* - T_m^*}{\Delta T^*}, \qquad T = \frac{T^* - T_m^*}{\Delta T^*}, \qquad x = \frac{x^*}{L}, \qquad t = \frac{t^*}{\tau}, \tag{6.11}$$

where ΔT^* is a temperature scale and τ the time-scale. In the Stefan problem without melting point depression the length-scale L may be unknown. With melting point depression L may be specified according to the equation governing the phase change temperature. Choosing the time-scale for heat flow in the liquid, $\tau = \rho c_l L^2/k_l$, the heat equations now reduce to

$$\frac{\partial \theta}{\partial t} = \frac{k}{c}\frac{\partial^2 \theta}{\partial x^2}, \qquad \frac{\partial T}{\partial t} = \frac{\partial^2 T}{\partial x^2}. \tag{6.12}$$

The Stefan condition becomes

$$\left[(1-c)\,T_I(t) + \beta\right] s_t = -\left.\frac{\partial T}{\partial x}\right|_{x=s(t)} + k\left.\frac{\partial \theta}{\partial x}\right|_{x=s(t)}, \tag{6.13}$$

where $\beta = L_f/(c_l \Delta T)$, $k = k_s/k_l$, $c = c_s/c_l$.

These equations are often simplified via a one-phase approximation. Say, for example we neglect the solid phase, then we only need to solve the heat equation in the liquid while the Stefan condition becomes

$$[(1-c)\,T_I(t)+\beta]\,s_t = -\left.\frac{\partial T}{\partial x}\right|_{x=s} . \tag{6.14}$$

The most familiar form of Stefan condition may be obtained by neglecting melting point depression, so setting $T_I = 0$ ($T_I^* = T_m^*$) in equation (6.14). Equation (6.14) may also be obtained by choosing $\theta(x,t)$ to be constant or a function of time. Wu *et al* [118] discuss papers where the solid phase is simply ignored, see [120, 85]. Many authors assume $\theta(x,t) = T_I(t)$ [15, 19, 38] or alternatively $\theta(x,t) = 0$ [39]. The first choice has the problem that it does not satisfy the heat equation, whilst the second does not satisfy the interface boundary condition. A more formal way to reduce the system is to let $k = 0$, so the liquid conducts heat infinitely faster than the solid. Then the solid temperature is removed from the Stefan condition while the heat equation in the solid becomes $\theta_t = 0$ and so θ may be set as a function of x: in practice it is usually taken as 0 or the initial temperature $\theta(x,0) = \theta_0$.

Evans and King [25] discuss a number of papers where the Stefan problem is incorrectly formulated and discuss in detail the approximation where (6.14) with $T_I = 0$ is used in conjunction with melting point depression. They point out that this form is popular since it arises in the case without supercooling and is accurate in the limit of large Stefan number. It may also be derived from (6.13) with the common assumption that $c = 1$ and then choosing $k = 0$ to remove the contribution of the solid phase. Wu *et al* [118] discuss similar reductions in the context of spherical nanoparticle melting. They state that when the initial temperature is different to the phase change temperature then the one-phase limit may only be derived under the assumption $k \ll 0$.

In [25] it is stated that the supercooled Stefan problem using (6.14) with $T_I = 0$ does not conserve energy. To understand this statement consider the total heat in the system

$$E = \int_0^s c\theta\,dx + \int_s^\infty T\,dx\ , \tag{6.15}$$

(note, we have chosen T_m^* as the reference temperature where $E = 0$). The rate of change of energy is

$$\frac{\partial E}{\partial t} = \int_0^s c\frac{\partial \theta}{\partial t}\, dx + c\theta(s,t)s_t + \int_s^\infty \frac{\partial T}{\partial t}\, dx - T(s,t)s_t\,. \tag{6.16}$$

Replacing the time derivatives via the heat equations and integrating gives

$$\frac{\partial E}{\partial t} \;=\; k\,\frac{\partial \theta}{\partial x}\bigg|_s - \frac{\partial T}{\partial x}\bigg|_s - k\,\frac{\partial \theta}{\partial x}\bigg|_0 + \left[c\theta(s,t) - T(s,t)\right] s_t\ , \tag{6.17}$$

where we have assumed $T_x \to 0$ as $x \to \infty$. The standard Stefan condition $T_x|_{x=s} = -\beta s_t$ may be obtained by setting $c = 1$, $\theta(x,t) = T_I(t)$ in (6.13). At the interface $\theta(s,t) = T(s,t) = T_I(t)$ and the above energy balance reduces to

$$\frac{\partial E}{\partial t} = \beta\frac{\partial s}{\partial t}\ . \tag{6.18}$$

This equation states that the rate of change of energy balances the heat released by the phase change, so in fact the standard Stefan condition may be consistent with energy conservation (although the choice $\theta(x,t) = T_I(t)$ does not satisfy the heat equation). However, if we arrive at the standard Stefan condition by setting $c = 1$, $\theta(x,t) = 0$ in equation (6.13) then the energy balance gives

$$\frac{\partial E}{\partial t} = \left[\beta - T_I\right] s_t\ , \tag{6.19}$$

and now energy is not conserved (but the heat equation is satisfied). So in fact using the standard Stefan condition it is possible to conserve energy in the system, provided the heat equation is not satisfied, conversely the heat equation may be satisfied but then energy is not conserved.

6.4 Asymptotic solutions

The problem of energy conservation has been tackled in a number of papers by making assumptions on the size of the conductivity ratio and seeking a series expansion in the temperature profiles. Most work has focussed on the limit of small solid to liquid conductivity ratio $k \ll 1$ [5, 25, 118]. However, in [74] it was pointed out that due to the way heat is conducted $k_s > k_l$ and so the limit $k \gg 1$ was investigated, we shall discuss both cases below.

6.4.1 The limit of small conductivity ratio, $k \ll 1$

The limit of small k was considered in [5, 25, 118]. In non-dimensional form the analysis of [25] simply incorporates a boundary layer in the solid, of thickness $\mathcal{O}(k)$, which allows the solid temperature to change between $T_I(t)$ at $x = s(t)$ to the initial temperature $\theta(x, 0)$ in the far-field which, for simplicity, is set to 0. Their analysis leads to the modified Stefan condition

$$[T_I(t) + \beta]\, s_t = -\left.\frac{\partial T}{\partial x}\right|_{x=s(t)} . \tag{6.20}$$

This is the correct form of Stefan condition for a far-field temperature $\theta = 0$ and it conserves energy. However, this solution is far from ideal. For the problem considered in [25] and by many other authors on the solidification of supercooled liquids the solid does not exist at $t = 0$, hence $\theta(x, 0)$ is undefined. Once solidification starts the solid forms at temperature $T_I(t) \neq 0$. Since the solid is assumed to be a poor conductor (infinitely poor compared to the liquid) there is no mechanism for the far-field to attain zero temperature. Then, there is the physical issue that solids are better conductors of heat than liquids. Hence this condition, although mathematically correct, is not of use for thermal problems.

6.4.2 Limit of large conductivity ratio, $k \gg 1$

Noting that physically $k_s > k_l$ it makes more sense to look for a large k reduction. Unlike the $k \to 0$ limit, when $k \to \infty$ the solid reacts almost instantaneously to the boundary temperature and so $\theta(x, t) \approx T_I(t)$.

Now consider the problem where $k \gg 1$ with boundary conditions on the solid $\theta(s,t) = T_I(t)$, $k\theta_x(0,t) = -Q$. Note, previously we ignored any heat input at the boundary $x = 0$ since the solid was deemed an infinitely poor conductor. In fact previous comparisons between one-phase and two-phase approximations have often been made by imposing $\theta_x = 0$ at the boundary, see [15, 74]. Now for generality we allow a non-zero heat flux. If we assume $1/k \ll 1$ and look for a perturbation solution in terms of the small parameter $1/k$ then to first order the solid temperature is

$$\theta(x,t) = T_I(t) + \frac{1}{k}\left[\frac{\partial T_I}{\partial t}\frac{(x^2 - s^2)}{2} - Q(x-s)\right] . \tag{6.21}$$

Using this to determine $\theta_x(s,t)$ in the Stefan condition (6.13) leads to

$$-cs\frac{\partial T_I}{\partial t} + Q + [(1-c)T_I + \beta]\, s_t = -\left.\frac{\partial T}{\partial x}\right|_{x=s} . \tag{6.22}$$

This is the appropriate one-phase Stefan condition, correct to first order, in the case where k is large. The version correct to leading order in $1/k$ has $\theta(x,t) = T_I(t)$ and the first two terms of equation (6.22) are neglected (thus reducing equation (6.22) to (6.14). That is the appropriate one-phase Stefan condition, when k is infinite, is given by equation (6.14). The most significant difference between using the leading order and first order results is the appearance of the time derivative of T_I. In the linear undercooling case examined in [74] $T_I = -s_t$ and so the Stefan condition becomes second order in time, rather than the usual first-order equation.

To verify that the new form conserves energy we may substitute for θ via equation (6.21) and $T_x(s,t)$ via (6.22) into the energy equation (6.17) to find

$$\frac{\partial E}{\partial t} = Q + \beta s_t . \tag{6.23}$$

This equation states that the rate of change of energy balances that released by the phase change and the energy input at the boundary, *i.e.* this formulation conserves energy. The heat equation is also satisfied by $\theta(x,t)$. Similarly, the leading order solution $\theta(x,t) = T_I(t)$

leads to a consistent, energy conserving solution (it satisfies the heat equation since the limit $k \to \infty$ results in $\theta_{xx} = 0$). Obviously the leading order solution will be less accurate than the first order approximation.

6.5 Formulation via equation (6.7)

In §6.2 we derived the dimensional Stefan formulation (6.7). If we compare this with the standard Stefan formulation (6.10), which is used in studies of melting point depression, we can see that (6.10) follows from equation (6.7) if the interface temperature of both phases is $T_I^*(t^*)$. *This implicit assumption, that both phases achieve the same temperature at the interface, is the root of the energy conservation problem.*

In non-dimensional form equation (6.7) may be written

$$[T(s,t) - c\theta(s,t) + \beta]\, s_t = -\left.\frac{\partial T}{\partial x}\right|_{x=s} + k \left.\frac{\partial \theta}{\partial x}\right|_{x=s}. \tag{6.24}$$

This equation should be used as the starting point for any one-phase reduction. For example, to retrieve the poor solid conductor model, $k \ll 1$, with initial temperature θ_0, we may impose $\theta(x,t) = \theta_0$ and so $\theta(s,t) = \theta_0$, $\theta_x = 0$. Substituting these values together with $T(s,t) = T_I(t)$ into equation (6.24) gives

$$[T_I(t) - c\theta_0 + \beta]\, s_t = -\left.\frac{\partial T}{\partial x}\right|_{x=s(t)}. \tag{6.25}$$

If we choose $\theta_0 = 0$ then equation (6.20) is retrieved (without the need for an asymptotic analysis).

In the limit of large k the solid is a good conductor and so the interface temperature is immediately transmitted through the material, hence $\theta(x,t) = T_I(t)$ and again $\theta_x = 0$. Equation (6.24) now reduces to

$$[(1-c)T_I(t) + \beta]\, s_t = -\left.\frac{\partial T}{\partial x}\right|_{x=s}. \tag{6.26}$$

These constitute the final two terms on the left hand side of equation (6.22), which are the

leading order terms in the large k expansion. The first two terms of equation (6.22) arise as a correction for finite k and come from the fact that for finite k the temperature gradient $\theta_x(s,t) \neq 0$.

Note, the popular form specified by equation (6.13) may be derived from equation (6.24) by setting $T(s,t) = \theta(s,t) = T_I(t)$. One-phase reductions must be consistent with this, either by choosing the temperature of the neglected phase to be $T_I(t)$ everywhere or by a boundary layer analysis to match the far-field to the interface temperature, as described in [5, 25, 74, 118]. On the other hand, any analysis based on equation (6.13) where the neglected phase is assigned a constant value not equal to T_I will be inconsistent and this manifests itself in the fact the energy balance is not satisfied.

6.6 Extension to cylindrical and spherically symmetric geometries

A common physical situation where the phase change temperature varies involves the melting of nanoparticles or nanowires [29, 86, 123, 118]. In this case the melting point depression is a consequence of the surface tension induced pressure. The interest in nano melting for a wide variety of practical applications provides us with the opportunity to investigate a different form of Stefan problem to that of previous sections. In keeping with the analyses of [29, 118] we will consider the radially symmetric melting of a sphere or cylinder where a fixed temperature is imposed at the outer boundary $T(1,t) = 1$. The appropriate nondimensional forms of (6.12) are

$$\frac{\partial \theta}{\partial t} = \frac{k}{c}\frac{1}{r^n}\frac{\partial}{\partial r}\left(r^n \frac{\partial \theta}{\partial r}\right), \qquad \frac{\partial T}{\partial t} = \frac{1}{r^n}\frac{\partial}{\partial r}\left(r^n \frac{\partial T}{\partial r}\right), \tag{6.27}$$

where the solid occupies $r \in [0, R(t)]$ and the liquid $r \in [R(t), 1]$. The length-scale has been chosen as the initial radius, R_0, and the temperature scale $\Delta T = T_H - T_m^*$ where T_H is the temperature imposed at the surface. The spherically symmetric model corresponds to $n = 2$, cylindrical to $n = 1$ and $n = 0$ gives us a one-dimensional Cartesian model. The appropriate

non-dimensional form for the Stefan condition (6.24) is

$$[T(R,t) - c\theta(R,t) + \beta]\, R_t = -\left.\frac{\partial T}{\partial r}\right|_{r=R} + k\left.\frac{\partial \theta}{\partial r}\right|_{r=R}. \tag{6.28}$$

Following the arguments of §6.5 we may immediately write down the one phase reductions for small and large k. For $k \ll 1$, $\theta(x,t) = \theta(R,t) = \theta_0$ and equation (6.28) reduces to the radial form of (6.25) (with s replaced by R and x by r). Choosing $\theta_0 = 0$ this is exactly the one-phase limit used in the study of nanoparticle melting of [5, 118] and derived through a boundary layer analysis. For infinite k, $\theta(x,t) = \theta(R,t) = T(R,t) = T_I$ and the radial version of (6.14) is obtained. The correction for large but finite k requires solving the solid heat equation in (6.27), subject to $\theta(R,t) = T_I(t), \theta_r(0,t) = 0$. This leads to

$$\theta = T_I + \frac{1}{k}\left[\frac{c}{n+1}\frac{\partial T_I}{\partial t}\left(\frac{r^2 - R^2}{2}\right)\right] + \mathcal{O}(k^{-2}). \tag{6.29}$$

Then the Stefan condition, correct to $\mathcal{O}(k^{-1})$, is

$$-\frac{cR}{n+1}\frac{\partial T_I}{\partial t} + [(1-c)T_I + \beta]\, R_t = -\left.\frac{\partial T}{\partial r}\right|_{r=R}. \tag{6.30}$$

Using the definition of total energy

$$E = \int_0^R c\theta r^n dr + \int_R^1 T r^n dr\,, \tag{6.31}$$

it is a simple matter to show that the above formulae all conserve energy.

In [74] the accuracy of the Cartesian one-phase formulations was discussed in detail. An example was given for the material salol, which has a low value of $k \approx 1.3$ and it was shown that the small k solution was far from the two-phase solution (with an approximately 40% slower melt rate). The standard formulation (corresponding to the infinite k limit) was more accurate than the small k solution and the large but finite k result was very accurate. With data appropriate for a water-ice system, $k \approx 4$, the same trend was observed: the small k solution gave the least accurate results, the large k solution was virtually indistinguishable from the two-phase solution. Since the accuracy of the Cartesian model has been

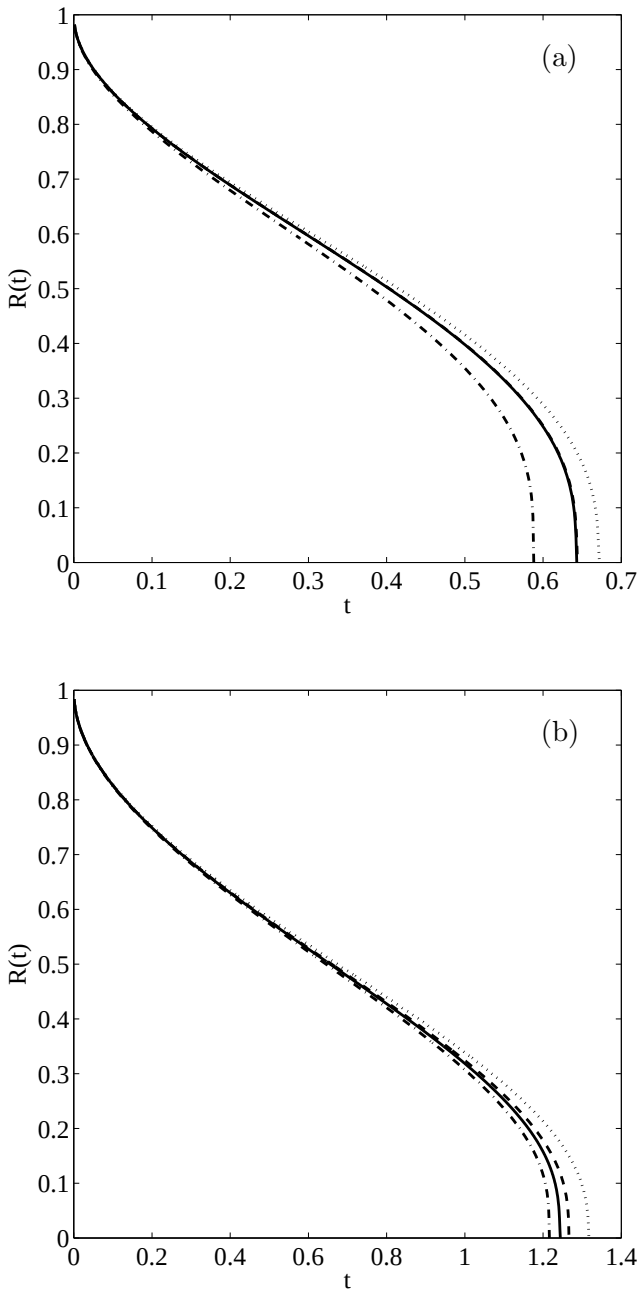

Figure 6.1: Evolution of the interface $R(t)$ for the two-phase (solid line), large k (dashed), small k (dash-dotted) and standard (dotted) formulations. Plot (a) corresponds to $n = 2$ (nanoparticle) and (b) to $n = 1$ (nanowire).

established we now focus on the radially symmetric formulations. In Figure 6.1 we present two sets of results for the evolution of a particle radius for the spherical and cylindrically symmetric models. Parameter values are chosen for gold: $T_m^* = 1337\text{K}$, $L_m 6.37 \times 10^4 \text{J/kg}$, $\rho(= \rho_s) = 1.93 \times 10^4 \text{kg/m}^3$, $k = 2.9906$, $c = 0.7914$, $\sigma_{sl} = 0.27\text{N/m}$, see [29]. The melt temperature is described by the standard Gibbs-Thomson relation, $T_I(t) = -n\Gamma/R(t)$ where $\Gamma = \sigma_{sl} T_m^*/(R_0 \rho L_f \Delta T)$ and σ_{sl} is the solid-liquid surface tension. Choosing an initial radius $R_0 = 20\text{nm}$ and temperature difference $\Delta T \approx 39\text{K}$ we find $\Gamma = 0.3755$, $\beta = 10$. Figure 6.1a shows the melting of a nanosphere, Figure 6.1b shows a melting nanowire. The four curves in each figure represent the solution of the two-phase model of equation (6.28) (solid line), the large k model of equation (6.30) (dashed line), the standard formulation (or infinite k) given by the radial version of (6.14) (dotted line) and the small k model, the radial version of equation (6.20), (dash-dot line). All curves show the expected feature that for $t \to 0^-$ and $R \to 0^+$ the velocity $R_t \to -\infty$, see [5, 29, 48, 119]. Note, the Gibbs-Thomson relation predicts a negative melt temperature for $R \approx 0.4\text{nm}$ while we expect continuum theory to no longer hold below $R = 2\text{nm}$, see the discussion in [29, 30]. Consequently the graphs should only be expected to hold for $R > 0.1 = 2\text{nm}/20\text{nm}$. In the first graph, for a nanosphere, the large k solution is virtually indistinguishable from the two-phase solution. The dotted line, which represents the infinite k model is close to the two-phase solution, while the small k approximation gives the worst result. For the melting of a nanowire, Fig. 6.1b, again the large k solution is the most accurate but, remarkably, the small k solution shows a similar, if slightly lower, level of accuracy.

6.7 Conclusion

It has been noted by several authors that the standard one-phase reduction to the Stefan problem in the presence of melting point depression does not conserve energy. In this chapter we show two important results:

1. Depending on the assumptions made to obtain the standard reduction it may conserve energy (but then the heat equation for the neglected phase is not satisfied).

2. Difficulties encountered in writing down a one-phase reduction which satisfies both energy conservation and the heat equation stem from using the wrong form of Stefan condition, which implicitly incorporates the assumption that both solid and liquid materials are at the phase change temperature at the interface. Provided the correct Stefan condition is used energy conserving forms may be written down immediately. Asymptotic expansions may subsequently be used to improve accuracy.

In the case of melting a semi-infinite solid, in a Cartesian frame, the appropriate two-phase Stefan condition is given by equation (6.24) and the leading order reduction by equation (6.26). A reduction accurate to first-order in $1/k$ is given by equation (6.22). Similar equations were also derived for spherical and cylindrically symmetric problems.

Obviously there are many varieties of Stefan problem and we have only analysed two particular types of problem. However, their adaptation to many other scenarios is straightforward. The key being to start with the correct form of Stefan condition.

Chapter 7

Conclusions

The main aim of this thesis was to extend the classical formulation of the Stefan problem to allow the modelling of recently discovered physical phenomena involving phase change. In particular the work has led to new insights into the melting of nanoparticles and the solidification from supercooled liquids. Our work on the nanoscale has been particularly groundbreaking, allowing us to explain the behaviour of a melting system at the limits of continuum theory. The introduction of a variable phase change temperature in the Stefan problem has been a common feature of the models developed in this thesis. This has led to the revision of standard one-phase reductions in order to ensure energy conservation in such systems.

In chapter 2 we analysed the melting process of nanoparticles. A generalised version of the Gibbs-Thomson equation was introduced in the Stefan problem to account for melting point depression. By means of a perturbation approach, the initial system consisting of two heat equations, the Stefan condition and the Gibbs-Thomson equation was reduced to a pair of ordinary differential equations, which were integrated numerically. The results successfully reproduced the characteristic abrupt melting of nanoparticles observed in experiments. Furthermore, the melting times predicted by our model agreed well with the limited experimental data available. The solution of the system assuming a constant phase change temperature, i.e. the standard Stefan problem, when compared to the solution of our model,

proved very inaccurate in describing the melting process of nanoparticles. In addition, we examined the response of the model to the reduction $c_l = c_s$, since this is a standard simplification. We concluded that for very small particles the system is very sensitive to this approximations.

In chapter 3 the goal was to study the effect of relaxing the standard condition of constant materials' density in the Stefan problem and examine the impact in the model for nanoparticle melting. The results showed that as the particle radius decreased the effect of the density change became increasingly important, leading to differences of more than 50% in melting times for nanoparticles with a radius of 10 nm. In addition, the results demonstrated that even for macroscopic particles, where the Gibbs-Thomson effect is negligible, the difference in the melting times from the models with and without density change tended to a limit of approximately 15%. In conclusion the density variation should always be included in phase change models.

The mathematical models studied in chapters 2 and 3 described a melting process where the phase change temperature varied with the curvature of the solid-liquid interface. In chapter 4 we dealt with a model describing the solidification of supercooled melts where the interface temperature depended on the velocity of the solidification front. While previous studies were restricted to the case where the relation between the interface temperature and the velocity was linear, valid only for small supercooling, we extended the theory to large supercooling by introducing a nonlinear relationship between the velocity of the front and the interface temperature. We presented solutions for three distinct scenarios: constant phase change temperature (Neumann solution), linear and nonlinear relationship between the interface temperature and the velocity. By examining the corresponding limits, the solutions with a nonlinear dependence could reproduce the behaviour of the Neumann solution and the solution with the linear relation. The main conclusion of this study was that for practical purposes the nonlinear relation should be employed even for small supercoolings, i.e., for Stefan numbers close to unity.

In chapter 4 we presented asymptotic, numerical and approximate solutions using the HBIM for the one-phase model with supercooling. Whilst asymptotic analysis is a popular

method to analyse the solution form in various limits it may only be valid over a very small range. In contrast, the HBIM solution was very close to the numerical solution, and in general proved more accurate than the small and large time asymptotics. In the nonlinear case, where the asymptotic solutions were not available the HBIM equations could still be analysed to predict the solution behaviour. In conclusion the HBIM is a useful tool in analysing this type of problem.

The Stefan problem with supercooling has been widely analysed in the past by means of its corresponding one-phase reduction. However, the standard one-phase reduction does not always conserve energy. Recent studies proposing one-phase reductions that conserved energy, but were physically inconsistent. In chapter 5 we developed a one-phase reduction of the supercooled Stefan problem that conserves energy, based on the assumption of a large ratio of solid to liquid thermal conductivity. When tested against the solution for the full two-phase system our model showed excellent agreement and improved remarkably on the performance of previous one-phase models.

The tangible link between the mathematical models analysed in this thesis is that of a time-dependent phase change temperature rather than the standard constant one. As discussed in chapter 5, for the case of supercooling, the one-phase reduction of the Stefan problem obtained by neglecting the temperature of one of the phases must be derived rigorously to ensure energy conservation. In chapter 6 we presented a detailed explanation of the difficulties encountered when formulating the one-phase reduction of the Stefan problem with a variable phase change temperature. We discovered that, depending on the assumption regarding the temperature of the neglected phase, the standard reduction may conserve energy. However, as an immediate consequence the heat equation for the neglected phase is not satisfied. Alternatively if one chooses to satisfy the heat equation then energy is not conserved. We concluded that by choosing the correct form of the Stefan condition for the two-phase problem, one-phase energy conserving formulations can be easily posed and asymptotic expansions may subsequently be used to improve the accuracy of the model. Furthermore, we provided a general one-phase model of the Stefan problem with a generic variable phase change temperature, valid for spherical, cylindrical and planar geometries.

Results from the one-phase formulation were compared to the two-phase model solution and showed excellent accuracy.

In summary this thesis has dealt with mathematical models describing special solid-liquid phase transitions, such as the solidification of a supercooled liquid, melting in the presence of high curvature and density effects. The research has opened the door to a number of future challenges. One exciting direction follows from the work on nanoparticle melting. In the final stages of our models the time-scales approached that of phonon transport, indicating that the diffusive heat transfer must be coupled to the ballistic heat transport due to the interaction of phonons. This process significantly modifies the heat equation. One appropriate description of the process leads to a form of 'relativistic heat equation', where a second time derivative is added to the standard heat equation, changing it from a parabolic to a hyperbolic problem. With the increasing interest in nanoscience and nanotechnology, this will be a hot topic of intense research and debate in the future, for instance to develop efficient methods for nanoparticle assembly or fabrication of nanometer scale structures for new electronic devices.

Conclusions

L'objectiu principal d'aquesta tesi ha estat el d'estendre la formulació clàssica del problema de Stefan per permetre la modelització de nous fenòmens físics en relació als canvis de fase. En particular, l'estudi dut a terme aporta nous aspectes sobre la transició sòlid-líquid en nanopartícules i en la solidificació de líquids sota-refredats. La nostra recerca en la nanoescala ha resultat particularment innovadora, permetent donar explicació al comportament de sistemes físics al límit de la teoria del continu. La introducció d'una temperatura variable de canvi de fase ha estat una característica comuna dels models desenvolupats en aquesta tesi, fet que ha portat a la revisió de la formulació estàndard del problema de Stefan d'una fase per tal de garantir la conservació de l'energia.

En el capítol 2 hem analitzat el canvi de fase sòlid-líquid en nanopartícules. Hem introduït una versió generalitzada de l'equació de Gibbs-Thomson al problema de Stefan per tenir en compte la depressió de la temperatura de fusió en les nanopartícules. Per mitjà del mètode de pertorbacions, el sistema inicial que consistia en dues equacions de la calor, la condició de Stefan i l'equació de Gibbs-Thomson, s'ha reduït a un parell d'equacions diferencials ordinàries d'integració numèrica fàcil. Els resultats han reproduït de manera satisfactòria la transició de fase abrupta característica de les nanopartícules. A més a més, els temps totals de transició calculats mitjançant el nostre model concorden amb les observacions experimentals existents. Per altra banda, la solució del model amb temperatura de canvi de fase constant, és a dir, la solució del problema estàndard de Stefan, s'ha mostrat totalment inapropiada per descriure la transició de fase sòlid-líquid en nanopartícules. A més, també hem examinat la resposta del model al imposar $c_s = c_l$, ja que aquesta és una aproximació estàndard, concloent que per partícules molt petites el sistema és molt sensible a aquest tipus d'aproximacions.

En el capítol 3 l'objectiu era estudiar l'efecte de relaxar la condició d'igual densitat ($\rho_s = \rho_l$) entre fases en el problema de Stefan, així com examinar l'impacte sobre els resultats en el model de transició de fase de nanopartícules desenvolupat al capítol anterior. Els resultats han mostrat com a mesura que el radi inicial de la partícula disminuïa l'efecte del canvi en la densitat esdevenia més i més important, fet que ha derivat en diferències de més

del 50% en els temps de transició per partícules amb radis de l'ordre de 10 nm. A més a més, els resultat han demostrat que, fins i tot per partícules macroscòpiques, on l'efecte de Gibbs-Thomson és menyspreable, la diferència entre el model amb densitat constat i el model amb densitat variable tendeix a un límit del 15%. En conclusió, la diferència entre la densitat de les fases sòlida i líquida sempre hauria de ser tinguda en compta en models matemàtics que descriguin transicions de fase.

Els models matemàtics estudiats en els capítols 2 i 3 han descrit de manera satisfactòria processos de transició de fase on la temperatura de canvi de fase depèn de la curvatura de interfície sòlid-líquid. En el capítol 4 hem desenvolupat un model que descriu la solidificació de líquids sota-refredats, on la temperatura de canvi de fase depèn de la velocitat del front de solidificació. Estudis previs s'havien restringit a casos on la relació entre la temperatura de canvi de fase i la velocitat del front era lineal, vàlida només per sota-refredaments moderats. En aquest capítol hem estès la teoria per a casos amb sota-refredaments elevats on la relació entre la temperatura de canvi de fase i la velocitat del front és no lineal. Hem presentat solucions pels tres escenaris possibles: temperatura de canvi de fase constant (solució de Neumann), relació lineal entre temperatura de transició i velocitat, i relació no lineal. Examinant els límits corresponents, les solucions tenint en compte la relació no lineal han reproduït el comportament de la solució de Neumann i el comportament de la solució mitjançant la relació lineal. La principal conclusió de l'anàlisi dut a terme és que, per aplicacions pràctiques, la relació no lineal ha de ser emprada fins i tot per a casos amb sota-refredament moderat, és a dir, per a valors del nombre de Stefan propers a la unitat.

En el capítol 4 hem presentat solucions asimptòtiques, numèriques i aproximades mitjançant el mètode HBIM per al problema de Stefan d'una fase amb sota-refredament. Així com l'anàlisi asimptòtic és un mètode popular per tal d'examinar el comportament de les solucions en diversos límits, sovint només dona aproximacions vàlides en rangs reduïts del domini. En canvi, tal i com s'ha comprovat en aquest capítol, el mètode HBIM permet obtenir solucions molt pròximes a la solució numèrica i, en general, més precises que les solucions asimptòtiques trobades per als diferents límits de temps. En els casos on l'anàlisi asimptòtic del problema per sota-refredaments elevats no ha estat possible, les equacions

resultants d'aplicar el mètode HBIM s'han analitzat i han permès extreure el comportament global de la solució. En conclusió, el mètode HBIM ha resultat una eina d'anàlisi molt útil per aquest tipus de problemes.

El problema de Stefan amb sota-refredament ha estat analitzat en estudis previs mitjançat la reducció d'una fase (una de les fases, sòlida o líquida, és suprimida i només es té en compte la fase resultant). Recentment, s'ha demostrat que la reducció estàndard del problema no sempre conserva l'energia. Estudis recents han proposat reduccions del problema d'una fase que conserven l'energia però que són poc consistents des d'un punt de vista físic. En el capítol 5 hem desenvolupat una reducció del problema de Stefan amb sota-refredament que conserva l'energia i que està basat en el fet que la raó entre les conductivitats tèrmiques de les fases sòlida i líquida és gran. Al comparar la solució del nostre model amb la solució del problema de dues fases el resultat ha estat satisfactori. També s'ha comprovat com la solució mitjançant el nostre model millora significativament els resultats dels models d'una fase en estudis anteriors.

El punt en comú dels diversos models matemàtics analitzats en aquesta tesi és el fet que la temperatura de canvi de fase depèn del temps, contràriament a la suposició estàndard de temperatura de canvi de fase constant. Tal i com s'ha exposat en el capítol 5 pel cas de líquids sota-refredats, la reducció d'una fase del problema de Stefan mitjançant la omissió d'una de les fases s'ha de derivar de manera rigorosa per tal garantir la conservació de l'energia. En el capítol 6 hem presentat una explicació detallada de les dificultats que es troben al formular les reduccions del problema de Stefan quan la temperatura de fusió és variable. Hem constatat que, depenent de la suposició inicial sobre la temperatura de la fase omesa, la reducció estàndard pot conservar l'energia però no satisfer l'equació de la calor (de la fase omesa), ò bé, es pot triar satisfer l'equació de la calor però no conservar l'energia. Hem conclòs que, escollint inicialment la condició de Stefan correcta del problema de dues fases, les reduccions d'una fase que conserven l'energia es poden obtenir de manera senzilla i mitjançant l'anàlisi asimptòtic es poden obtenir formulacions molt precises del problema reduït. A més a més, al final d'aquest capítol, hem proporcionat una model general d'una fase amb una temperatura de canvi de fase genèrica, vàlid per geometries esfèriques, cilíndriques

i planes. El resultat obtingut de comparar les solucions d'aquest model amb la solució del problema de dues fases ha esdevingut molt satisfactori.

En resum, en aquesta tesi hem desenvolupat i analitzat models matemàtics que descriuen transicions de fase en situacions especials, com és el cas de la transició de líquid a sòlid en condicions de sota-refredament o la transició de sòlid a líquid en presència de superfícies amb molta curvatura. La recerca realitzada ha obert la porta a tot un seguit de reptes futurs. En particular, un d'aquests reptes deriva dels models estudiats que descriuen el canvi de fase sòlid-líquid en nanopartícules. En aquests models, l'escala de temps al final del procés s'acosta a l'escala de temps d'interacció entre fonons, indicant que la transferència de calor per difusió s'hauria d'acoblar amb el transport balístic dels fonons. En aquest cas, l'equació de la calor s'ha de modificar de manera significativa. Una de les descripcions de la transferència de calor a escales nano o sub-nano mètriques es basa en la utilització de l'equació de la calor relativista, on una segona derivada del temps apareix i transforma el problema de parabòlic a hiperbòlic. Amb el creixent interès en la nanociència i la nanotecnologia, aquest serà un tema de gran debat i recerca intensa, per exemple alhora de desenvolupar mètodes eficients de producció de nanopartícules o mecanismes per fabricar estructures nanomètriques per nous dispositius electrònics.

Chapter 8

Appendix

8.1 Rankine-Hugoniot conditions

Given the functions $f(x,t)$ and $g(x,t)$, with g the flux of f, the divergence form

$$\frac{\partial f}{\partial t} + \frac{\partial g}{\partial x} = 0\,, \tag{8.1}$$

implies that for any smooth space-time curve $x = x_i(t)$, the following jump relation (Rankine-Hugoniot or shock condition) must hold

$$\dot{x}_i\,[f]^+_- = [g]^+_-\,, \tag{8.2}$$

where the notation '+' and '−' implies evaluation on both sides of the curve $x_i(t)$. The jump occurring at $x_i(t)$ is depicted in figure 8.1.

In order to obtain the relation (8.2) one needs to integrate (8.1) over the domain $[x_1, x_2]$,

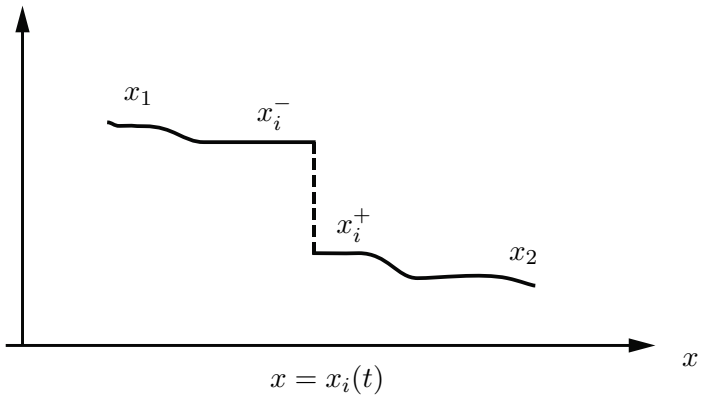

Figure 8.1: Representation of the jump at $x_i(t)$.

then

$$0 = \int_{x_1}^{x_2} \left(\frac{\partial f}{\partial t} + \frac{\partial g}{\partial x} \right) \, dx \tag{8.3}$$

$$= \int_{x_1}^{x_2} \frac{\partial f}{\partial t} \, dx + [g]_{x_1}^{x_2} \tag{8.4}$$

$$= \frac{d}{dt} \int_{x_1}^{x_2} f \, dx + [g]_{x_1}^{x_2} \tag{8.5}$$

where we have utilized the Leibnitz integral rule

$$\frac{d}{dt} \int_{a(t)}^{b(t)} h(x,t) \, dx = \int_{a(t)}^{b(t)} \frac{\partial h}{\partial t} \, dx + h(b(t),t) \, \frac{\partial b}{\partial t} - h(a(t),t) \, \frac{\partial a}{\partial t} \,, \tag{8.6}$$

to progress from (8.4) to (8.5). Assuming $x_i^- > x_1$ and $x_i^+ < x_2$ to be the left and right sides of x_i, respectively, the domain $[x_1, x_2]$ may be split in two, leading to

$$\frac{d}{dt} \int_{x_1}^{x_2} f \, dx = \frac{d}{dt} \left(\int_{x_1}^{x_i^-} f \, dx + \int_{x_i^+}^{x_2} f \, dx \right) \tag{8.7}$$

$$= \int_{x_1}^{x_i^-} \frac{\partial f}{\partial t} \, dx + \dot{x}_i^- f(x_i^-, t) + \int_{x_i^+}^{x_2} \frac{\partial f}{\partial t} \, dx - \dot{x}_i^+ f(x_i^+, t). \tag{8.8}$$

Then, substituting (8.8) in (8.5) and letting $x_1 \to x_i^-$ and $x_2 \to x_i^+$, the integrals vanish and

$$\dot{x}_i^- f(x_i^-, t) - \dot{x}_i^+ f(x_i^+, t) = - [g]_{x_i^-}^{x_i^+} \,. \tag{8.9}$$

Finally, noting that $\dot{x}_i^- = \dot{x}_i^+ = \dot{x}_i$, one obtains the jump condition (8.2).

Chapter 9

Bibliography

[1] P. Abragall and N-T Nguyen. *Nanofluidics*. Artech House, 1st edition, 2009.

[2] F. Ahmad, A.K. Pandey, A.B. Herzog amd J.B. Rose, C.P. Gerba, and S.A. Hashsham. Environmental applications and potential health implications of quantum dots. *Journal of Nanoparticle Research*, 14(8):1–24, 2012.

[3] V. Alexiades and A.D. Solomon. *Mathematical Modelling of Freezing and Melting Processes*. Hemisphere Publishing Corporation, 1st. edition, 1993.

[4] M. F. Ashby and D. R. H. Jones. *Engineering materials 2: an introduction to microstructures, processing and design*. Butterworth-Heinemann, 3rd edition, 2006.

[5] J.M. Back, S.W. McCue, M.H-N. Hsieh, and T.J. Moroney. The effect of surface tension and kinetic undercooling on a radially-symmetric melting problem. *Applied Mathematics and Computation*, 229:41–52, 2014.

[6] P. Bergese, I. Colombo, D. Gervasoni, and L.E. Depero. Melting of nanostructured drugs embedded into a polymeric matrix. *Journal of Physical Chemistry B*, 108:15488–15493, 2004.

[7] R.B. Bird, W.E. Stewart, and E.N. Lightfoot. *Transport Phenomena*. John Wiley and Sons, 2nd edition, 2007.

[8] P. Buffat and J. P. Borel. Size effect on the melting temperature of gold particles. *Physical Review A*, 13(6):2287–2297, 1976.

[9] C. Cagran, B. Wilthan, and G. Pottlacher. Enthalpy, heat of fusion and specific electrical resistivity of pure silver, pure copper and the binary Ag–28Cu alloy. *Thermochimica Acta*, 445(2): 104–110, 2006.

[10] J. Caldwell and C. K. Chiu. Numerical solution of one-phase stefan problems by the heat balance integral method, part i: cylindrical and spherical geometries. *Communications in Numerical Methods in Engineering*, 16(8):569–583, 2000.

[11] W. L. Chan, R. S. Averback, D. G. Cahill, and Y. Ashkenazy. Solidification velocities in deeply undercooled silver. *Physical Review Letters*, 102(95701): 1230–1234, 2009.

[12] I. E. Chang. Navier-stokes solutions at large distances from a finite body. *Journal of Mathematics and Mechanics*, 10: 811–876, 1961.

[13] C. Charach and I. Rubinstein. Pressure-temperature effects in planar stefan problems with density change. *Journal of Applied Physics*, 71:1128, 1992.

[14] C. Charach and B. Zaltzman. Planar solidification from an undercooled melt: Asymptotic solutions to a continuum model with interfacial kinetics. *Physical Review E*, 47(2): 1230–1234, 1993.

[15] C. Charach and B. Zaltzman. Analytic model for planar growth of a solid germ from an undercooled melt. *Physical Review E*, 49(5): 4322–4327, 1994.

[16] J. Crank. *Free and Moving Boundary Problems*. Oxford University Press, 1st. edition, 1996.

[17] J. Crepeau. Josef stefan: His life and legacy in the thermal sciences. *Experimental Thermal and Fluid Science*, 31:795–803, 2007.

[18] T. Ben David, Y. Lereah, G. Deutscher, R. Kofman, and P. Cheyssac. Solid-liquid transition in ultra-fine lead particles. *Philosophical Magazine A*, 71(5):1135–1143, 1995.

[19] S.H. Davis. *Theory of Solidification*. Cambridge University Press, 2001.

[20] P. G. Debenedetti. Supercooled and glassy water. *Journal of Physics: Condensed Matter*, 15: 1669–1726, 2003.

[21] P.G. Debenedetti. *Metastable liquids, concepts and principles*. Princeton University Press, 1996.

[22] Andrey I. Denisyuk, Kevin F. MacDonald, F. Javier Garca de Abajo, and Nikolay I. Zheludev. Towards femtojoule nanoparticle phase-change memory. *Japanese Journal of Applied Physics*, 48(3S1):03A065, 2009.

[23] J. N. Dewynne, S. D. Howison, J. R. Ockendon, and W. Xie. Asymptotic behaviour of solutions to the Stefan problem with a kinetic condition at the free boundary. *Journal of the Australian Mathematical Society Series B*, 31: 81–96, 1989.

[24] U. Düring, J. H. Bilgram, and W. Känzing. Properties of the solid-liquid interface of growing salol crystals: A dynamic light scattering investigation. *Physical Review A*, 30(2): 946–959, 1984.

[25] J. D. Evans and J. R. King. Asymptotic results for the Stefan problem with kinetic undercooling. *Quarterly Journal of Mechanics and Applied Mathematics*, 53: 449–473, 2000.

[26] C. Faivre, D. Bellet, and G. Dolino. Phase transitions of fluids confined in porous silicon: A differential calorimetry investigation. *European Physical Journal B*, 7(1):19–36, 1999.

[27] M. Farid. The moving boundary problems from melting and freezing to drying and frying food. *Chemical Engineering and Processing*, 41:1–10, 2002.

[28] F. Font, S. L. Mitchell, and T.G. Myers. One-dimensional solidification of supercooled melts. *International Journal of Heat and Mass Transfer*, 62:411–421, 2013.

[29] F. Font and T.G. Myers. Spherically symmetric nanoparticle melting with a variable phase change temperature. *Journal of Nanoparticle Research*, 15(12):1–13, 2013.

[30] F. Font, T.G. Myers, and S. L. Mitchell. Mathematical model for nanoparticle melting with density change. *Microfluidics and Nanofluidics*, pages 1–11, 2014.

[31] P. Ghosh, G. Han, M. De, C.K. Kim, and V.M. Rotello. Gold nanoparticles in delivery applications. *Advanced Drug Delivery Reviews*, 60:1307–1315, 2008.

[32] T. R. Goodman. The Heat-Balance Integral and its application to problems involving a change of phase. *Transactions of the ASME*, 80: 335–342, 1958.

[33] A. O. Govorov, W. Zhang, T. Skeini, H. Richardson, J. Lee, and N. A. Kotov. Gold nanoparticle ensembles as heaters and actuators: melting and collective plasmon resonances. *Nanoscale Research Letters*, 1(1):84–90, 2006.

[34] A Lindsay Greer. A cloack of liquidity. *Nature*, 464:1137–1138, 2010.

[35] G. Guisbiers. Schottky defects in nanoparticles. *The Journal of Physical Chemistry C*, 115(6):2616–2621, 2011.

[36] G. Guisbiers, M. Kazan, O. Van Overschelde, M. Wautelet, and S. Pereira. Mechanical and thermal properties of metallic and semiconductive nanostructures. *Journal of Physical Chemistry C*, 112:4097–4103, 2008.

[37] O. Gulseren, F. Ercolessi, and E. Tosatti. Premelting of thin wires. *Physical Review B*, 51(11):7377–7380, 1995.

[38] S.C. Gupta. *The Classical Stefan Problem.* Elsevier, 1st. edition, 2003.

[39] L.A. Herraiz, M.A. Herrero, and J.J.L. Velzquez. A note on the dissolution of spherical crystals. *Proceedings of the Royal Society of Edinburgh*, 131:371–389, 2001.

[40] J. M. Hill. *One-Dimensional Stefan Problems: An Introduction.* Longman Scientific & Technical, 1st. edition, 1987.

[41] J.M. Hill and A. Kucera. On boundary fixing transformations for the classical stefan problem. *Mechanics Research Communications*, 11(2):91 – 96, 1984.

[42] E.J. Hinch. *Perturbation methods.* Cambridge University Press, 2000.

[43] H. Hu and S.A. Argyropoulos. Mathematical modelling of solidification and melting: a review. *Modelling and Simulation in Matererial Science Engineering*, 4:371–396, 1996.

[44] Prashant K. Jain, Ivan H. El-Sayed, and Mostafa A. El-Sayed. Au nanoparticles target cancer. *Nano Today*, 2(1):18–29, 2007.

[45] S. Karmakar, S. Kumar, R. Rinaldi, and G. Maruccio. Nano-electronics and spintronics with nanoparticles. *Journal of Physics: Conference Series*, 292(012002):doi:10.1088/1742–6596/292/1/012002, 2011.

[46] J.M. Khodadadi and S.F. Hosseinizadeh. Nanoparticle-enhanced phase change materials (nepcm) with great potential for improved thermal energy storage. *International Communications in Heat and Mass Transfer*, 34(5):534 – 543, 2007.

[47] J. R. King and J. D. Evans. Regularization by kinetic undercooling of blow-up in the ill-posed stefan problem. *SIAM Journal of Applied Mathematics*, 65(5): 1677–1707, 2005.

[48] R. Kofman, P. Cheyssac, Y. Lereah, and A. Stella. Melting of clusters approaching 0D. *The European Physical Journal D*, 9(1-4):441–444, 1999.

[49] K. Koga, T. Ikeshoj, and K-I Sugawara. Size- and temperature-dependent structural transitions in gold nanoparticles. *Physical Review Letters*, 92(11):DOI: 10.1103/PhysRevLett.92.115507, 2004.

[50] C.-L. Kuo and P. Clancy. Melting and freezing characteristics and structural properties of supported and unsupported gold nanoclusters. *Journal of Physical Chemistry B*, 109:13743–13754, 2005.

[51] P. A. Lagerstrom and R. G. Casten. Basic concepts underlying singular perturbation techniques. *SIAM Review*, 14(1): 63–120, 1972.

[52] S. L. Lai, J. Y. Guo, V. Petrova, G. Ramanath, and L. H. Allen. Size-dependent melting properties of small tin particles: Nanocalorimetric measurements. *Physical Review Letters*, 77(1):99–102, 1996.

[53] G. Lame and B.P. Clapeyron. Mémoire sur la solidification par refroidissement d'un globe solide. *Annales Chimie Physique*, 47:250–256, 1831.

[54] Bing Li and Da-Wen Sun. Novel methods for rapid freezing and thawing of foods – a review. *Journal of food engineering*, 54:175–182, 2002.

[55] F. Liu and D. L. S. Mcelwain. A computationally efficient solution technique for moving-boundary problems in finite media. *IMA Journal of Applied Mathematics*, 59(1):71–84, 1997.

[56] R.P. Liu, T. Volkmann, and D. M. Herlach. Undercooling and solidification of Si by electromagnetic levitation. *Acta Materialla*, 49:439–444, 2001.

[57] X. Liu, P. Yangb, and Q. Jiang. Size effect on melting temperature of nanostructured drugs. *Materials Chemistry and Physics*, 103:1–4, 2007.

[58] H. Löwen, J. Bechhoefer, and L. S. Tuckerman. Crystal growth at long times: Critical behaviour at the crossover from diffusion to kinetics-limited regimes. *Physical Review A*, 45(4): 2399–2415, 1992.

[59] S. W. McCue, J. R. King, and D. S. Riley. Extinction behaviour for two-dimensional inward-solidification problems. *Proceedings of the Royal Society A*, 459(2032):977–999, 2003.

[60] S. W McCue, B. Wu, and J. M. Hill. Micro/nanoparticle melting with spherical symmetry and surface tension. *IMA Journal of Applied Mathematics*, 74:439–457, 2009.

[61] J. Mei and J. W. Davenport. Molecular-dynamics study of self-diffusion in liquid transition metals. *Physical Review B*, 42(15): 9682–9684, 1990.

[62] M. Merder. Solidification fronts with unusual long-time behaviour. *Physical Review A*, 45(4): 2158–2160, 1992.

[63] S. L. Mitchell. Applying the combined integral method to one-dimensional ablation. *Appl. Math. Modelling*, 36: 127–138, 2012.

[64] S. L. Mitchell and T. G. Myers. Application of standard and refined heat balance integral methods to one-dimensional Stefan problems. *SIAM Review*, 52(1): 57–86, 2010.

[65] S. L. Mitchell and T. G. Myers. Improving the accuracy of heat balance integral methods applied to thermal problems with time dependent boundary conditions. *International Journal of Heat and Mass Transfer*, 53: 3540–3551, 2010.

[66] S. L. Mitchell and M. Vynnycky. Finite-difference methods with increased accuracy and correct initialization for one-dimensional Stefan problems. *Applied Mathematics and Computation*, 215: 1609–1621, 2009.

[67] S. L. Mitchell, M. Vynnycky, I. G. Gusev, and S. S. Sazhin. An accurate numerical solution for the transient heating of an evaporating droplet. *Applied Mathematics and Computation*, 217: 9219–9233, 2011.

[68] Hisashi Moriguchi, Yue Zhang, Makoto Mihara, and Chifum Sato. Successful cryopreservation of human ovarian cortex tissues using supercooling. *Nature. Scientific Reports*, 2:537, 2012.

[69] F. Mosally, A.S. Wood, and A. Al-Fhaid. An exponential heat balance integral method. *Applied Mathematics and Computation*, 130(1):87 – 100, 2002.

[70] T. G. Myers. Optimizing the exponent in the heat balance and refined integral methods. *International Communications in Heat and Mass Transfer*, 36: 143–147, 2009.

[71] T. G. Myers. Optimal exponent heat balance and refined integral methods applied to Stefan problems. *International Journal of Heat and Mass Transfer*, 53: 1119–1127, 2010.

[72] T. G. Myers, J. P. F. Charpin, and C. P. Thompson. Slowly accreting ice due to supercooled water impacting on a cold surface. *Physics of Fluids*, 14(1):240–256, 2002.

[73] T. G. Myers and S. L. Mitchell. Application of the combined integral method to Stefan problems. *Applied Mathematical Modelling*, 35: 4281–4294, 2011.

[74] T. G. Myers, S. L. Mitchell, and F. Font. Energy conservation in the one-phase supercooled Stefan problem. *International Communications in Heat and Mass Transfer*, 39: 1522–1525, 2012.

[75] T.G. Myers and F. Font. On the one-phase reduction of the stefan problem. *Submitted to International Communications on Heat and Mass Transfer*, 2014.

[76] T.G. Myers and J. Low. An approximate mathematical model for solidification of a flowing liquid in a microchannel. *Microfluidics and Nanofluidics*, 11:417428, 2011.

[77] T.G. Myers and J. Low. Modelling the solidification of a power-law fluid flowing through a narrow pip. *International Journal of Thermal Sciences*, 70:127–131, 2013.

[78] K.K. Nanda. Size dependent melting of nanoparticles. *Pramana Journal of Physics*, 72(4): 617–628, 2009.

[79] NASA. Nasa science news: Liquids on pause. `http://science.nasa.gov/science-news/science-at-nasa/2003/16oct_viscosity/`, last accessed 12 May 2012, 2003.

[80] M.F. Natale, E.A. Santillan Marcus, and D.A. Tarzia. Explicit solutions for one-dimensional two-phase free boundary problems with either shrinkage or expansion. *Nonlinear analysis: Real World Applications*, 11:1946–1952, 2010.

[81] N-T Nguyen and S.T. Werely. *Fundamentals and applications of microfluidics*. Artech House, 1st edition, 2006.

[82] J. Ockendon, A. Lacey, A. Movchan, and S. Howison. *Applied Partial Differential Equations*. Oxford University Press, 1999.

[83] O. Petrov and I. Furó. Curvature-dependent metastability of the solid phase and the freezing-melting hysteresis in pores. *Physical Review E*, 73:011608, 2006.

[84] A. Plech, V. Kotaidis, S. Grésillon, C. Dahmen, and G. von Plessen. Laser-induced heating and melting of gold nanoparticles studied by time-resolved x-ray scattering. *Physical Review B*, 70(19):195423, 2004.

[85] Zhu Q., Peirce A., and Chadam J. Initiation of shape instabilities of free boundaries in planar cauchy-stefan problems. *Eurpoean Journal of Applied Mathematics*, 4:419–436, 1993.

[86] W.H. Qi. Size effect on melting temperature of nanosolids. *Physica B: Condensed Matter*, 368(1-4):46–50, 2005.

[87] W.H. Qi and M.P. Wang. Size effect on the cohesive energy of nanoparticle. *Journal of Materials Science Letters*, 21(22):1743–1745, 2002.

[88] S. Rana, A. Bajaj, R. Mout, and V.M. Rotello. Monolayer coated gold nanoparticles for delivery applications. *Advanced Drug Delivery Reviews*, 64:200–216, 2012.

[89] D. S. Riley, F. T. Smith, and G. Poots. The inward solidification of spheres and circular cylinders. *International Journal of Heat and Mass Transfer*, 17:1507–1516, 1974.

[90] C. Ruan, Y. Murooka, R. K. Raman, and R. A. Murdick. Dynamics of size-selected gold nanoparticles studied by ultrafast electron nanocrystallography. *Nano Letters*, 7(5):1290–1296, 2007.

[91] Nacer Sadoun, El-Khider Si-Ahmed, and Pierre Colinet. On the refined integral method for the one-phase stefan problem with time-dependent boundary conditions. *Applied Mathematical Modelling*, 30(6):531 – 544, 2006.

[92] O.V. Salata. Applications of nanoparticles in biology and medicine. *Journal of Nanobiotechnology*, 2(3), 2004.

[93] V.M. Samsonov, A.N. Bazulev, and N.Yu. Sdobnyakovy. On applicability of Gibbs thermodynamics to nanoparticles. *Central European Journal of Physics*, 1(3):474–484, 2003.

[94] Bozidar Sarler. Stefan's work on solid-liquid phase changes. *Engineering Analysis with Boundary Elements*, 16:83–92, 1995.

[95] Jan Schroers and William L. Johnson. Ductile bulk metallic glass. *Physical Review Letters*, 93(255506), 2004.

[96] T. U. Schülli, R. Daudin, G. Renaud, A. Vaysset, O. Geaymond, and A. Pasturel. Substrate-enhanced supercooling in AuSi eutectic droplets. *Nature*, 464:1174–1177, 2010.

[97] H. W. Sheng, G. Ren, L. M. Peng, Z. Q. Hu, and K. Lu. Superheating and melting-point depression of Pb nanoparticles embedded in Al matrices. *Phiolosophical Magazine Letters*, 73(4):179–186, 1996.

[98] J.-H. Shim, B.-J. Lee, and Y. W. Cho. Thermal stability of unsupported gold nanoparticle: a molecular dynamics study. *Surface Science*, 512:262–268, 2002.

[99] Bruno F. Soares, Fredrik Jonsson, and Nikolay I. Zheludev. All-optical phase-change memory in a single gallium nanoparticle. *Physical Review Letters*, 98:153905, 2007.

[100] J. Stefan. Versuche über die verdampfung. *Sitzungsberichte der Mathematisch-Naturwissenschaftlichen Klasse der Kaiserlichen Akademie der Wissenschaften in Wien. Mathem.-naturw.*, 68(2A):385–423, 1873.

[101] J. Stefan. Über die diffusion von säuren und basen gegen einander. *Sitzungsberichte der Mathematisch-Naturwissenschaftlichen Klasse der Kaiserlichen Akademie der Wissenschaften in Wien. Mathem.-naturw.*, 98(2A):616–636, 1889.

[102] J. Stefan. Über die theorie der eisbildung, insbesondere über die eisbildung im polarmeere. *Sitzungsberichte der Mathematisch-Naturwissenschaftlichen Klasse der Kaiserlichen Akademie der Wissenschaften in Wien. Mathem.-naturw.*, 98(2A):965–983, 1889.

[103] J. Stefan. Über die verdampfung und die auflösung als vorgänge der diffusion. *Sitzungsberichte der Mathematisch-Naturwissenschaftlichen Klasse der Kaiserlichen Akademie der Wissenschaften in Wien. Mathem.-naturw.*, 98(2A):1418–1442, 1889.

[104] J. Stefan. Über einige probleme der theorie der wärmeleitung. *Sitzungsberichte der Mathematisch-Naturwissenschaftlichen Klasse der Kaiserlichen Akademie der Wissenschaften in Wien. Mathem.-naturw.*, 98(2A):473–484, 1889.

[105] J. Stefan. Über die theorie der eisbildung. *Monatshefte für Mathematik und Physik*, 1(1):1–6, 1890.

[106] J. Stefan. Über die verdampfung und die auflösung als vorgänge der diffusion. *Annalen der Physik und Chemie*, 277(12):725–747, 1890.

[107] J. Stefan. Über die theorie der eisbildung, insbesondere über die eisbildung im polarmeere. *Annalen der Physik und Chemie*, 278(2):269–286, 1891.

[108] D. Tarzia. *A Bibliography on Moving-Free Boundary Problems for the Heat-Diffusion Equation. The Stefan Problem.* Progetto Nazionale M.P.I., *Equazioni di evoluzione e applicazioni fisico-matematiche*, 1st. edition, 1988.

[109] M. Telford. The case for bulk metallic glass. *Materials Today*, 7(3): 36–43, 2004.

[110] M. Vert *et al.* Terminology for biorelated polymers and applications (iupac recommendations 2012). *Pure and Applied Chemistry*, 84(2):377–410, 2012.

[111] Marios D. Demetriou *et al.* A damage-tolerant glass. *Nature Materials*, 10:123–128, 2011.

[112] K. P. Travis, B. D. Todd, and D. J. Evans. Departure from navier-stokes hydrodynamics in confined liquids. *Physical Review E*, 55(4):4288–4295, 1997.

[113] V. Voller and M. Cross. Accurate solutions of moving boundary problems using the enthalpy method. *International Journal of Heat and Mass Transfer*, 24(3):545 – 556, 1981.

[114] S. Volz, J-B Saulnier, M. Lallemand, B. Perrin, and P. Depondt. Transient fourier-law deviation by molecular dynamics in solid argon. *Physical Review B*, 54(1):340–347, 1996.

[115] C. Vuik. Some historical notes about the Stefan problem. *Delft University of Technology Report*, 93-07, 1993.

[116] Xiang-Qi Wang and Arun S. Mujumdar. Heat transfer characteristics of nanofluids: a review. *International Journal of Thermal Sciences*, 46(1):1 – 19, 2007.

[117] H. Weber. *Die Partiellen Differential-Gleichungen der Mathematischen Physik*. Vieweg & sohn, 2nd edition, 1901.

[118] B. Wu, S. W. McCue, P. Tillman, and J. M. Hill. Single phase limit for melting nanoparticles. *Applied Mathematical Modelling*, 33: 2349–2367, 2009.

[119] B. Wu, P. Tillman, S. W. McCue, and J. M. Hill. Nanoparticle melting as a Stefan moving boundary problem. *Journal of Nanoscience and Nanotechnology*, 9(2):885–888, 2009.

[120] T. Wu, H.-C. Liaw, and Y.-Z. Chen. Thermal effect of surface tension on the inward solidication of spheres. *International Journal of Heat and Mass Transfer*, 45(10):2055–2065, 2002.

[121] Bin Yang, Yulai Gao, Changdong Zou, Qijie Zhai, A.S. Abyzov, E. Zhuravlev, J.W.P. Schmelzer, and C. Schick. Cooling rate dependence of undercooling of pure sn single drop by fast scanning calorimetry. *Applied Physics A*, 104(1):189–196, 2011.

[122] Z. Yang, M. Sen, and S. Paolucci. Solidification of a finite slab with convective cooling and shrinkage. *Applied Mathematical Modelling*, 27:733–762, 2003.

[123] Wen Y.H., Zhu Z.Z., Zhu R., and Shao G.F. Size effects on the melting of nickel nanowires: a molecular dynamics study. *Physica E*, 25(1):47–54, 2004.

[124] J. Zhong, L. H. Zhang, Z. H. Jin, M. L. Sui, and K. Lu. Superheating of Ag nanoparticles embedded in Ni matrix. *Acta Materiala*, 49(15):2897–2904, 2001.